UNIVERSITEIT VAN PRETORIA
UNIVERSITY OF PRETORIA
YUNIBESITHI YA PRETORIA

Potential of selected South African plant extracts in reducing eczema associated symptoms

By

Marizé Nel

Submitted in fulfillment of the requirements for the degree

MAGISTER SCIENTAE (**Medicinal Plant Sciences)**

In the Faculty of Natural & Agricultural Sciences

University of Pretoria

Pretoria

(May, 23/05/2022)

Supervisor: Prof N Lall

Co-supervisor: Dr. D Twilley

Declaration of originality

I, Marizé Nel declare that the dissertation, which I hereby submit for the degree in MSc Medicinal Plant Science at the University of Pretoria, is my own work and has not previously been submitted by me for a degree at this or any other tertiary institution.

SIGNATURE.…  DATE: 19/05/2022.

Acknowledgments

I would like to thank my supervisor, Prof Namrita Lall for her advice, guidance and the opportunity to complete my masters under her supervision. Without her, none of this would have been possible.

I would like to thank my co-supervisor, Dr. Danielle Twilley for her patience, willingness to help and her encouragement throughout this study. She was a huge source of inspiration and motivation.

To the National Research Foundation, Water Research Commission, the Department of Science and Innovation (DSI) and the University of Pretoria for their financial support during this study.

To my friends, colleagues, family and my fiancé for their unwavering support, love and motivation. Specifically, my fiancé for being my rock throughout this opportunity.

Lastly and most importantly, I would like to thank The Lord for the opportunities; he has given me and for the guidance needed to complete this work.

Conferences and research outputs

i. Conferences:

- Nel M and Lall N. (20-22 September 2021). From Wetland to counter: developing cosmeceutical prototypes from hydrophytes. Water Research Commission (WRC), Fifth WRC Symposium, Digital.
- Nel M and Lall N. (4-7 July 2022). 24th Indigenous Plant Use Forum (IPUF), Digital.

ii. Research outputs

Book Chapters:

- Marizé Nel and Namrita Lall. 2022. "Medicinal Plants for Eczema" In Medicinal Plants in 'Cosmetics, Health and Disease", edited by Prof Namrita Lall. Taylor and Francis **(Accepted).**
- Marizé Nel and Namrita Lall 2023. "*Juncus lomatophyllus* Spreng." In Medicinal Plants from Sub-Saharan Africa-Undiscovered Therapeutic potential edited by Prof Namrita Lall and Dr. Anna-Mari Kok. Springer Nature **(Expected submission date, March 2023).**
- Marizé Nel and Namrita Lall 2023. "*Elegia tectorum* (L. f.) Moline & H. P. Linder" In Medicinal Plants from Sub-Saharan Africa-Undiscovered Therapeutic potential edited by Prof Namrita Lall and Dr. Anna-Mari Kok. Springer Nature **(Expected submission date, March 2023).**
- Marizé Nel and Namrita Lall 2023. "*Bulbine frutescens* (L.) Willd." In Medicinal Plants from Sub-Saharan Africa-Undiscovered Therapeutic potential edited by Prof Namrita Lall and Dr. Anna-Mari Kok. Springer Nature **(Expected submission date, March 2023).**

Publications under preparation:

- Marizé Nel, Danielle Twilley and Namrita Lall. 2023. "Anti-inflammatory response of gold nanoparticles synthesized from *Juncus lomatophyllus* Spreng. against TNF-α production" Frontiers in Molecular Biosciences (IF: 5.246).

- Marizé Nel, Danielle Twilley and Namrita Lall. 2023. “Anti-elastase potential of *Elegia tectorum* (L. f.) Moline & H. P. Linder” Journal of Aging Research (IF: 2.400).
- Marizé Nel, Danielle Twilley and Namrita Lall. 2023. “Potential antihistamine activity of gold nanoparticles biosynthesized from *Bulbine frutescens* (L.) Willd.” PLoS One (IF: 3.240).

Table of Contents

List of Figures

List of Tables

List of abbreviations

ACK:	Ammonium-chloride-potassium
AD:	Atopic dermatitis
ANOVA:	One-way analysis of variance
aSMase:	Acidic sphingomyelinase

Au: Gold metal

AuNPs: Gold nanoparticles

BF: *Bulbine frutescens*

BFE: *Bulbine frutescens* ethanolic leaf juice extract obtained from Botanica

BFE^+: *Bulbine frutescens* ethanolic whole leaf extract collected and prepared at UP

BFE^+AuNP: *Bulbine frutescens* ethanolic whole leaf extract collected and prepared at UP gold nanoparticle

BFEAuNP: *Bulbine frutescens* ethanolic leaf juice extract obtained from Botanica gold nanoparticle

BFG: *Bulbine frutescens* gel extract collected and prepared at UP

BFGAuNP: *Bulbine frutescens* gel extract collected and prepared at UP gold nanoparticle

BFS: *Bulbine frutescens* commercial spray obtained from Botanica

BFSAuNP: *Bulbine frutescens* commercial spray obtained from Botanica gold nanoparticle

BSA: Bovine serum albumin

BSM: Bifidus Selective Medium

dH_2O: Distilled water

DLS: Dynamic light scattering

DMEM: Dulbecco's modified Eagle's Medium

DMSO: Dimethyl sulfoxide

DSI: Department of Science and Inovation

EDS: Energy dispersive spectrometer

EDTA: Ethylenediaminetetraacetic acid

ET: *Elegia tectorum*

ETAuNP: *Elegia tectorum* gold nanoparticle

ET-EtOH: *Elegia tectorum* ethanolic extract

ETF: *Elegia tectorum* fermented extract

FADD: Fas-associated protein with death domain

FBS: Fecal bovine serum

FLG: Filaggrin gene

FTIR: Fourier-transform infrared spectrometry

GC-MS: Gas chromatography-mass spectrometry

HaCaT: Human keratinocyte cells

HRTEM: High-resolution transmission electron microscopy

IAP: Inhibitors of apoptosis proteins

IC_{50}: Concentration at which 50% of the enzyme was inhibited

IFN-α: Interferon-alpha

IFN-γ:	Interferon gamma
IgE:	Immunoglobulin E
IKK-β:	IκB kinase beta
IL:	Interleukin
IL-1β:	Interleukin 1 beta
iNOS:	Inducible nitric oxide synthase
IκB:	Inhibitors of nuclear factor kappa beta
JL:	*Juncus lomatophyllus*
JLAuNP:	*Juncus lomatophyllus* gold nanoparticles
JLB:	*Juncus lomatophyllus* butanol partition
JL-EtOH:	*Juncus lomatophyllus* ethanol extract
JLF:	*Juncus lomatophyllus* fermented extract
LPS:	Lipopolysaccharide
Na_2CO_3:	Sodium bicarbonate
NaCl:	Sodium chloride
NF-κB:	Nuclear factor kappa beta
NIST:	National Institute of Standards and Technology
PBMCs:	Peripheral blood mononuclear cells
PBS:	Phosphate-buffered saline
PMA:	Phorbol 12-myristate 13-acetate
RIP1:	Receptor-interacting serine/threonine kinase 1
RPMI-1640:	Roswell Park Memorial Institute medium
SAED:	Selective area diffraction pattern
SOD	Silencer of death
sPLA2:	Phospholipase
SPR:	Surface plasmon resonance
SPRR3:	Small proline-rich protein 3 gene
TACE:	Tumor necrosis factor-alpha converting enzyme
Th:	T-helper
TLC:	Thin layer chromatography
TNF:	Tumor necrosis factor
TNFR:	Tumor necrosis factor receptor
TNF-α:	Tumor necrosis factor-alpha
TRADD:	Tumor necrosis factor-alpha receptor-associated death domain
TRAF2:	Tumor necrosis factor receptor-associated factor 2

UP:	University of Pretoria
UV-Vis:	Ultraviolet-visible spectrometry
XIAP:	X-chromosome-linked inhibitors of apoptosis proteins
β-GlcCer'ase:	Beta glucocerebrosidase
λ_{max}:	Surface plasmon resonance peak

Abstract

Two main hypotheses have been accepted as the potential cause of eczema. The inside-out hypothesis states that eczema is caused by an immunological defect involving the overproduction of tumor necrosis factor-alpha (TNF-α), which further causes post-inflammatory hyperpigmentation. The outside-in hypothesis states that eczema is due to a skin barrier disruption including the skin becoming cracked. This promotes histamine production which could lead to wrinkle formation when overproduced.

The aim of this study was to determine whether three South African plants namely *Juncus lomatophyllus* (JL), *Elegia tectorum* (ET) and *Bulbine frutescens* (BF) reduce symptoms associated with eczema and inhibit the production of either TNF-α or histamine. Furthermore, this study evaluated whether synthesized gold nanoparticles (AuNPs) using JL, ET and BF or fermenting the ethanolic extracts (Et-OH) of JL (JLF) and ET (ETF), using *Bifidobacterium bifidum*, would enhance biological activity.

Bioassay-guided fractionation was conducted due to the limited information found on JL's compound composition. Gas chromatography-mass spectrometry (GC-MS) of two semi-pure fractions, pooled from the butanol partition (JLB), indicated volatile compounds with a peak area above 5%. Furthermore, JLAuNP (50% inhibitory concentration (IC_{50}): 268.8 ± 5.64 µg/mL) displayed enhanced anti-tyrosinase activity when compared to JL-EtOH and JLF (IC_{50} > 400 µg/mL). JLB, JLAuNP and JL-EtOH effect on TNF-α production using lipopolysaccharide (LPS) stimulated peripheral blood mononuclear cells (PBMCs) was evaluated. None of the selected samples displayed antiproliferative activity against human keratinocytes (HaCaT) and PBMCs (IC_{50} > 400 µg/mL). JLAuNP (23.59 ± 1.95 pg/mL), compared to the untreated control (46.17 ± 9.51 pg/mL), significantly inhibited TNF-α production while JLB and JL-EtOH showed no effect at 200 µg/mL.

ET-EtOH displayed anti-elastase activity (IC_{50}: 28.27 ± 2.02 µg/mL), while ETF and ETAuNP displayed no inhibition (IC_{50} > 500 µg/mL). ET-EtOH was further evaluated on histamine production using phorbol 12-myristate 13-acetate (PMA) stimulated granulocytes. No antiproliferative activity was observed against HaCaT cells and granulocytes (IC_{50} > 400 µg/mL). Furthermore, ET-EtOH (0.10 ± 0.009 ng/mL) significantly inhibited histamine production at 6 µg/mL compared to the vehicle control (0.26 ± 0.02 ng/mL).

BF samples (eight) were evaluated for their potential wound healing activity using HaCaT cells. The commercial spray (BFS) and BFSAuNP displayed antiproliferative activity (IC_{50} of 4.63 ± 0.05 and 3.50 ± 0.40%), while the ethanolic leaf juice (BFE), ethanolic whole leaf (BFE^{+}), gel extract (BFG) and their AuNPs showed no activity (IC_{50} > 400 µg/mL and 10%). BFE (31.40 ± 0.88 %) and BFEAuNP (20.87 ± 0.69%) when compared to the controls showed significant closure at 100 µg/mL and were further evaluated. None of the samples displayed antiproliferative effects against granulocytes. Compared to the untreated control (0.30 ± 0.02 ng/mL), BFEAuNP at 100 µg/mL (0.12 ± 0.04 ng/mL) significantly inhibited histamine production.

This study concluded that JLAuNP's, ET-EtOH and BFEAuNPs potentially reduce eczema associated symptoms based on the *in vitro* results obtained. This is the first report of the synthesis of AuNPs from JL, ET and BF and their potential biological activity. Lastly, this study is the first to identify potential volatile compounds present in JL.

Chapter 1. General introduction

1.1) Background and motivation

Atopic dermatitis, commonly known as eczema is a prevalent chronic inflammatory skin condition that is increasing in prevalence every year, specifically in developed countries (Buddenkotte et al., 2010; Chamlin et al., 2002; Gelmetti and Wollenberg, 2014). Common symptoms experienced by eczema patients include an intolerable itching sensation, dry skin, eczematous skin lesions, epidermal barrier dysfunctions and immunoregulation (Buddenkotte et al., 2010; Lee and Lee, 2014). Currently, there is no cure and treatments such as phototherapy, oral glucocorticosteroids, cyclosporine A and methotrexate, aid in reducing associated symptoms (Buddenkotte et al., 2010). However, these treatments pose numerous adverse effects ranging from steroid atrophy, tachyphylaxis and steroid acne to neurotoxicity, hypertension, diarrhea and anemia (Hengge et al., 2006; Rezzani, 2004). Other known adverse effects include photosensitivity, nausea, gastrointestinal bleeding, headache and serositis (Albrecht and M ler-Ladner, 2010). Thus, effective alternative treatments for eczema are in demand.

For the purpose of this study, three South African plants namely *Juncus lomatophyllus* Spreng., *Elegia tectorum* (L. f.) Moline & H. P. Linder and *Bulbine frutescens* (L.) Willd. were investigated for their potential in reducing symptoms associated with eczema namely post-inflammatory hyperpigmentation, the formation of wrinkles and skin damage as well as their effects on tumor necrosis factor-alpha (TNF-α) and histamine production.

1.2) Research question, aim and objectives

The main research questions and aims for this study were whether South African plants reduce eczema-associated symptoms, if synthesizing gold nanoparticles using the samples enhances the biological activity and whether the samples reduced the production of TNF-α and histamine. It was hypothesized that the selected South African plant extracts would reduce the production of TNF-α and histamine, which causes eczema-associated symptoms. Furthermore, it was hypothesized that the formation of nanoparticles would significantly enhance the biological activity of the samples.

The objectives of the study were to:

i. Synthesis and characterize gold nanoparticles (AuNPs) from *J. lomatophyllus*, *E. tectorum* and *B. frutescens* extracts using gold (III) chloride trihydrate.

ii. Ferment the extracts of *J. lomatophyllus* and *E. tectorum* using *Bifidobacterium bifidum*.
iii. Identify potential volatile compounds using gas chromatography-mass spectrometry (GC-MS) in *J. lomatophyllus*.
iv. Determine whether the ethanolic extract, most active partition and synthesized AuNP's of *J. lomatophyllus* reduce the production of TNF-α, which initiates post-inflammatory hyperpigmentation when overexpressed.
v. Determine whether the crude and synthesized AuNP of *E. tectorum* and *B. frutescens* inhibit the production of histamine, which contributes to the formation of wrinkles and skin damage

1.3) Structure of thesis

The format of four of the six chapters has been prepared for publication as a book chapter and research articles in peer-reviewed journals.

Chapter 2

Provided a review of the two main hypotheses associated with the cause of eczema and elaborates on eight South African indigenous plants that have been traditionally used to treat the condition. Furthermore, this chapter includes plant compounds that have been shown to reduce symptoms associated with eczema including the overproduction of TNF-α and nuclear factor kappa beta (NF-κB).

Chapter 3

This chapter investigated the effect of *Juncus lomatophyllus* Spreng. on symptoms associated with the inside-out hypothesis. Adverse effects caused by the overproduction of TNF-α include post-inflammatory hyperpigmentation. which is due to the over-expression of tyrosinase. Furthermore, this chapter evaluates whether the biological activity of the ethanolic extract was enhanced when fermented or used to synthesize gold nanoparticles. Lastly, due to limited information that could be found on this species, bioassay-guided fractionation was conducted and potential volatile compounds were identified.

Chapter 4

This chapter evaluated the effect of *Elegia tectorum* (L. f.) Moline & H. P. Linder on symptoms associated with the outside-in hypothesis, which included wrinkle formation due to the over-

expression of elastase caused by the increased levels of histamine. Moreover, the effect of fermenting and synthesizing gold nanoparticles using the ethanolic extract was investigated.

Chapter 5

This chapter evaluated the wound healing properties of five extracts prepared from *Bulbine frutescens* (L.) Willd. and whether synthesizing gold nanoparticles using these extracts would enhance the activity. Furthermore, this chapter investigated whether *B. frutescens* would reduce the production of histamine as increased levels causes the skin barrier to become damaged.

Chapter 6

This chapter provided an overview of the results that were obtained throughout the study and indicates future studies that could be conducted to support the above-mentioned findings.

References

Albrecht, K., M ler-Ladner, U., 2010. Side effects and management of side effects of methotrexate in rheumatoid arthritis. Clinical and Experimental Rheumatology-Incl Supplements 28 (5), S95.

Buddenkotte, J., Maurer, M., Steinhoff, M., 2010. Histamine and antihistamines in atopic dermatitis, *Histamine in Inflammation*. Springer, Boston, 73-80.

Chamlin, S.L., Kao, J., Frieden, I.J., Sheu, M.Y., Fowler, A.J., Fluhr, J.W., Williams, M.L., Elias, P.M., 2002. Ceramide-dominant barrier repair lipids alleviate childhood atopic dermatitis: changes in barrier function provide a sensitive indicator of disease activity. Journal of the American Academy of Dermatology 47 (2), 198-208. 10.1067/mjd.2002.124617

Gelmetti, C., Wollenberg, A., 2014. Atopic dermatitis–all you can do from the outside. British Journal of Dermatology 170 (1), 19-24. 10.1111/bjd.12957

Hengge, U.R., Ruzicka, T., Schwartz, R.A., Cork, M.J., 2006. Adverse effects of topical glucocorticosteroids. Journal of the American Academy of Dermatology 54 (1), 1-15.

Lee, H., Lee, S., 2014. Epidermal permeability barrier defects and barrier repair therapy in atopic dermatitis. Allergy, asthma & immunology research 6 (4), 276-287. 10.4168/aair.2014.6.4.276

Rezzani, R., 2004. Cyclosporine A and adverse effects on organs: histochemical studies. Progress in histochemistry and cytochemistry 39 (2), 85-128.

Chapter 2. Medicinal Plants for Eczema

Medicinal Plants for Eczema [1]

Graphical abstract

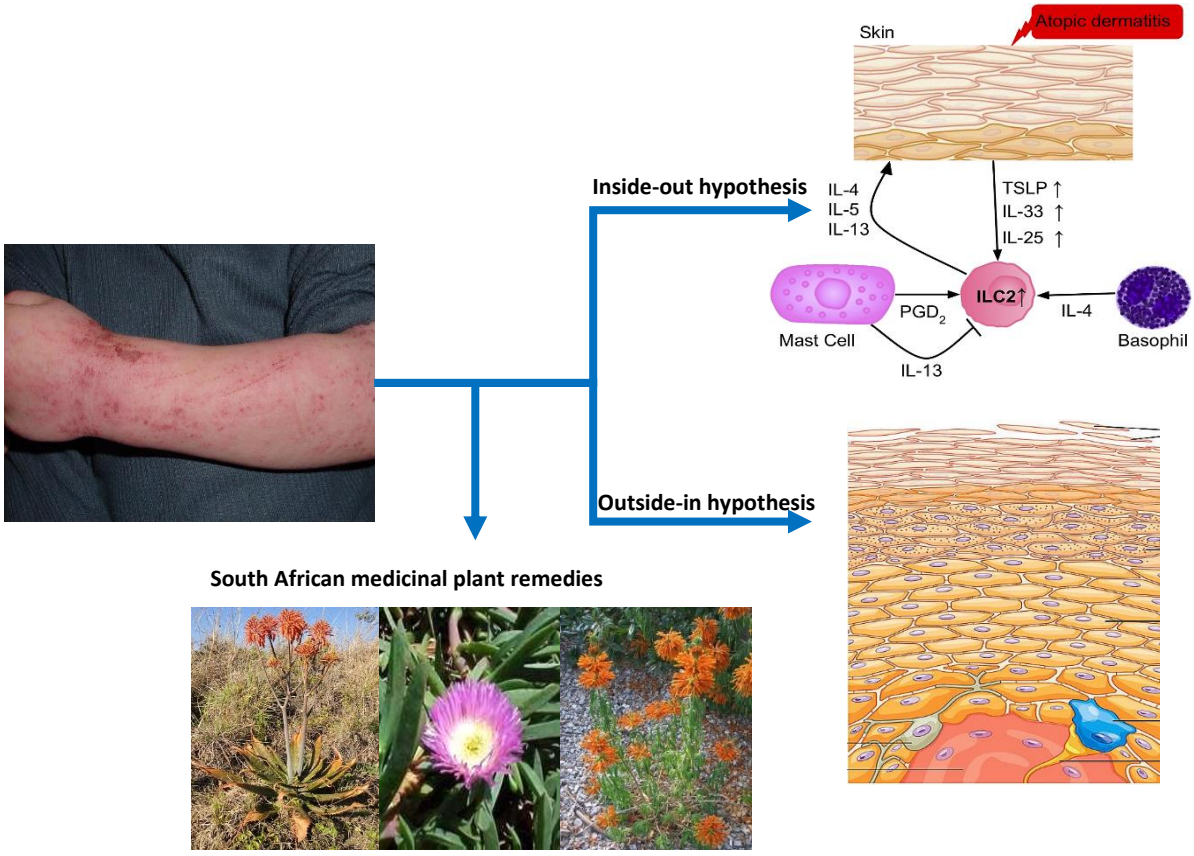

Abstract

Approximately, 15 to 20% of children and 1 to 3% of adults worldwide are affected with some form of eczema. As the exact cause of eczema has not been identified, different hypotheses have been proposed. These hypotheses include (i) the inside-out hypothesis, which states that the condition could be caused by an immunological defect allowing patients to become sensitive to immunoglobulin E (IgE) while (ii) the outside-in hypothesis concludes that eczema could be due to a disruption occurring in the skin barrier. Albeit, conventional medicine is used to reduce symptoms associated with the condition, alternative treatments are favored as they

[1] This chapter will be published by Taylor and Frances In: *Medicinal Plants in Cosmetics, Health and Disease* edited by Prof Namrita Lall (Accepted).

are used throughout the world and pose fewer adverse effects. An estimated 80–99% of the world's population use alternative medicine, most of which consist of medicinal plants used for primary health care. For this chapter, eight South African indigenous plants were selected that are traditionally used to treat eczema. Furthermore, plant compounds that have previously been shown to possess anti-eczematous properties in literature have been mentioned.

2.1) Introduction

Approximately 22.6 and 17.1% of children and adults are diagnosed with atopic dermatitis (AD) annually (Gelmetti and Wollenberg, 2014; Chamlin et al., 2002; Bylund et al., 2020). In 2017, a study was conducted in the United States, which indicated that approximately a quarter to one-third of the population suffers from some form of the condition with the most pronounced side effects including eczema eczematous lesions, epidermal barrier dysfunctions and immune dysregulations (Sullivan and Silverberg, 2017; Lee and Lee, 2014).

Though the condition is non-contagious, eczema can occur at any stage in one's life, is often hereditary and worsens over time (Akdis et al., 2006; Palmer et al., 2006). The exact cause of eczema has not been fully identified; however, different hypotheses have been developed. The two most accepted hypotheses are the inside-out and outside-in hypothesis (Brandt and Sivaprasad, 2011).

Medicinal plants have been and are currently used in numerous cultures around the world as a source of medicine. Though plants are primarily used as a food source, developed and developing countries are favoring the use of plants as an alternative to conventional medicines (Tadeg et al., 2005). In this chapter, each of the hypotheses was elaborated on and information on traditionally used South African plants was mentioned as well as bioactive compounds that reduce symptoms associated with the condition.

2.1.1) Inside-out hypothesis

The inside-out hypothesis states that atopic dermatitis is caused by an immunological defect, which alters the permeability of the skin allowing these patients to be sensitive to allergens (Brandt and Sivaprasad, 2011; Chamlin et al., 2002). The original model indicates that the condition is caused by an imbalance of T helper (Th) 1 and Th-2 lymphocytes, which stimulate cytokine production within the epidermal hyperplasia (Sullivan and Silverberg, 2017). Depending on the age and prevalence of the condition there are several subtypes, which include intrinsic and extrinsic subtypes (FIGURE 2.1) (Mansouri and Guttman-Yassky, 2015).

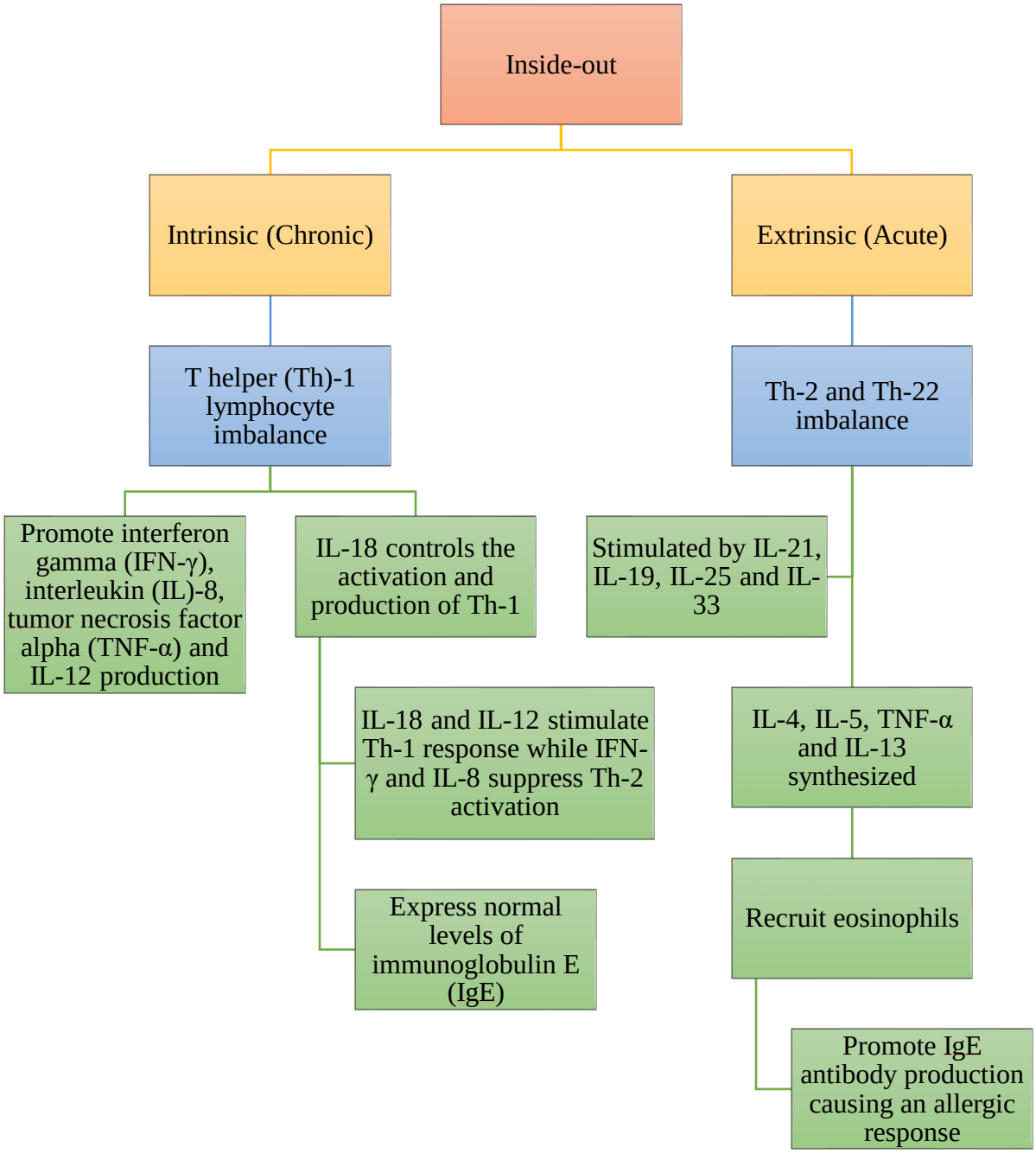

FIGURE 2.1.
Intrinsic and extrinsic pathways associated with the Inside-out hypothesis

The extrinsic subtype occurs in patients that experience acute atopic dermatitis commonly known as contact dermatitis (Mansouri and Guttman-Yassky, 2015). In these patients, Th-2 and Th-22 lymphocytes are imbalanced, which promotes the synthesis of interleukin 4 (IL-4), IL-5, tumor necrosis factor-alpha (TNF-α) and IL-13 and recruits eosinophils to the infected

site (Sullivan and Silverberg, 2017; Mansouri and Guttman-Yassky, 2015; Malajian and Guttman-Yassky, 2015; Nedoszytko et al., 2014). These cytokines promote immunoglobulin E (IgE) antibodies, which reduce extracellular pathogens and induce an allergic response (Sullivan and Silverberg, 2017).

In an earlier study conducted by Malajian and Guttman-Yassky (2015), it was found that IL-4 and IL-13 inhibited the production of IL-17, which is prominent within psoriasis patients while other authors have indicated that IL-4, IL-31 and TNF-α compromise the epidermal barrier function and reduce the expression of filaggrin and ceramide, which maintain the epidermal barrier (Gschwandtner et al., 2013; Malajian and Guttman-Yassky, 2015; Cornelissen et al., 2012; Howell et al., 2009; Kim et al., 2011; Hatano et al., 2005).

Other cytokines that are stimulated by Th-2 and Th-22 include IL-21, IL-19, IL-25 and IL-33, which induce the expression of IL-5 and IL-13, modulate Th-2 responses and recruit dendritic cells, basophils and eosinophils to the infected site (Brandt and Sivaprasad, 2011; Mansouri and Guttman-Yassky, 2015). In some cases, bacteria such as *Staphylococcus aureus* can trigger IgE antibody production due to the abnormal amount of bacterial colonization found in the infected sites. These bacteria present antigens or superantigens, which, once detected, cause the stimulation of the proteolytic activity of the immune system resulting in a cytokine storm (hypercytokinemia) that damages the skin barrier (Gelmetti and Wollenberg, 2014).

The intrinsic subtype occurs in patients that experience chronic atopic dermatitis. In these patients, Th-1 lymphocytes are imbalanced, which promotes the synthesis of interferon-gamma (IFN-γ), IL-8, TNF-α and IL-12 (Mansouri and Guttman-Yassky, 2015; Nedoszytko et al., 2014). Pro-inflammatory cytokines, such as IL-18, are used to control the activation of Th-1 and Th-2 lymphocytes' responses. During the acute stage, IL-18 increases the secretion of IL-4 and IL-13, thereby promoting IgE synthesis; however, during the chronic stage, IL-18 and

IL-12 stimulate the Th-1 response (Nedoszytko et al., 2014). Cytokines, such as IFN-γ and IL-8, suppress Th-2 lymphocyte activation and reduce intracellular pathogens (Sullivan and Silverberg, 2017). These patients express normal levels of IgE antibodies and synthesize other cytokines such as CCL20, IFN-alpha (IFN-α) and IL-1 beta (IL-1β) (Mansouri and Guttman-Yassky, 2015). This subtype causes patients to experience the condition throughout their lives or when exposed to stressful situations (Nedoszytko et al., 2014).

TNF-α is a pro-inflammatory cytokine, produced by macrophages, that modulates inflammation within the acute and chronic phases of eczema (FIGURE 2.2) (Song et al., 2008). When synthesized and released into the cytoplasm, TNF-α can bind to two receptors known as TNF-α receptor 1 (TNFR1) and TNFR2, which are found on cell membranes (FIGURE 2.2) (Palladino et al., 2003). During the synthesis of TNF-α, a pro-TNF trimer is cleaved from the cell membrane by the TNF-α converting enzyme (TACE) to form a mature TNF trimer that binds to the extracellular domain of TNFR1 (Palladino et al., 2003; Xu and Shi, 2007). This allows the release of the silencer of death (SOD) inhibitory from the intracellular domain. Thereafter, adaptor proteins, known as TNF-α receptor-associated death domain (TRADD), recruit TNFR-associated factor 2 (TRAF2) and receptor-interacting serine/ threonine kinase 1 (RIP1), forming a plasma membrane-bound complex known as Complex I (Xu and Shi, 2007).

Once Complex I has formed, inhibitors of nuclear factor kappa B (IκB) become phosphorylated and dissociate from nuclear factor kappa B (NF-κB) transcription factors. This allows NF-κB to become active and translocate into the nucleus (Miller et al., 2010). Inside the nucleus, NF-κB transcribes sections of the DNA that are required to activate the synthesis of cytokines and chemokines such as TNF-α, IL-1β, IL-6, IL-8 and IFN-γ (Palladino et al., 2003). If IκB is unable to dissociate from NF-κB, the TNFR1 intracellular domain, known as the death domain, recruits a cytoplasmic complex, Complex II, which is comprised of RIP1 or TRADD and fas-

associated protein with death domain (FADD). Once formed, FADD recruits caspase 8 or 10 that are activated upon self-cleavage and cause a protease cascade, which results in apoptosis (Xu and Shi, 2007). To prevent this, active NF-κB transcribes inhibitors of apoptosis proteins (IAP) such as X-chromosome-linked IAP (XIAP), which bind to and inhibit active caspases (Van Antwerp et al., 1998).

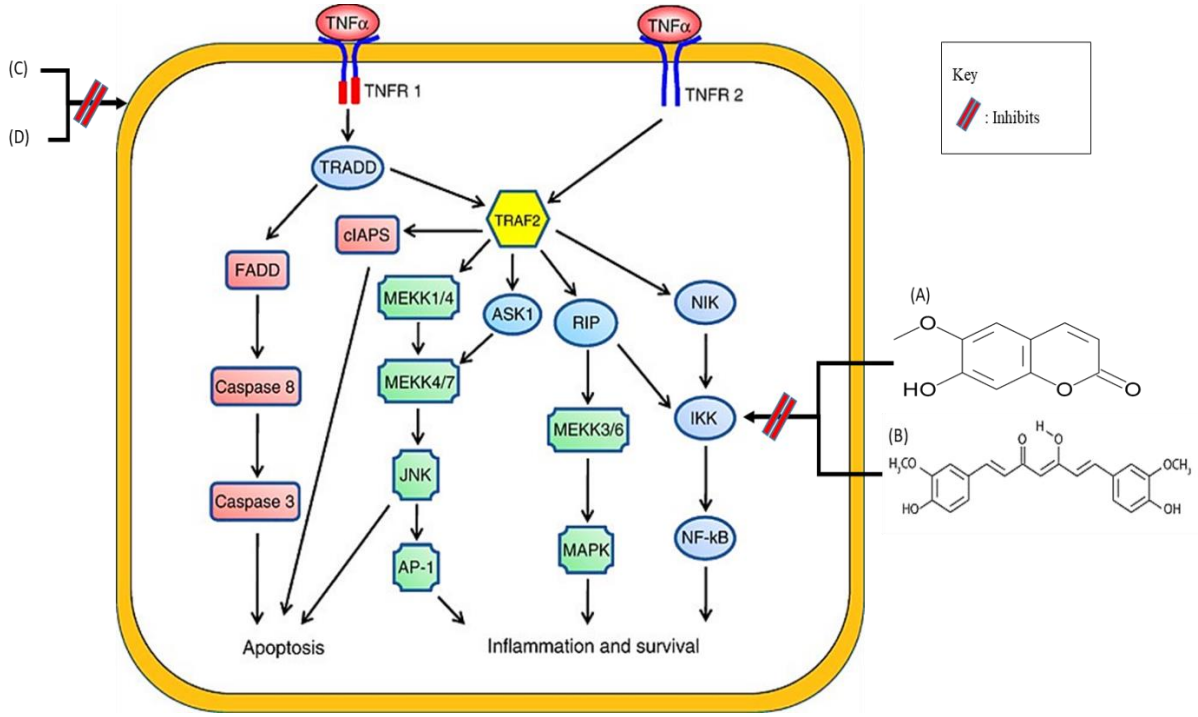

FIGURE 2.2.
Tumor necrosis factor-alpha (TNF-α) pathway. A, Scopoletin; B, Curcumin; C, Magnosalin; D, Andamanicin. Adapted from (Wu and Zhou, 2010; Chrumps, 2010; Biophysik, 2008)

2.1.2) Outside-in hypothesis

The outside-in hypothesis, commonly known as the hygiene hypothesis, is based on the condition occurring due to a disruption within the skin barrier (Brandt and Sivaprasad, 2011). The skin is an interface between the organism's body and the environment, providing protection and support. The primary mediator of the epidermal barrier is the stratum corneum (FIGURE 2.3) (Lee and Lee, 2014). The stratum corneum is comprised of corneocytes, which

secrete intercellular or intracellular substances such as filaggrin (Sullivan and Silverberg, 2017).

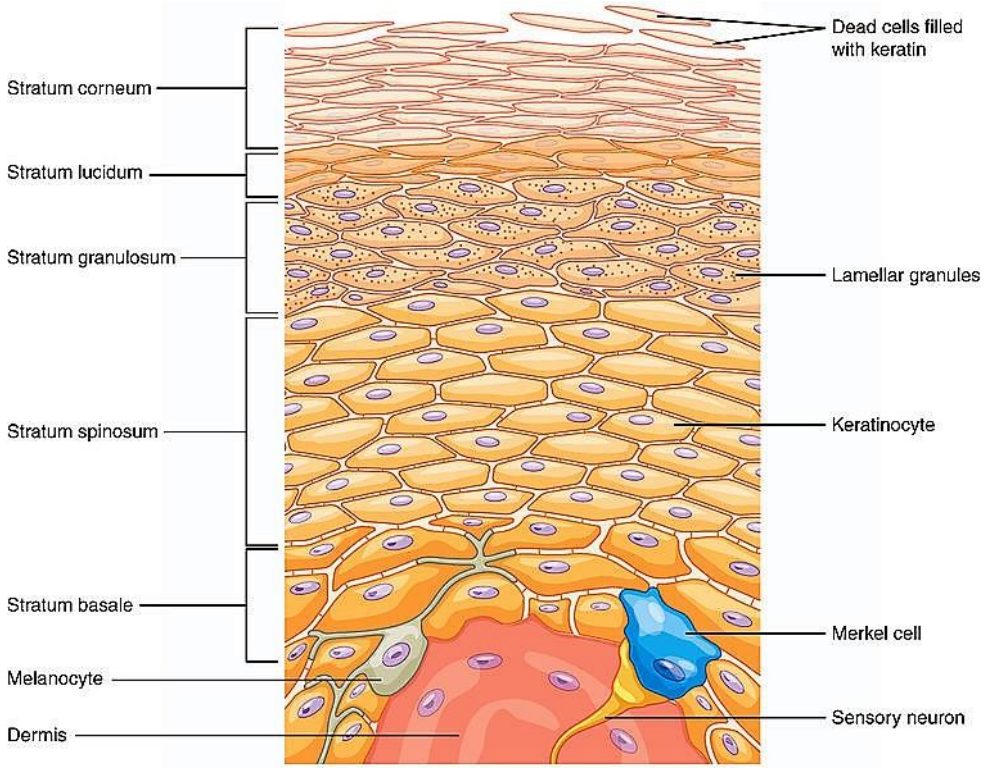

FIGURE 2.3.
Different layers of the epidermis (OpenStax College, 2013)

These intercellular or intracellular substances degrade amino acids such as urocanic acid, pyrrolidone carboxylic acid, alanine, glutamine, arginine and histidine, and lipids such as ceramide 1, fatty acids and cholesterol responsible for creating the barrier layer and maintaining its integrity (Sullivan and Silverberg, 2017; Lee and Lee, 2014; Varothai, Nitayavardhana, and Kulthanan, 2013). Below the stratum corneum are keratinocyte membranes that contain tight junctions. These junctions form an additional barrier that protects the organism from the environment when the stratum corneum is dysfunctional. However, in eczema patients, the expression of claudins is downregulated causing these tight junctions to become dysfunctional (Malajian and Guttman-Yassky, 2015).

The degradation of amino acids maintains hydration within the epidermis and reduces the pH of the skin to between 4.7 and 5.75 (Gelmetti and Wollenberg, 2014; Lee and Lee, 2014). This low skin pH maintains the epidermal barrier homeostasis and ensures that the stratum corneum is intact, ceramide metabolism is activated and the serine protease cascade is modulated (Lee and Lee, 2014). In eczema patients, the skin pH is slightly higher than normal (pH 6), which causes lipid processing enzymes, such as beta-glucocerebrosidase (β-GlcCer'ase), acidic sphingomyelinase (aSMase) and phospholipase A2 (sPLA2), to be inhibited and stimulates the production of serine proteases (Gelmetti and Wollenberg, 2014; Lee and Lee, 2014). This increase in serine proteases downregulates the secretion of lamellar bodies, inhibits protective resident bacterial flora on the skin and causes barrier dysfunction (Gelmetti and Wollenberg, 2014).

Furthermore, a dysfunctional skin barrier can be caused by several genetic mutations that impair the function of genes required to maintain structural integrity (Elias and Wakefield, 2014). This includes the missense and nonsense mutations of *TMEM79*, which leads to skin lesions and inflammation (Voisin and Chiu, 2018). Another mutation linked to atopic dermatitis is the overexpression of the small proline-rich protein 3 (*SPRR3*) gene due to a 24 base pair defect and an in-frame insertion and deletion (Elias and Wakefield, 2014).

The basis of this theory is the loss-of-function mutation within the filaggrin (*FLG*) gene, which further impairs the barrier function (Sullivan and Silverberg, 2017). Studies have shown that patients with these mutations have a higher chance of developing atopic dermatitis than those who do not, by a third to a fifth (Langan, Irvine, and Weidinger, 2020). The filaggrin gene is located on chromosome 1q21 and translates into a polyprotein known as profilaggrin, which is the main component of keratohyalin granules (Lee and Lee, 2014; Palmer et al., 2006). These profilaggrins are comprised of calcium-binding N-terminal domain and are dephosphorylated

and cleaved into 10-12 filaggrin monomers that contribute to the strength and integrity of the epidermis (Lee and Lee, 2014; Brown and McLean, 2012).

When these monomers aggregate, the keratin cytoskeleton forms a protein-lipid matrix, which maintains epidermal hydration (Voisin and Chiu, 2018). In eczema patients who have an impaired barrier function, there is an increase in transepidermal water loss and a decrease in water-binding capacity, which manifests as dry skin (Sullivan and Silverberg, 2017; Lee and Lee, 2014). This is due to the low ratio of intercellular lipids, an imbalance of protease and anti-protease present within the stratum corneum and an increase in cystatin A production, which leads to the degradation of the corneodesmosome (Gelmetti and Wollenberg, 2014).

In eczema patients, there is an increase in histamine production, which leads to an intolerable itching sensation (Buddenkotte, Maurer, and Steinhoff, 2010). This biogenic amine is synthesized during the decarboxylation of histidine when this amino acid is exposed to histidine decarboxylase (1-histidine decarboxylase, EC 4.1.1.22) (Castells, 2006; Abe et al., 1993). Once synthesized, the histamine is stored in secretory granules within mature mast cells and basophils along with other mediators such as proteoglycan heparin and chondroitin sulfate E (Castells, 2006; Abe et al., 1993; Hogan and Schwartz, 1997). This causes a large number of mast cells to be present within the skin, that express NF-κB related genes and Th-2 cytokines when exposed to an allergen (Jensen, Falkencrone, and Skov, 2014). However, these allergens release histamine into the extracellular space during a process known as degranulation (Abe et al., 1993; Hogan and Schwartz, 1997). Some of the histamines are metabolized via two alternative pathways (Abe et al., 1993). One of the pathways involves a catalyst known as histamine N-methyltransferase (EC 2.1.1.8), while the other involves a catalyst known as diamine oxidase (EC 1.4.3.6) (Castells, 2006; Abe et al., 1993).

Increased levels of histamine can affect the expression of genes associated with maintaining the epidermal barrier, which includes filaggrin, keratins and proteases. In response to this, filaggrin levels are reduced and the mRNA expression of some keratins is downregulated (Gschwandtner et al., 2013; Gutowska-Owsiak et al., 2014). However, the expression of proteases such as cathepsins and elastase are increased which contributes to the inflammatory response and the dry effect that occurs around eczematous skin lesions (Agrawal and Woodfolk, 2014; Voegeli et al., 2009). These proteases cause the pH of the skin to increase, which enhances their effect on the inflammatory system and the epidermal barrier (Gelmetti and Wollenberg, 2014). Elastase is mainly used to remove foreign proteins during wound healing, however, when overexpressed these proteases degrade elastin, which leads to wrinkle formation (Thring, Hili, and Naughton, 2009).

2.2) South African medicinal plants used to treat eczema

In South Africa, traditional healers use various indigenous plants to treat patients that suffer from eczema (TABLE 2.1) (Mabona and Van Vuuren, 2013). Of these, eight indigenous plants were selected based on the amount of information available on how they are prepared and used to treat eczema were described below. This was done to promote the use of plants as an alternative to conventional medicine.

TABLE 2.1
Traditional methods using South African plants to treat eczema

SOUTH AFRICAN MEDICINAL PLANTS	PLANT PARTS	TRADITIONAL METHODS USED	REFERENCES
Aloe greatheadii Schonland	The sap of the leaves	Applied topically to the infected areas	(Fern, 2019; Lall and Kishore, 2014)
Aspalathus linearis (Burm f.) R. Dahlgren	Shoots from the stems	Cut into smaller pieces, bruised and left to dry. After fermentation, the plants are brewed at low	(Joubert and de Beer, 2011; Joubert et al., 2008)

		temperatures and then applied topically to infected areas	
Carpobrotus edulis (L.) L. Bolus	The juice and pulp from the leaves	Applied topically to the infected areas	(Deutschländer, Lall, and Van De Venter, 2009; Lall and Kishore, 2014)
Harpephyllum caffrum Bernh ex. Krauss	The bark of the tree	Applied topically to infected areas	(Lall and Kishore, 2014)
Leonotis leonurus (L.) R. Br.	Leaves and stems	Infusions and decoctions are applied externally to infected areas	(El-Ansari et al., 2009)
Trichilia emetica Vahl	Roots, leaves and fruits	Leaves and roots are made into a poultice and applied externally. The roots are made into a powder and mixed with potassium hydroxide in water	(Lall and Kishore, 2014; Komane, Olivier, and Viljoen, 2011)
Olea europaea L. subsp. *africana* (mill.) P. S. Green	Bark, leaves and oils from the seeds	Bark decoctions and leaf infusions are used topically and internally to treat different types of dermatitis and inflammation. The oils are applied topically to treat hand, contact and atopic dermatitis.	(Lall and Kishore, 2014; Long, Tilney, and Van Wyk, 2010; Hashmi et al., 2015)
Pelargonium graveolens L. 'Hér	Oils from the seeds and leaves	The leaves are applied directly onto infected areas while the oils are used topically.	(Lall and Kishore, 2014; Saraswathi et al., 2011)

2.2.1) *Aloe greatheadii* Schonland

Aloe greatheadii Schonland (FIGURE 2.4.1), commonly known as the spotted aloe, is part of the Aloacea family and is an important indigenous plant (Lall and Kishore, 2014; Human and Nicolson, 2006). This plant is widespread throughout South Africa and is used in winter as a food source to increase the bee population within Pretoria (Human and Nicolson, 2006). Though these bees favor this plant, they become aggressive when exclusively bred on

A. greatheadii (Grace et al., 2009). This evergreen succulent is harvested mainly for food and its medicinal properties (Fern, 2019).

FIGURE 2.4.
Plants that are traditionally used against eczema. 1) *Aloe greatheadii*, 2) *Aspalathus linearis*, 3) *Carpobrotus edulis*, 4) *Harpephyllum caffrum*, 5) *Leonotis leonurus*, 6) *Trichilia emetic*, 7) *Olea europaea* subsp. *africana*, 8) *Pelargonium graveolens* (DerHexer, 2010; JMK, 2012; Bruenken, 2005; JoJan, 2005; Richfield, 2011; Giraud, 2011; Hectonichus, 2018; BotBln, 2010)

The sap of the leaves is used as eye drops for chronic conjunctivitis and applied topically for skin cancer, arthritis, and skin irritation (Lall and Kishore, 2014; Fern, 2019). However, adverse side effects of the sap include congestion and irritation when consumed and if used for a prolonged time may cause colorectal cancer. The leaves are made into infusions and decoctions to treat gonorrhea and purgatives to treat other diseases (Fern, 2019).

2.2.2) *Aspalathus linearis* (Burm f.) R. Dahlgren

Aspalathus linearis (Burm f.) R. Dahlgren (FIGURE 2.4.2), commonly known as rooibos, is part of the Fabaceae family and is natively found in the Cedarberg Mountains in the Western Cape Province (Lall and Kishore, 2014; McKay and Blumberg, 2007). This shrub-like leguminous bush is used worldwide as a beverage and for its medicinal properties (McKay and Blumberg, 2007).

In some cultures, the shoots are cut into smaller pieces that are bruised with a hammer and pasteurized using steam. The steam prevents microbes from entering and contaminating the plant material. Afterward, the plants are left to dry and made into infusions (Joubert and de Beer, 2011). These infusions are red, however, if the fermentation step is skipped and plant material is dried then the infusions are green in color (McKay and Blumberg, 2007). By drying the leaves before fermentation, the moisture content is reduced to prevent oxidation from occurring, which allows the leaves to retain their green coloration (Joubert and Schultz, 2012).

The Khoisans chop the shoots with an ax and crush the material with a mallet. The bruised sections are placed inside a hollow stone reef to allow fermentation to occur. Afterward, the plants are dried and boiled in hot water. Once brewed, the concentration of the infusion can be altered by adding water or shoots depending on the condition (Joubert et al., 2008).

2.2.3) *Carpobrotus edulis* (L.) L. Bolus

Carpobrotus edulis (L.) L. Bolus (FIGURE 2.4.3), commonly known as sour fig, is part of the Aizoaceae family and is native to South Africa, however, invades numerous coastal areas (Lall and Kishore, 2014; Mudimba and Nguta, 2019). These plants mainly inhabit sandy coastal areas, however, have been found within sandy and marshy inland areas. The fruit, leaves and flowers are traditionally used for various ailments depending on the preparation method used (Mudimba and Nguta, 2019).

To treat bacterial and fungal infections, the leaves, fruit or flowers are chewed raw or boiled in water. The boiled leaves are used for tuberculosis and other respiratory diseases (Mudimba and Nguta, 2019). The juice from the leaves is gargled for throat infections, however, when taken orally can be used as a diuretic and a styptic, while the juice from the fruit is often gargled to treat throat and mouth infections (Deutschländer, Lall, and Van De Venter, 2009). When applied topically, the leaf juice and leaf pulp are used to treat burns, wounds and infections (Lall and Kishore, 2014; Deutschländer, Lall, and Van De Venter, 2009).

2.2.4) *Harpephyllum caffrum* Bernh. ex Krauss

Harpephyllum caffrum Bernh. ex Krauss (FIGURE 2.4.4), commonly known as the wild plum, is part of the Anacardiaceae family, which is the largest tree family in South Africa (Lall and Kishore, 2014; Chinyama, 2009). The bark of this evergreen tree is applied topically for acne and made into decoctions to be used as a blood purifier and emetic (Lall and Kishore, 2014; Chinyama, 2009; Maroyi, 2019). The fruit is consumed and made into marketable products such as jams, jellies, and non-alcoholic and alcoholic beverages (Chinyama, 2009; Maroyi, 2019). However, the fruit can be applied topically to treat wounds and sprains (Maroyi, 2019).

2.2.5) *Leonotis leonurus* (L.) R. Br.

Leonotis leonurus (L.) R. Br. (FIGURE 2.4.5), commonly known as wild dagga, is part of the Lamiaceae family and is found throughout South Africa (Lall and Kishore, 2014; Nsuala et al., 2017). These broadleaf evergreen woody shrubs are drought tolerant and are found nearby riverbanks and rocky hillsides (Nsuala et al., 2017; Nsuala, Enslin, and Viljoen, 2015). For many years, different sections of the plant have been used traditionally for numerous ailments. Leaf decoctions involve chopping leaves into small pieces and boiling them in water for an extended time. Once cooled and strained these decoctions are applied topically and taken orally (Nsuala, Enslin, and Viljoen, 2015). Oral decoctions are used against coughs, colds, headaches,

diarrhea and diabetes, while topical decoctions treat boils, muscular pains and reduce itching (Nsuala, Enslin, and Viljoen, 2015; El-Ansari et al., 2009).

The leaves are sometimes dried and crushed into a powder and applied topically as an ointment to relieve pain. Stems and seeds are made into a powder and boiled with water to make decoctions before being used orally to treat hemorrhoids or topically for sores. Finally, the flowers are made into a purgative or a tonic to treat tuberculosis, influenza and sores (Nsuala, Enslin, and Viljoen, 2015).

2.2.6) *Trichilia emetica* Vahl.

Trichilia emetica Vahl. (FIGURE 2.4.6), commonly-known as Natal mahogany, is part of the Meliaceae family that is mainly located within tropical and subtropical regions, however, has been found within the savanna region of South Africa (Lall and Kishore, 2014; Diallo et al., 2003). This widespread small tree is used throughout Africa for its medicinal uses (Diallo et al., 2003; Komane, Olivier, and Viljoen, 2011).

The leaves are made into a poultice to soothe bruises and decoctions are taken orally for coughs and headaches (Lall and Kishore, 2014; Komane, Olivier, and Viljoen, 2011). However, in Nigeria, leaf poultices are used topically to treat syphilis (Komane, Olivier, and Viljoen, 2011). To treat fevers and coughs, the bark of the tree is dried up and crushed into a powder (Diallo et al., 2003). The Xhosa tribe uses bark decoctions to treat kidney disorders and anemia, whereas, the Zulu tribe uses this decoction against stomach ailments and backaches (Komane, Olivier, and Viljoen, 2011).

Powdered roots are used as a poison antidote when mixed with milk and for asthma when mixed with honey (Diallo et al., 2003). When combined with potassium hydroxide and water,

these powdered roots are used to reduce inflammation. Lastly, roasted roots that have been crushed into a powder are used topically to heal wounds (Komane, Olivier, and Viljoen, 2011).

2.2.7) *Oleo europaea* L. subsp. *africana* (Mill.) P. S. Green

Olea europaea L. subsp. *africana* (Mill.) P. S. Green (FIGURE 2.4.7), commonly known as the olive tree, is part of the Oleaceae family and is mainly found within the eastern regions of Africa and extends towards the Southern tip of Africa (Lall and Kishore, 2014; Cuneo and Leishman, 2006). This small evergreen tree is found in woodland and mountain habitats and has a distinctive purple-black fruit color (Cuneo and Leishman, 2006). *Olea europaea* is one of the oldest cultivated trees dating back to around 7000 years ago. These plants were mainly cultivated for commercial purposes, however, the oils are known for their medicinal properties (Hashmi et al., 2015).

To treat diabetes, diarrhea, urinary tract infections and hypertension, the leaves are made into decoctions and taken orally, while infusions are used to treat hypotension, eye lotion, sore throat, inflammation and hypoglycemia (Hashmi et al., 2015; Long, Tilney, and Van Wyk, 2010). The bark of the tree is used to treat colic when made into infusions, while decoctions are used to reduce rashes and itching (Long, Tilney, and Van Wyk, 2010). The oil obtained from the seeds is used as a laxative when taken orally, while oils obtained from the fruit are applied on fractured limbs (Hashmi et al., 2015).

2.2.8) *Pelargonium graveolens* L 'Hér

Pelargonium graveolens L 'Hér (FIGURE 2.4.8), commonly known as rose-scented pelargonium, is part of the Geraniaceae family and is indigenous to South Africa, however, was introduced to other parts of the world, including Europe (Lall and Kishore, 2014; Asgarpanah and Ramezanloo, 2015). This aromatic perennial shrub is found in moist habitats

and the oils are used commercially as a substitute for rose perfume in the cosmetic and aromatherapy industry (Asgarpanah and Ramezanloo, 2015; Lawrence, 2002).

Traditionally, the oils are used to treat acne, while fresh leaves are used topically to reduce skin diseases, rashes and ulcers (Lall and Kishore, 2014; Saraswathi et al., 2011). The roots are made into decoctions and are used to treat malaria and urinary disorders. Infusions and decoctions of the leaves and stems are used topically for wound healing and used orally for syphilis, duodenal ulcers, shingles and herpes (Asgarpanah and Ramezanloo, 2015; Saraswathi et al., 2011).

2.3) Plant compounds that reduce eczema

Plants contain secondary metabolites that can be used to reduce specific symptoms of eczema, such as inflammation, intolerable itching, the formation of wrinkles and hyperpigmentation. Though there are clinical treatments available that are used to reduce symptoms associated with eczema, such as inflammation caused by the overexpression of TNF-α and NF-κB production, these treatments are mainly used against other conditions such as rheumatoid arthritis, cancer and psoriasis (Song et al., 2008; Miller et al., 2010; Parameswaran and Patial, 2010; Bradley, 2008; Serasanambati and Chilakapati, 2016). Below are some plant compounds that can be used to reduce either the internal aspects of the condition, such as the overexpression of cytokines and transcription factors, or physical aspects such as rashes, dry skin and itching sensation.

2.3.1)Tumor necrosis factor alpha (TNF-α) production

Some plant-based compounds that are used to reduce TNF-α production include scopoletin, curcumin, magnosalin and andamanicin (FIGURE 2.2). Scopoletin (FIGURE 2.2 A), isolated from aqueous extracts of *Artemisia feddie* H. Lev. & Vaniot and prevents the release of TNF-

α, while curcumin (FIGURE 2.2 B), derived from the rhizomes of *Curcurma longa* L., inhibits the production of pro-inflammatory cytokines in lipopolysaccharide (LPS) induced macrophages (Paul, Gohil, and Bhutani, 2006). Both of these compounds target the IκB cascade by inhibiting the activation of NF-κB (Moon et al., 2007; Kahkhaie et al., 2019). Magnosalin and andamanicin (FIGURE 2.2 C and D), isolated from the leaves of *Perilla frutescens* (L.) Britton was suggested to reduce TNF-α in L929 cells at a concentration of 10 μM (Paul, Gohil, and Bhutani, 2006).

2.3.2)Nuclear factor kappa beta (NF-κB) production

Compounds that are used to modulate NF-κB activity include kamebakaurin, acanthoic acid, isohelenin and parthenolide. Both kamebakaurin, isolated from *Isodon japonicus* (Burm. f.) H. Hara and acanthoci acid, derived from *Acanthopanax koreanum* Nakai have been shown to interfere with the NF-κB activation cascade. While isohelenin, isolated from *Arnica montana* L., prevents IκB degradation by alkylating the p69 subunit of NF-κB and parthenolide, derived from *Tanacetum parthenium* (L.) Sch. Bip., binds to and inhibits I kappa B kinase beta (IKK-β) (Palladino et al., 2003).

2.3.3)Physical aspects

Several compounds have been used to reduce common symptoms associated with eczema (TABLE 2.2). This includes the itching sensation, rash formation and dry skin. Some of the compounds are used to reduce *Staphylococcus aureus* formation on eczematous lesions, which are thought to promote the formation of these lesions (Arima et al., 2003).

TABLE 2.2
Plant metabolites and compounds that are used to reduce common side effects associated with eczema

MEDICINAL PLANTS	FAMILY	PLANT PART	SECONDARY METABOLITES AND COMPOUNDS	GEOGRAPHICAL LOCATION	REFERENCES
Albizia adianthifolia (Schumach.) W. Wight	Fabaceae	Bark, leaves and stem roots	Anthraquinones, flavonoids, tannins, triterpenoids, sesquiterpene hydrocarbons, oxygenated sesquiterpenes and saponins	North Maputaland in South Africa and tropical areas of Africa	(Dlova and Ollengo, 2018; Maroyi, 2018)
Aloe ferox Mill.	Xanthorrhoeaceae	Leaves and the roots	Chrysophanol, aloe-emodin, aloin a, aloesin, aloenin and aloeresin a	Eastern Cape and cape coastal areas in South Africa	(Dlova and Ollengo, 2018; Chen et al., 2012)
Dysphania ambrosioides (L.) Mosyakin & Clements	Amaranthaceae	Leaves	Chenopodiumamine a, b and c	Eastern Cape in South Africa	(Dlova and Ollengo, 2018; Song et al., 2015)
Momordica balsamina L.	Cucubitaceae	Leaves	Anthraquinones, flavonoids, tannins and saponins	North Maputaland in South Africa, Namibia and Botswana	(Dlova and Ollengo, 2018; Thakur et al., 2009)
Portulacaria afra Jacq.	Portulacaceae	Leaves	Anthraquinones, flavonoids, tannins and saponins	North Maputaland, South Africa	(Dlova and Ollengo, 2018)
Chamaecyparis obtusa (Siebold & Zucc.) Endl.	Cupressaceae	Wood	B-thujaplicin, limonene, bornyl acetate and elemol	Native to Japan and Southern parts of Korea	(Arima et al., 2003; Joo et al., 2010)

2.4) Conclusion

Both the inside-out and outside-in hypotheses are considered viable theories related to the cause of eczema. Recently, more studies supported the outside-in hypothesis due to the discovery of the loss-of-function mutation within the filaggrin gene. However, there are aspects of the inside-out hypothesis that have not been explored before. For future recommendations, more studies should be focused on the inside-out hypothesis and using plants to reduce aspects within this hypothesis. This chapter promotes the advantages of bioactive compounds that possess anti-eczematous properties. Moreover, this study concluded that numerous plants contain compounds that can be used to reduces various aspects of the condition. Further investigation into plant compounds that reduce NF-κB and TNF-α as a potential candidate for in vivo trials should be considered. Furthermore, this chapter promotes the need to analyze indigenous plants for anti-eczematous properties using the same method of extraction as traditional healers.

References

Abe, Y, S Ogino, M Irifune, *et al.* 1993. "Histamine content, synthesis and degradation in human nasal mucosa." *Clinical & Experimental Allergy* 23, 2: 132-136. doi: 10.1111/j.1365-2222.1993.tb00308.x.

Agrawal, Rachana, and Judith A Woodfolk. 2014. "Skin barrier defects in atopic dermatitis." *Current allergy and asthma reports* 14, 5: 1-11. doi: 10.1007/s11882-014-0433-9.

Akdis, C. A., M. Akdis, T. Bieber, *et al.* 2006. "Diagnosis and treatment of atopic dermatitis in children and adults: European Academy of Allergology and Clinical Immunology/American Academy of Allergy, Asthma and Immunology/PRACTALL Consensus Report." *The Journal of Allergy and Clinical Immunology* 118, 1: 152-169. doi: https://doi.org/10.1111/j.1398-9995.2006.01153.x.

Arima, Yaeno, Yoriko Nakai, Ritsuko Hayakawa, and Takeshi Nishino. 2003. "Antibacterial effect of β-thujaplicin on *Staphylococci* isolated from atopic dermatitis: relationship between changes in the number of viable bacterial cells and clinical improvement in an eczematous lesion of atopic dermatitis." *Journal of antimicrobial Chemotherapy* 51, 1: 113-122. doi: 10.1093/jac/dkg037.

Asgarpanah, J., and F. Ramezanloo. 2015. "An overview on phytopharmacology of *Pelargonium graveolens* L." *Indian Journal of Traditional Knowledge* 14, 4: 558-563.

Biophysik. 2008. "Curcumin-enol.png." Obtained from Wikimedia under the Public Domain License. https://commons.wikimedia.org/wiki/File:Curcumin-enol.png (Accessed 20 March 2021).

BotBln. 2010. "*Olea europaea africana.* ." Obtained from Wikimedia under a Creative Common Attribution-Share Alike 3.0 Unported license https://commons.wikimedia.org/wiki/File:Olea_europaea_africana_KirstenboshBotGard09292010C.JPG (Accessed 8 June 2020).

Bradley, JR. 2008. "TNF-mediated inflammatory disease." *The Journal of Pathology: A Journal of the Pathological Society of Great Britain and Ireland* 214, 2: 149-160. doi: 10.1002/path.2287.

Brandt, E. B., and U. Sivaprasad. 2011. "Th2 Cytokines and Atopic Dermatitis." *Journal of clinical & cellular immunology* 2, 3: 1-25. doi: 10.4172/2155-9899.1000110.

Brown, S. J., and W. H. I. McLean. 2012. "One remarkable molecule: filaggrin." *Journal of Investigative Dermatology* 132, 3: 751-762. doi: 10.1038/jid.2011.393.

Bruenken, W. . 2005. "Rooibos (*Aspalathus linearis*)." Obtained from Wikimedia under a Creative Common Attribution-Share Alike 2.5 Generic license https://commons.wikimedia.org/wiki/File:Rooibos_(Aspalathus_linearis).jpg (Accessed 8 June 2020).

Buddenkotte, Jörg, Marcus Maurer, and Martin Steinhoff. 2010. "Histamine and antihistamines in atopic dermatitis." In *Histamine in Inflammation*, 73-80. Boston: Springer doi: 10.1007/978-1-4419-8056-4_8.

Bylund, Simon, Laura B von Kobyletzki, Marika Svalstedt, and Åke Svensson. 2020. "Prevalence and Incidence of Atopic Dermatitis: A Systematic Review." *Acta dermato-venereologica* 100: 320-329. doi: 10.2340/00015555-3510.

Castells, Mariana. 2006. "Mast cell mediators in allergic inflammation and mastocytosis." *Immunology and Allergy Clinics* 26, 3: 465-485. doi: 10.1016/j.iac.2006.05.005.

Chamlin, S. L., J. Kao, I. J. Frieden, *et al.* 2002. "Ceramide-dominant barrier repair lipids alleviate childhood atopic dermatitis: changes in barrier function provide a sensitive indicator of disease activity." *Journal of the American Academy of Dermatology* 47, 2: 198-208. doi: 10.1067/mjd.2002.124617.

Chen, Weiyang, Ben-Erik Van Wyk, Ilze Vermaak, and Alvaro M Viljoen. 2012. "Cape aloes—A review of the phytochemistry, pharmacology and commercialisation of *Aloe ferox*." *Phytochemistry Letters* 5, 1: 1-12. doi: 10.1016/j.phytol.2011.09.001.

Chinyama, R. F. 2009. "Biological activities of medicinal plants traditionally used to treat septicaemia in the Eastern Cape, South Africa." Masters, Biomedical Technology, Nelson Mandela Metropolitan University.

Chrumps. 2010. "Scopoletin.png." Obtained from Wikimedia under the Public Domain License. https://commons.wikimedia.org/wiki/File:Scopoletin.png (Accessed 20 March 2021).

Cornelissen, C., Y. Marquardt, K. Czaja, *et al.* 2012. "IL-31 regulates differentiation and filaggrin expression in human organotypic skin models." *Journal of allergy and clinical immunology* 129, 2: 426-433.

Cuneo, P., and M. R. Leishman. 2006. "African Olive (*Olea europaea* subsp. *cuspidata*) as an environmental weed in eastern Australia: a review." *Cunninghamia* 9, 4: 545-577.

DerHexer. 2010. "*Pelargonium graveolens.*" Obtained from Wikimedia under a Creative Common Attribution-Share Alike 3.0 Unported license https://commons.wikimedia.org/wiki/File:Pelargonium_graveolens_in_Hel.jpg (Accessed 8 June 2020).

Deutschländer, M. S., N. Lall, and M. Van De Venter. 2009. "Plant species used in the treatment of diabetes by South African traditional healers: An inventory." *Pharmaceutical Biology* 47, 4: 348-365. doi: 10.1080/13880200902752959.

Diallo, D., B. S. Paulsen, T. H. A. Liljebäck, and T. E. Michaelsen. 2003. "The malian medicinal plant *Trichilia emetica*; studies on polysaccharides with complement fixing

ability." *Journal of Ethnopharmacology* 84, 2: 279-287. doi: 10.1016/S0378-8741(02)00330-6.

Dlova, Ncoza C, and Moses A Ollengo. 2018. "Traditional and ethnobotanical dermatology practices in Africa." *Clinics in dermatology* 36, 3: 353-362. doi: 10.1016/j.clindermatol.2018.03.009.

El-Ansari, M. A., E. A. Aboutabl, A. R. H. Farrag, *et al.* 2009. "Phytochemical and pharmacological studies on *Leonotis leonurus.*" *Pharmaceutical biology* 47, 9: 894-902. doi: 10.1080/13880200902942428.

Elias, P. M., and J. S. Wakefield. 2014. "Mechanisms of abnormal lamellar body secretion and the dysfunctional skin barrier in patients with atopic dermatitis." *Journal of allergy and clinical immunology* 134, 4: 781-791. doi: 10.1016/j.jaci.2014.05.048.

Fern, K. 2019. "*Aloe greatheadii.*" www.tropical.theferns.info/viewtropical.php?id=Aloe+greatheadii (Accessed 14 June 2020).

Gelmetti, C., and A. Wollenberg. 2014. "Atopic dermatitis–all you can do from the outside." *British Journal of Dermatology* 170, 1: 19-24. doi: 10.1111/bjd.12957.

Giraud, G. 2011. "*Leonotis leonurus*." Obtained from Wikimedia under a Creative Commons Universal Public Domain Dedication license. https://commons.wikimedia.org/wiki/File:Leonotis_leonurus_03.jpg (Accessed 8 June 2020).

Grace, O. M., M. S. J. Simmonds, G. F. Smith, and A. E. van Wyk. 2009. "Documented utility and biocultural value of *Aloe* L. (Asphodelaceae): a review." *Economic Botany* 63, 2: 167-178. doi: 10.1007/s12231-009-9082-7.

Gschwandtner, M, M Mildner, V Mlitz, *et al.* 2013. "Histamine suppresses epidermal keratinocyte differentiation and impairs skin barrier function in a human skin model." *Allergy* 68, 1: 37-47. doi: 10.1111/all.12051.

Gutowska-Owsiak, D, L Greenwald, C Watson, *et al.* 2014. "The histamine-synthesizing enzyme histidine decarboxylase is upregulated by keratinocytes in atopic skin." *British Journal of Dermatology* 171, 4: 771-778. doi: 10.1111/bjd.13199.

Hashmi, M. A., A. Khan, M. Hanif, U. Farooq, and S. Perveen. 2015. "Traditional uses, phytochemistry, and pharmacology of *Olea europaea* (olive)." *Evidence-Based Complementary and Alternative Medicine* 2015: 1-30. doi: 10.1155/2015/541591.

Hatano, Y., H. Terashi, S. Arakawa, and K. Katagiri. 2005. "Interleukin-4 suppresses the enhancement of ceramide synthesis and cutaneous permeability barrier functions induced by tumor necrosis factor-α and interferon-γ in human epidermis." *Journal of investigative dermatology* 124, 4: 786-792. doi: 10.1111/j.0022-202X.2005.23651.x.

Hectonichus. 2018. "Meliaceae -*Trichilia emetica.*" Obtained from Wikimedia under a Creative Common Attribution-Share Alike 4.0 International license https://commons.wikimedia.org/wiki/File:Meliaceae-Trichilia_emetica_(Natal_Mahogany).JPG (Accessed 8 June 2020).

Hogan, Angela Duff, and Lawrence B Schwartz. 1997. "Markers of mast cell degranulation." *Methods* 13, 1: 43-52. doi: 10.1006/meth.1997.0494.

Howell, M. D., B. E. Kim, P. Gao, *et al.* 2009. "Cytokine modulation of atopic dermatitis filaggrin skin expression." *Journal of Allergy and Clinical Immunology* 124, 3: R7-R12. doi: 10.1016/j.jaci.2009.07.012.

Human, H., and S. W. Nicolson. 2006. "Nutritional content of fresh, bee-collected and stored pollen of *Aloe greatheadii* var. *davyana* (Asphodelaceae)." *Phytochemistry* 67, 14: 1486-1492. doi: 10.1016/j.phytochem.2006.05.023.

Jensen, Bettina M, Sidsel Falkencrone, and Per S Skov. 2014. "Measuring histamine and cytokine release from basophils and mast cells." In *Methods in Molecular Biology*,

edited by Bernhard F. Gibbs and Franco H. Falcone, 135-145. New York: Springer doi: 10.1007/978-1-4939-1173-8_10.

JMK. 2012. "*Aloe greatheadii* var *davyana*." Obtained from Wikimedia under a Creative Common Attribution-Share Alike 3.0 Unported license https://commons.wikimedia.org/wiki/File:Aloe_greatheadii_var_davyana,_habitus,_Louwsburg.jpg (Accessed 8 June 2020).

JoJan. 2005. "*Carpobrotus edulis*01.jpg." Obtained from Wikimedia under a public domain license. https://commons.wikimedia.org/wiki/File:Carpobrotus_edulis01.jpg (Accessed 8 June 2020).

Joo, Seong Soo, Yeong-Min Yoo, Sang-Hwan Ko, *et al.* 2010. "Effects of essential oil from Chamaecypris obtusa on the development of atopic dermatitis-like skin lesions and the suppression of Th cytokines." *Journal of dermatological science* 60, 2: 122-125. doi: 10.1016/j.jdermsci.2010.08.008.

Joubert, E., and D. de Beer. 2011. "Rooibos (*Aspalathus linearis*) beyond the farm gate: From herbal tea to potential phytopharmaceutical." *South African Journal of Botany* 77, 4: 869-886. doi: 10.1016/j.sajb.2011.07.004.

Joubert, E., W. C. A. Gelderblom, A. Louw, and D. de Beer. 2008. "South African herbal teas: *Aspalathus linearis*, *Cyclopia* spp. and *Athrixia phylicoides*—A review." *Journal of ethnopharmacology* 119, 3: 376-412. doi: 10.1016/j.jep.2008.06.014.

Joubert, Elizabeth, and H Schultz. 2012. "Production and quality aspects of rooibos tea and related products. A review." *Journal of Applied Botany and Food Quality* 80, 2: 138-144.

Kahkhaie, Kolsoum Rezaie, Ali Mirhosseini, Ali Aliabadi, *et al.* 2019. "Curcumin: a modulator of inflammatory signaling pathways in the immune system." *Inflammopharmacology* 27, 5: 885-900. doi: 10.1007/s10787-019-00607-3.

Kim, B. E., M. D. Howell, E. Guttman, *et al.* 2011. "TNF-α downregulates filaggrin and loricrin through c-Jun N-terminal kinase: role for TNF-α antagonists to improve skin barrier." *Journal of Investigative Dermatology* 131, 6: 1272-1279. doi: 10.1038/jid.2011.24.

Komane, B. M., E. I. Olivier, and A. M. Viljoen. 2011. "*Trichilia emetica* (Meliaceae)–A review of traditional uses, biological activities and phytochemistry." *Phytochemistry Letters* 4, 1: 1-9. doi: 10.1016/j.phytol.2010.11.002.

Lall, N., and N. Kishore. 2014. "Are plants used for skin care in South Africa fully explored?" *Journal of ethnopharmacology* 153, 1: 61-84. doi: 10.1016/j.jep.2014.02.021.

Langan, Sinéad M., Alan D. Irvine, and Stephan Weidinger. 2020. "Atopic dermatitis." *The Lancet* 396, 10247: 345-360. doi: 10.1016/S0140-6736(20)31286-1.

Lawrence, E. 2002. "*Pelargonium graveolens*." http://pza.sanbi.org/pelargonium-graveolens (Accessed 15 June 2020).

Lee, H., and S. Lee. 2014. "Epidermal permeability barrier defects and barrier repair therapy in atopic dermatitis." *Allergy, asthma & immunology research* 6, 4: 276-287. doi: 10.4168/aair.2014.6.4.276.

Long, H. S., P. M. Tilney, and B. E. Van Wyk. 2010. "The ethnobotany and pharmacognosy of *Olea europaea* subsp. *africana* (Oleaceae)." *South African Journal of Botany* 76, 2: 324-331. doi: 10.1016/j.sajb.2009.12.005.

Mabona, U., and S. F. Van Vuuren. 2013. "Southern African medicinal plants used to treat skin diseases." *South African Journal of Botany* 87: 175-193. doi: https://doi.org/10.1016/j.sajb.2013.04.002.

Malajian, D., and E. Guttman-Yassky. 2015. "New pathogenic and therapeutic paradigms in atopic dermatitis." *Cytokine* 73, 2: 311-318. doi: 10.1016/j.cyto.2014.11.023.

Mansouri, Y., and E. Guttman-Yassky. 2015. "Immune pathways in atopic dermatitis, and definition of biomarkers through broad and targeted therapeutics." *Journal of clinical medicine* 4, 5: 858-873. doi: 10.3390/jcm4050858.

Maroyi, A. 2019. "Medicinal Uses, Biological and Chemical Properties of Wild Plum (*Harpephyllum caffrum*): An Indigenous Fruit Plant of Southern Africa." *Journal of Pharmacy and Nutrition Sciences* 9, 5: 258-268. doi: 10.29169/1927-5951.2019.09.05.4.

Maroyi, Alfred. 2018. "Albizia Adianthifolia: Botany, Medicinal Uses, Phytochemistry, and Pharmacological Properties." *The Scientific World Journal* 2018. doi: 10.1155/2018/7463584.

McKay, D. L., and J. B. Blumberg. 2007. "A review of the bioactivity of South African herbal teas: rooibos (*Aspalathus linearis*) and honeybush (*Cyclopia intermedia*)." *Phytotherapy Research* 21, 1: 1-16. doi: 10.1002/ptr.1992.

Miller, Susanne C, Ruili Huang, Srilatha Sakamuru, *et al.* 2010. "Identification of known drugs that act as inhibitors of NF-κB signaling and their mechanism of action." *Biochemical pharmacology* 79, 9: 1272-1280. doi: 10.1016/j.bcp.2009.12.021.

Moon, Phil-Dong, Byung-Hee Lee, Hyun-Ja Jeong, *et al.* 2007. "Use of scopoletin to inhibit the production of inflammatory cytokines through inhibition of the IκB/NF-κB signal cascade in the human mast cell line HMC-1." *European Journal of Pharmacology* 555, 2-3: 218-225. doi: 10.1016/j.ejphar.2006.10.021.

Mudimba, T. N. , and J. M. Nguta. 2019. "Traditional uses, phytochemistry and pharmacological activity of *Carpobrotus edulis*: A global perspective." *The Journal of Phytopharmacology* 8, 3: 111-116. doi: 10.31254/phyto.2019.8305.

Nedoszytko, Bogusław, Małgorzata Sokołowska-Wojdyło, Katarzyna Ruckemann-Dziurdzińska, Jadwiga Roszkiewicz, and Roman J Nowicki. 2014. "Chemokines and cytokines network in the pathogenesis of the inflammatory skin diseases: atopic dermatitis, psoriasis and skin mastocytosis." *Advances in Dermatology and Allergology* 31, 2: 84-91. doi: 10.5114/pdia.2014.40920.

Nsuala, B. N., G. Enslin, and A. Viljoen. 2015. "“Wild cannabis”: A review of the traditional use and phytochemistry of *Leonotis leonurus.*" *Journal of ethnopharmacology* 174: 520-539. doi: 10.1016/j.jep.2015.08.013.

Nsuala, B. N., G. P. Kamatou, M. Sandasi, G. Enslin, and A. Viljoen. 2017. "Variation in essential oil composition of *Leonotis leonurus*, an important medicinal plant in South Africa." *Biochemical systematics and ecology* 70: 155-161. doi: 10.1016/j.bse.2016.11.009.

OpenStax College. 2013. "Layers of epidermis." Obtained from Wikimedia under a Creative Common Attribution-Share Alike 3.0 Unported license https://commons.wikimedia.org/wiki/File:502_Layers_of_epidermis.jpg (Accessed 12 June 2020).

Palladino, Michael A, Frances Rena Bahjat, Emmanuel A Theodorakis, and Lyle L Moldawer. 2003. "Anti-TNF-α therapies: the next generation." *Nature reviews Drug discovery* 2, 9: 736-746. doi: 10.1038/nrd1175.

Palmer, C. N. A., A. D. Irvine, A. Terron-Kwiatkowski, *et al.* 2006. "Common loss-of-function variants of the epidermal barrier protein filaggrin are a major predisposing factor for atopic dermatitis." *Nature Genetics* 38: 441-446. doi: https://doi.org/10.1038/ng1767.

Parameswaran, Narayanan, and Sonika Patial. 2010. "Tumor necrosis factor-α signaling in macrophages." *Critical Reviews™ in Eukaryotic Gene Expression* 20, 2: 87-103. doi: 10.1615/CritRevEukarGeneExpr.v20.i2.10.

Paul, Atish T, Vikrantsinh M Gohil, and Kamlesh K Bhutani. 2006. "Modulating TNF-α signaling with natural products." *Drug discovery today* 11, 15-16: 725-732. doi: 10.1016/j.drudis.2006.06.002.

Richfield, J. 2011. "*Harpephyllum caffrum* Anacardiaceae." Obtained from Wikimedia under a Creative Common Attribution-Share Alike 3.0 Unported license https://commons.wikimedia.org/wiki/File:Harpephyllum_caffrum_Anacardiaceae_6397s.jpg (Accessed 8 June 2020).

Saraswathi, J., K. Venkatesh, N. Baburao, M. H. Hilal, and A. R. Rani. 2011. "Phytopharmacological importance of *Pelargonium* species." *Journal of Medicinal Plants Research* 5, 13: 2587-2598.

Serasanambati, Mamatha, and Shanmuga Reddy Chilakapati. 2016. "Function of nuclear factor kappa B (NF-kB) in human diseases-a review." *South Indian Journal of Biological Sciences* 2, 4: 368-387. doi: 10.22205/sijbs/2016/v2/i4/103443.

Song, Kun, Jian Zhang, Peng Zhang, *et al.* 2015. "Five new bioactive compounds from *Chenopodium ambrosioides*." *Journal of Asian natural products research* 17, 5: 482-490. doi: 10.1080/10286020.2015.1042872.

Song, Moo-Young, Sang-Koo Park, Chang-Suk Kim, *et al.* 2008. "Characterization of a novel anti-human TNF-α murine monoclonal antibody with high binding affinity and neutralizing activity." *Experimental & molecular medicine* 40, 1: 35-42. doi: 10.3858/emm.2008.40.1.35.

Sullivan, M., and N. B. Silverberg. 2017. "Current and emerging concepts in atopic dermatitis pathogenesis." *Clinics in dermatology* 35, 4: 349-353. doi: 10.1016/j.clindermatol.2017.03.006.

Tadeg, H., E. Mohammed, K. Asres, and T. Gebre-Mariam. 2005. "Antimicrobial activities of some selected traditional Ethiopian medicinal plants used in the treatment of skin disorders." *Journal of ethnopharmacology* 100, 1-2: 168-175. doi: 10.1016/j.jep.2005.02.031.

Thakur, Gulab S, Manoranjan Bag, Bhagwan S Sanodiya, *et al.* 2009. "*Momordica balsamina*: a medicinal and neutraceutical plant for health care management." *Current pharmaceutical biotechnology* 10, 7: 667-682. doi: 10.2174/138920109789542066.

Thring, Tamsyn SA, Pauline Hili, and Declan P Naughton. 2009. "Anti-collagenase, anti-elastase and anti-oxidant activities of extracts from 21 plants." *BMC complementary and alternative medicine* 9, 1: 27. doi: 10.1186/1472-6882-9-27.

Van Antwerp, Daniel J, Seamus J Martin, Inder M Verma, and Douglas R Green. 1998. "Inhibition of TNF-induced apoptosis by NF-κB." *Trends in cell biology* 8, 3: 107-111. doi: 10.1016/S0962-8924(97)01215-4.

Varothai, S., S. Nitayavardhana, and K. Kulthanan. 2013. "Moisturizers for patients with atopic dermatitis." *Asian pacific journal of allergy and immunology* 31, 2: 91-98.

Voegeli, R, AV Rawlings, M Breternitz, *et al.* 2009. "Increased stratum corneum serine protease activity in acute eczematous atopic skin." *British Journal of Dermatology* 161, 1: 70-77. doi: 10.1111/j.1365-2133.2009.09142.x.

Voisin, T., and I. M. Chiu. 2018. "Molecular link between itch and atopic dermatitis." *Proceedings of the National Academy of Sciences* 115, 51: 12851-12853. doi: 10.1073/pnas.1818879115.

Wu, Ya-di, and BP Zhou. 2010. "TNF-α/NF-κ B/Snail pathway in cancer cell migration and invasion." *British journal of cancer* 102, 4: 639-644. doi: 10.1038/sj.bjc.6605530. Obtaind under the Creative Commons CC-BY license.

Xu, Guangwu, and Yufang Shi. 2007. "Apoptosis signaling pathways and lymphocyte homeostasis." *Cell research* 17, 9: 759-771. doi: 10.1038/cr.2007.52.

Chapter 3. Anti-inflammatory response of gold nanoparticles synthesized from *Juncus lomatophyllus* Spreng. against TNF-α production

Anti-inflammatory response of gold nanoparticles synthesized from *Juncus lomatophyllus* Spreng. against TNF-α production [2]

Keywords: Anti-tyrosinase, atopic dermatitis, bioassay-guided fractionation, gold nanoparticles, inside-out hypothesis, TNF-α.

Abstract

Atopic dermatitis has been increasing in prevalence with the exact cause of the condition unknown, however, two main hypotheses have been accepted. The inside-out hypothesis states that atopic dermatitis is caused by immunological defects including the over-production of tumor necrosis factor-alpha (TNF-α), which in turn causes post-inflammatory hyperpigmentation. Clinical treatments pose adverse effects including skin atrophy and tachyphylaxis, resulting in a demand for an alternative option. The aim was to determine whether the ethanolic extract of *Juncus lomatophyllus* Spreng. (JL-EtOH) inhibited tyrosinase and TNF-α production and if the biological activity was enhanced when fermented using *Bifidobacterium bifidum* (JLF) or when used to form gold nanoparticles (JLAuNP). Lasty, this study aimed to identify potentially active compounds present. Though, JL-EtOH and JLF showed no anti-tyrosinase activity (fifty percent inhibitory concentration (IC_{50}) > 400 µg/mL), JLAuNP displayed inhibition (IC_{50} of 268.8 ± 5.64 µg/mL). Five partitions were prepared from JL-EtOH of which the butanol partition (JLB) displayed the highest anti-tyrosinase activity (IC_{50}: 40.4 ± 2.31 µg/mL). Seven major fractions were pooled from JLB of which P4 (105.55 ± 7.28) and P5 (125.60 ± 3.68 µg/mL) displayed the highest inhibitory activity. Gas chromatography-mass spectrometry (GC-MS) indicated the presence of seven major volatile compounds of which n-hexadecanoic acid has previously displayed anti-tyrosinase activity. The cytotoxic effects of the JLB, JLAuNP and JL-EtOH were evaluated on human keratinocytes (HaCaT) and peripheral blood mononuclear cells (PBMCs) and displayed no effect (IC_{50} > 400 µg/mL). Furthermore, JL-EtOH (25.48 ± 7.27) and JLB (30.79 ± 5.80 pg/mL) displayed no effect, whereas JLAuNP (23.59 ± 1.95 pg/mL) significantly inhibited ($p < 0.05$) the production of TNF-α at a concentration of 200 µg/mL. Further isolation and characterization of P4 and P5 and the effect JLAuNP may have on translators associated with TNF-α production as a potential mode of action should be considered.

3.1 Introduction

Chronic inflammatory skin conditions, specifically atopic dermatitis, have been increasing in prevalence over the past 10 years while the exact cause of this condition remains unknown. Two main hypotheses that have been accepted as the likely cause of atopic dermatitis are known as the inside-out and outside-in hypotheses (Chamlin et al., 2002; Brandt and Sivaprasad, 2011). The inside-out hypothesis states that atopic dermatitis is caused by an immunological defect, which alters the permeability of the skin causing patients to experience a higher sensitivity to allergens (Chamlin et al., 2002; Brandt and Sivaprasad, 2011). The hypothesis is divided into two main subtypes known as acute (extrinsic) and chronic (intrinsic) eczema both of which involve the overproduction of the pro-inflammatory cytokine tumor necrosis factor-alpha (TNF-α), within macrophages (Song et al., 2008; Mansouri and Guttman-Yassky, 2015). A known adverse effect caused by the overproduction

[2] This chapter will be submitted as an original research article to Frontiers in Molecular Biosciences with an impact factor of 5.246. The format of the chapter was written based on the guidelines set by Frontiers.

of TNF-α is post-inflammatory hyperpigmentation (Davis and Callender, 2010). During melanogenesis, the rate-limiting enzyme, tyrosinase, initiates the oxidization of tyrosine into dopaquinone leading to the production of melanin, however, TNF-α stimulates the proliferation of melanocytes resulting in the overexpression of this enzyme (Davis and Callender, 2010) (Parvez et al., 2007; Narayanaswamy and Ismail, 2015). Clinical treatments, such as phytotherapy and glucocorticosteroids alleviate symptoms associated with eczema, however, patients experience adverse effects including skin atrophy and tachyphylaxis, thus an effective alternative treatment is in high demand (Chamlin et al., 2002; Rezzani, 2004; Hengge et al., 2006; Gelmetti and Wollenberg, 2014).

Juncus lomatophyllus Spreng. is part of the Juncaceae family that consists of eight genera, of which this genus is the most well-known (El-Shamy et al., 2015). Most species within the *Juncus* genus are located in salty marshes throughout the world. These species are known for their sympodial rhizomes that produce shoots that are slender and nodeless (Bús et al., 2018). Although there is limited information on the biological activity of *J. lomatophyllus*, it is a widely distributed endemic sedge located in wetlands that are situated in Gauteng, North West and the Free State province of South Africa (Wentzel and Wentzel, 2020). Secondary metabolites that have been isolated from plants within the Juncaceae family include terpenes, sterols, carotenoids, stilbenes, phenolic acid derivatives, coumarins, phenanthrenoids and flavonoids (El-Shamy et al., 2015; Bús et al., 2018). These metabolites are similar to those traditionally used to treat eczema including *Aloe vera* L. and *Avena sativa* L., which contain flavonoids, sterols and terpenes (Zari and Zari, 2015). In Chinese Traditional medicine, the stem pith of *Juncus effusus* L. is used to reduce insomnia, pain and mouth ulcers, while the medulla of this plant is used to treat traumatic bleeding and pharyngitis (Bús et al., 2018). The fruit of *Juncus acutus* L. is used in infusions to treat colds, while the rhizome of *Juncus maritimus* Lam. is used for insomnia (El-Shamy et al., 2015). In the Zulu culture, *J. effusus* is used to treat venereal diseases and reduce pain during childbirth, while *Juncus kraussii* Hochst. and *J. lomatophyllus* are used for sexually transmitted diseases (Mhlongo and Van Wyk, 2019). Egyptians use the seeds of *Juncus rigidus* Desf. to treat diarrhea (Bús et al., 2018).

This study aimed to determine the anti-tyrosinase potential of the ethanolic extract of *Juncus lomatophyllus* and whether this extract reduces the production of TNF-α. Furthermore, this study focused on whether the biological activity of the ethanolic extract was enhanced when fermented using *Bifidobacterium bifidum* or used to form gold nanoparticles. Lastly, due to the limited information on the chemical composition of *J. lomatophyllus*, this study aimed to identify potential active compounds present using bioassay-guided fractionation.

3.2 Materials and methods

3.2.1 Materials, chemicals, and reagents

The human keratinocytes (HaCaT) were donated by Dr. Lester Davids from the University of Cape Town. The Dulbecco's modified Eagle's Medium (DMEM), Roswell Park Memorial Institute (RPMI-1640) medium, phosphate-buffered saline (PBS), fetal bovine serum (FBS), ammonium-chloride-potassium (ACK) lysing buffer, PrestoBlue Cell Viability reagent, amphotericin B, streptomycin, and penicillin, Eutech pH buffer solutions (pH 4, 7 and 10) and 0.25% trypsin were obtained from ThermoFisher Scientific (Johannesburg, South Africa). Cell culture plates and flasks were purchased from LasecSA (Pty) Ltd. (Midrand, South Africa). Tumor necrosis factor-alpha (TNF-α) (ab181421) ELISA kit was sourced from BIOCOM Africa (Pty) Ltd. (Lyttleton Manor, South Africa). Histopaque,

ethylenediaminetetraacetic acid (EDTA) and other chemicals and reagents such as dimethyl sulfoxide (DMSO), gum arabic, actinomycin D (purity >95%), gold (III) chloride trihydrate ($HAuCl_4.3H_2O$), kojic acid (purity >98%), sodium chloride (NaCl), Bifidus Selective Medium (BSM)-Agar, BSM-Supplement, BSM-Broth, bovine serum albumin (BSA), silica (SiO_2) powder, quartz sand, lipopolysaccharides (LPS) extracted from *Escherichia coli* (O111:B4), *L*-tyrosine substrate and mushroom tyrosinase enzyme were obtained from Sigma-Aldrich (Johannesburg, South Africa).

3.2.2 Plant collection and extraction

The whole plant of *J. lomatophyllus* was collected in March (2016) from the Manie van der Schijff Botanical Garden at the University of Pretoria (PRU 122255), rinsed with distilled water (dH_2O), and placed in a -80˚C freezer for three days. Afterward, the samples were freeze-dried for a week. Once dry, the samples were ground into a fine powder using an IKA grinder (MF 10.1 Head 2870900) with a 2 mm sieve. Afterward, 737 g of powder was mixed with 3.69 mL of absolute ethanol (1:5) and placed on a shaker for seven days. Thereafter, the solution was filtered using a Whatman no. 3 filter paper, concentrated using a rotary evaporator and freeze-dried for three days. The percentage yield was calculated for each extract using the following equation:

$$\%\text{Yield} = \left(\frac{Extract\ weight\ (g)}{Powdered\ or\ fresh\ material\ weight\ (g)}\right) \times 100$$

The final quantity of the concentrated extract was 39.9 g with a percentage yield of 5.4%. The dried extract was stored at 4˚C.

3.2.3 Bioassay-guided fractionation

3.2.3.1 Liquid-liquid partition

Twenty grams of *J. lomatophyllus* ethanolic extract (JL-EtOH) was dissolved in 500 mL of distilled water (dH_2O) and partitioned using *n*-hexane, ethyl acetate and *n*-butanol. Briefly, 500 mL of *n*-hexane was added to the solution (1:1), thoroughly mixed and left to stand. Once two distinct layers were seen, the top layer (*n*-hexane) was collected by removing the bottom layer. Thereafter, the bottom layer, consisting of the water solution, was added to the funnel and the process was repeated three times. Using the remaining water solution in the funnel same method was used to collect the ethyl-acetate and butanol partition. A sublayer between *n*-butanol and ethyl acetate was formed which was collected separately and labeled as sub-1. The collected partitions were concentrated using a rotary evaporator and left to dry overnight in a fume hood. The water partition (consisting of the remaining water solution) was left overnight in a -80˚C freezer and freeze-dried for a week. The partition that showed the highest anti-tyrosinase activity was further purified.

3.2.3.2 Column chromatography

A slurry consisting of 2.45 g of the butanol partition (JLB) was dissolved in minimal amounts of methanol and combined with silica. Once dry, the slurry was added to a column containing silica that was saturated with *n*-hexane. A total of 165 fractions were collected and the following solvent systems were used to elute the column: fraction 1 with 100% hexane, fraction 2-3 with 100% dichloromethane, 3-4 with 80% chloroform in hexane, 5-109 with 80% chloroform in methanol, 110-136 with 80% ethyl acetate in methanol, 137-157 with 70% ethyl acetate in methanol and 158-164 with 50% ethyl acetate in methanol. Fractions

that displayed similar TLC profiles were pooled together. A total of seven main fractions were collected and were evaluated for anti-tyrosinase activity.

3.2.3.3 Gas chromatography-mass spectrometry (GC-MS)

GC-MS of the major fractions that displayed the highest anti-tyrosinase activity was performed using a LECO Pegasus 4D GC-TOFMS (LECO Africa (Pty) Ltd., Kempton Park, South Africa) that was equipped with a capillary column (Rxi-5SiMS (30 m × 0.25 mm ID with a film thickness of 0.2 mm)) (Restek, Bellefonte, PA, USA). The carrier gas used consisted of high-grade helium (99.999%) (Afrox, Gauteng, South Africa) that was flowing at a constant rate of 1 mL/min. Furthermore, the injector was maintained at a constant temperature (250°C) and a splitless mode set at every 30 s was used to operate the inlet. The temperature program that was set for the GC oven was 40°C for three minutes with an increase of 10°C per minute to reach a final temperature of 300°C for five minutes. The MS transfer line and ion source were set at a temperature of 280 and 230°C, respectively. Spectroscopic detection was operated in electron impact ionization mode (EI^+) with an electron energy of 70 eV with a data acquisition rate of 10 spectra per second. The total running time of the analysis was 35 minutes with a solvent delay of five minutes. The national institute of standards and technology (NIST) database was used to compare and identify the phytochemical constituent of each peak.

3.2.4 Fermentation

JL-EtOH was fermented using *Bifidobacterium bifidum* (ATCC 11863) according to the method described by Park and Bae (2016), with modifications. *Bifidobacterium bifidum* colonies were cultures from Kwik Sticks on Bifidus Selective Medium (BSM)-Agar supplemented with BSM-Supplement (stock solution of 23.2 g/L) while single colonies were grown on BSM-Broth at 37˚C for 48 hours. Bacterial suspensions were prepared in accordance with an 8 McFarland standard (112×10^8 CFU/mL) at a wavelength of 600 nm. JL-EtOH (10 mg/mL) was supplemented with 1% ethanol solution (w/v), warmed BSM-Broth and inoculated with 4% bacterial suspension (v/v) at a final volume of 50 mL. After fermentation for six weeks at 37˚C with weekly agitations, the extract was sonicated for five minutes at 45˚C, freeze-dried and stored at 4˚C. A vehicle and negative control was included consisting of all the components with one exception. The negative control did not contain any bacteria while the JL-EtOH was substituted with 0.5 mL of EtOH in the vehicle control.

3.2.5 Synthesis of gold nanoparticles

To synthesize gold nanoparticles using *Juncus lomatophyllus*, JL-EtOH was dissolved in dH_2O (2 mg/mL) and heated until 60˚C was reached. Due to the inability of JL-EtOH to homogenize with water, the solution was centrifuged and 20 mL of collected supernatant was combined with 60 mg of gum arabic powder, which was used as a stabilizer. Thereafter, the mixture was heated to 60˚C whereby 100 mM of gold salt ($HAuCl_4.3H_2O$) solution was added. Immediately after the solution was exposed to the gold salt a color change from green to wine was observed.

3.2.6 Characterization of synthesized gold nanoparticles

3.2.6.1 Ultraviolet-visible spectrometry (UV-Vis)

To confirm the formation of gold nanoparticles, a full spectral scan was conducted using ultraviolet-visible spectrometry (UV-Vis) to determine if the surface plasmon resonance

(SPR) was similar to gold metal (Au). In a 96-well plate, 100 µL of the synthesized gold nanoparticles (JLAuNPs) solution was added and the absorbance was read between 450-800 nm at 50 nm increments using a Victor Nivo plate reader (PerkinElmer, Midrand, South Africa).

3.2.6.2 *In vitro* stability

In vitro stability of the JLAuNPs was evaluated in various mediums consisting of buffer solutions and cell culture mediums, which included 0.5% bovine serum albumin (BSA), 5% sodium chloride (NaCl), pH buffer solutions at 4, 7 and 10, phosphate buffer (pH 6.5), Dulbecco's Modified Eagles medium (DMEM) and Roswell Park Memorial Institute (RPMI-1640) medium. JLAuNPs were added to the abovementioned solutions at a 1:1 ratio with a final volume of 1.5 mL and were incubated at 37˚C. To confirm whether the nanoparticles were stable, the SPR peaks (λ_{max}) between 450 and 800 nm were measured using a Victor Nivo plate reader at 0, 2, 24 (Day 1), 48 (Day 2), 72 (Day 3), 96 (Day 4) and 120 hours (Day 5).

3.2.6.3 High-resolution transmission electron microscopy (HRTEM)

High-resolution transmission electron microscopy was used to identify the particle size and shape of JLAuNPs. Furthermore, the crystallinity was identified through selected area electron diffraction (SAED). Five microlitres of JLAuNPs solution were loaded onto a carbon-coated copper TEM grid and allowed to dry. Thereafter, the grids were loaded into a JEOL JEM- ARM200F double Cs-corrected transmission electron microscope equipped with a large solid angle energy dispersive spectrometer (EDS) (Akishima, Tokyo, Japan) and images were captured.

3.2.6.4 Quantification of the total phenolic content present in the synthesized nanoparticles

The total phenolic content was quantified using Folin Cioalteau as described by De Canha et al. (2021). A standard curve was prepared from JL-EtOH that was serially diluted two-fold, in dH_2O, resulting in a final concentration range of 2000-15.63 µg/mL. In a 2 mL Eppendorf tube, 125 µL of 7.5% (w/v) sodium bicarbonate solution (Na_2CO_3) and 125 µL 10% (v/v) Folin Cioalteau reagent (1 in 10 mL dH_2O) were added to 250 µL of each dilution and to 250 µL of the JLAuNPs solution. Thereafter, 100 µL of each solution was transferred into a 96-well plate and incubated at 30˚C for 30 minutes in the dark. Blanks for JL-EtOH and JLAuNPs consisted of 250 µL of sample, 7.5% Na_2CO_3 and dH_2O in the place of 10% Folic Cioalteau. The absorbance was measured at 765 nm using a Victor Nivo plate reader and the phenolic content of JLAuNPs was determined using the equation generated from the standard curve ($y = 0.0002x + 0.0014$, $R^2 = 0.9898$). The quantified phenolic content was used as the highest stock concentration in each of the bioassays that were conducted.

3.2.6.5 Dynamic light scattering (DLS)

To determine the hydrodynamic size of the JLAuNPs, 1 mL of the JLAuNPs was transferred into a zeta cell and read using a Zetasizer Nano ZS instrument (Malvern Instruments Ltd., Malvern, Worcestershire, UK). Three reads were performed, and the average was obtained.

3.2.6.6 Zeta potential

The electrostatic charge of JLAuNPs was obtained by transferring 1 mL into a cuvette, which was measured three times using a Zetasizer Nano ZS instrument and the average was after three reads were recorded.

3.2.6.7 Fourier transform infrared spectrometry (FTIR)

To identify potential phytochemical groups, present in JLAuNPs, Fourier transform infrared spectrometry was conducted using 9 mg of JL-EtOH as a blank. The percentage transmittance was detected over an infrared range of 550-4000 cm^{-1} using a Perkin Elmer spectrum 100 FTIR spectrometer (Perkin Elmer, Midrand, South Africa).

3.2.7 Tyrosinase inhibition

The method used to determine tyrosinase inhibition was described by Lall et al. (2019) with slight modifications to the concentration range. Briefly, in 24 well-plates the partitions, major fractions, and the positive control (kojic acid) were dissolved in DMSO (40 µg/mL) and serially diluted two-fold to achieve a final concentration range of 200-1.56 µg/mL. The same method was applied to JL-EtOH and JLF (80 µg/mL) with a final concentration range of 400-3.12 µg/mL. JLAuNPs stock solution was serially diluted to achieve a concentration range of 400-3.12 µg/mL. A 1% DMSO (vehicle control) was prepared in the same manner as the solvent partitions. A 0% control was prepared which consisted of phosphate buffer (pH 6.5). Using a BIO-TEK Power-Wave XS plate reader (Analytical and Diagnostic Products CC, Roodepoort, South Africa), the absorbance values were determined at a wavelength of $OD_{492\ nm}$ for 30 minutes. To calculate the percentage inhibition the following equation was used.

$$\%\ Inhibition = 100 - \left(\frac{Absorbance\ sample}{Absorbance\ control}\right) \text{ x } 100$$

The $Absorbance_{control}$ was determined by subtracting the absorbance of DMSO at 30 min from the absorbance of DMSO at 0 min. The $Absorbance_{sample}$ was determined by subtracting the absorbance of the extract or positive control at 30 min from the absorbance of the extract or positive control at 0 min. GraphPad Prism 4 was used to calculate the 50% inhibitory concentration (IC_{50}) of the samples.

3.2.8 Cell culture

Human keratinocytes (HaCaT) were used to determine the antiproliferative activity of JL-EtOH, JLAuNPs and JLB. To maintain the cell line, DMEM media was used, which was supplemented with 1% antibiotics (consisting of penicillin (100 U/mL), streptomycin (100 µg/mL) and amphotericin B (250 µg/mL)) and 10% fetal bovine serum. The cells were incubated at 5% CO_2 and 37˚C until a confluent monolayer was obtained. The cells were sub-cultured using 0.25% trypsin-EDTA once the monolayer had formed.

3.2.9 Antiproliferative activity

The PrestoBlue viability reagent method used was described by Lall et al. (2019). Within a 96-well microtiter culture plate, cells were seeded at a concentration of 5×10^4 cells/mL and incubated overnight at 37˚C and 5% CO_2. A stock solution of JL-EtOH and JLB was prepared at a concentration of 40 mg/mL in DMSO. JL-EtOH, JLB and JLAuNPs stock solutions were diluted two-fold with 20% DMSO and actinomycin D used as a positive control. Once the cells adhered, JL-EtOH, JLB, JLAuNPs, 20% DMSO and actinomycin D

were added in triplicate. The final concentration ranged between 400-3.125 µg/mL with 20% DMSO between 20-0.155% and actinomycin D between 0.05-3.9×10^{-4} µg/mL. Media (100%), PrestoBlue reagent and a 1% DMSO control were added, however, the PrestoBlue control contained no cells (0%). After 72 hours, PrestoBlue reagent was added and incubated for a further two hours. The fluorescence was measured at an excitation/emission wavelength of 560/590 nm using a Victor Nivo plate reader. To calculate cell viability the following equation was used and the IC_{50} values were determined using GraphPad Prism 4:

$$\%\ Viability = \frac{Fluorescence\ \ sample - Fluorescence\ 0\%\ control}{(Fluorescence\ \ 100\%\ control - Fluorescence\ \ 0\%\ control)} \text{ x } 100$$

3.2.10 PBMC isolation

Peripheral blood mononuclear cells (PBMCs) were isolated from whole blood using Histopaque®-1077. The selection criteria of the volunteer were based on whether they had eczema and were above the age of 21 with no history of major diseases. Ethics approval was obtained by the ethics committee of the Faculty of Natural and Agricultural Science (EC120411-046, University of Pretoria, South Africa). To isolate the PBMCs, a method described by Oosthuizen et al. (2017) was followed. Briefly, 15 mL of freshly collected blood was diluted with incomplete RPMI-1640 media at a 1:1 ratio, at room temperature. Thereafter, 15 mL of diluted blood was layered on 7.5 mL of histopaque and centrifuged at 1500×*g* for 30 minutes. After centrifugation, the buffy coat was collected and transferred into a falcon tube. The collected coat was resuspended in incomplete media and centrifuged at 810×*g* for 10 min at room temperature. The supernatant was discarded, and the pellet was resuspended in approximately 5 mL ACK lysing buffer, to remove the remaining erythrocytes. After 5 minutes, complete RPMI-1640 media containing 10 % fetal bovine serum and 1 % antibiotics, containing penicillin (100 U/mL), streptomycin (100 µg/mL) and 1 % amphotericin B (250 µg/mL), was added. The PBMCs were centrifuged at 240×*g* for 10 min at room temperature. The supernatant was discarded and the PBMCs were resuspended in 10 % RPMI-1640 media. Further investigation into JL-EtOH, JLAuNPs and JLB effect on TNF-α production was conducted and the samples were tested for antiproliferative activity against PBMCs as described in section 3.2.9.

3.2.11 TNF-α quantification

Quantification of TNF-α from PBMCs cell supernatant was conducted using a TNF-α ELISA kit, following the manufacturer's protocol. PBMC monocytes were differentiated into macrophages using lipopolysaccharide (LPS) at a final concentration of 5 µg/mL. The cells were seeded in a 96-well plate at a concentration of 1.5×10^5 cells/mL and incubated for 24 hours at 5% CO_2 and 37˚C. Thereafter, the samples were serially diluted two-fold and added in duplicate at final concentrations of 200, 100 and 50 µg/mL. A vehicle control consisting of 0.25% DMSO was prepared in the same manner. After 24 hours of incubation, 100 µL of cell supernatant was transferred to a 96-well plate and stored at -80˚C until use. Cell viability was measured by adding 10 µL of PrestoBlue reagent to the remaining cells and calculated as described in section 3.2.9 to ascertain that the modulation of TNF-α was not due to cell death. TNF-α quantification was measured at a wavelength of 450 nm using a Victor Nivo plate reader. A standard curve was prepared from the controls provided, ranging from a concentration of 1000-15.63 and 0 pg/mL (blank control). For each sample, the blank was deducted from the absorbance and the resulting value was quantified using the equation generated from the standard curve ($y = 0.0029x + 0.1636$, $R^2 = 0.9902$).

3.2.12 Statistical analysis

Results are reported as mean ± standard error (or standard deviation) as displayed in the results section. Three repeats were performed for each of the assays, with two repeats conducted for TNF-α quantification. Furthermore, JLAuNPs, where applicable, were compared to the untreated control as the stock solution did not contain DMSO. To obtain the IC_{50} values, a nonlinear regression analysis of the sigmoidal dose-response curves (4-parameter logistic) using GraphPad Prism 4 was conducted. Statistical analysis was done using one-way analysis of variance (ANOVA) followed by Dunnett's multiple comparison tests (GraphPad, version 4), where $p < 0.05$ (*), $p < 0.01$ (**) and $p < 0.001$ (***) were considered statistically significant.

3.3 Results

3.3.1 Bioassay-guided fractionation

Though JL-EtOH displayed no anti-tyrosinase activity ($IC_{50} > 200$ µg/mL), the butanol partition (JLB) (40.4 ± 2.31 µg/mL) displayed the lowest IC_{50} value against tyrosinase. Column chromatography was conducted on JLB of which seven major fractions were pooled. When evaluated against tyrosinase, P1 (155.70 ± 4.95), P4 (105.55 ± 7.28) and P5 (125.60 ± 3.68 µg/mL) displayed inhibition.

3.3.2 GC-MS analysis

To identify potential bioactive constituents present in P4 and P5, GC-MS was conducted. A total of 78 and 92 peaks in P4 (Table 3.1) and P5 (Table 3.2) were observed using GC-MS (Figures 3.1 and 3.2). Major constituents present in P4, above a peak area of 2%, included 9-octadecenamide (34.89%), dodecanamide (25.32%), [1,1'-biphenyl]-4,4'-diamine, N, N'-diphenyl- (4.16%), octadecanoic acid (4.09%), hexasiloxane, tetradecamethyl- (3.75%) and n-hexadecanoic acid (2.81%). Furthermore, major constituents discovered in P5 above a peak area of 5% included diisooctyl phthalate (20.50%), 9-octadecenamide (13.43%), 1-octanamine (8.01%), sulfurous acid, butyl octyl ester (7.80%) and dodecanamide (5.99%). Furthermore, it was noted that P4 and P5 shared similar constituents with varying peak area percentages.

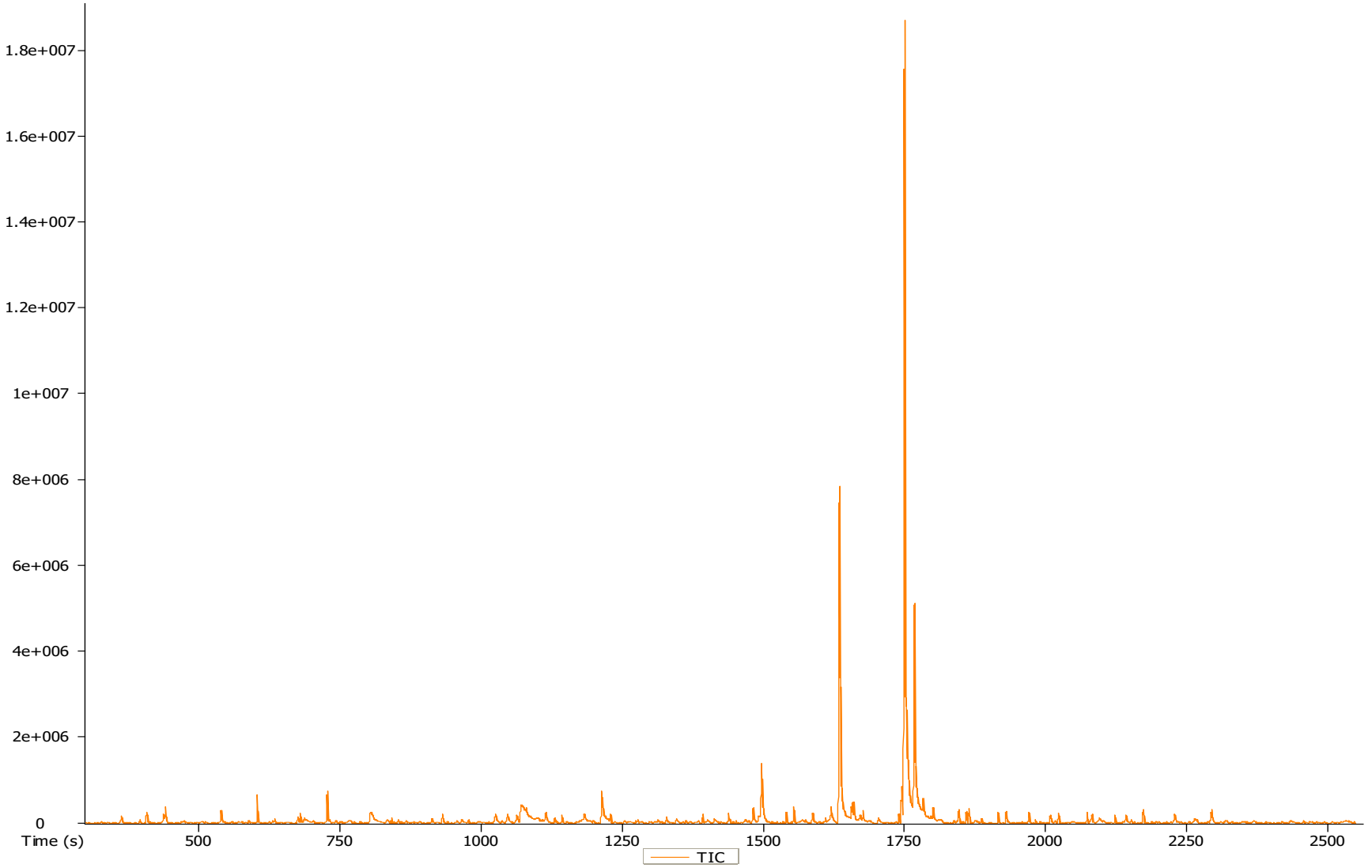

Figure 3.1. GC-MS chromatogram of a semi-pure bioactive fraction (P4) isolated from the butanol partition of *Juncus lomatophyllus.*

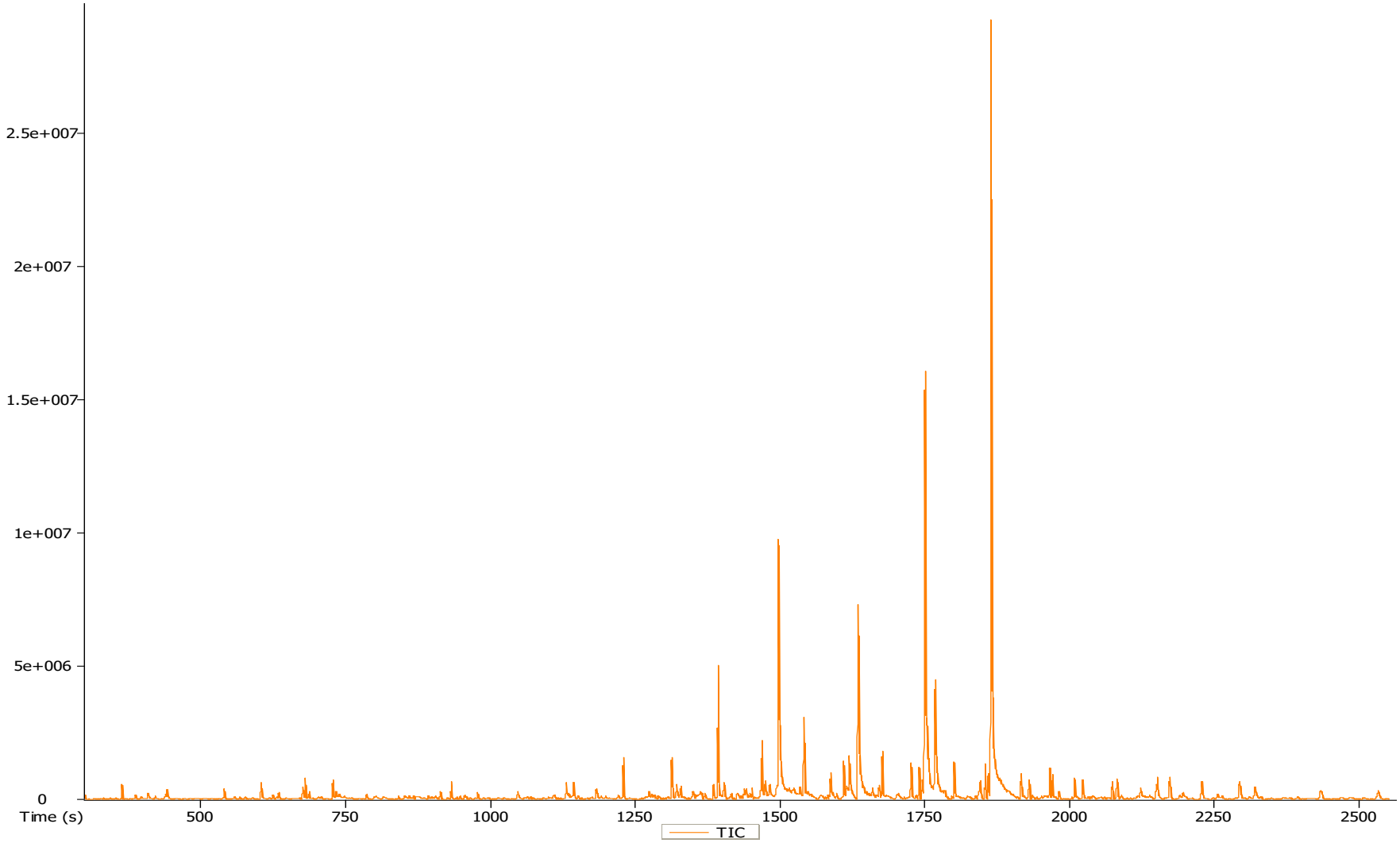

Figure 3.2. GC-MS chromatogram of a semi-pure bioactive fraction (P5) isolated from the butanol partition of *Juncus lomatophyllus.*

331 **Table 3.1. Chemical composition of P4 isolated from the butanol partition of *Juncus lomatophyllus.***

Peak#	Name	Molecular weight	Formula	Similarity [A]	Area % [B]
1	Benzene, 1,3-dimethyl-	106	C_8H_{10}	924	0.12
2	o-Xylene	106	C_8H_{10}	938	0.49
3	p-Xylene	106	C_8H_{10}	951	0.25
4	Ethane, 1,1,2,2-tetrachloro-	166	$C_2H_2Cl_4$	844	0.62
5	Ethane, pentachloro-	200	C_2HCl_5	748	0.39
6	Decane	142	$C_{10}H_{22}$	929	0.80
7	Ethane, hexachloro-	234	C_2Cl_6	883	0.18
8	Octane, 2,3,6,7-tetramethyl-	170	$C_{12}H_{26}$	866	0.27
9	Undecane	156	$C_{11}H_{24}$	930	1.00
10	Silane, cyclohexyldimethoxymethyl-	188	$C_9H_{20}O_2Si$	869	0.05
11	1,4:3,6-Dianhydro-à-d-glucopyranose	144	$C_6H_8O_4$	850	1.44
12	Benzothiazole	135	C_7H_5NS	864	0.27
13	Hexadecane	226	$C_{16}H_{34}$	894	0.59
14	p-Nitrophenyl hexanoate	237	$C_{12}H_{15}NO_4$	830	0.16
15	D-Allose	180	$C_6H_{12}O_6$	898	1.05
16	4H-Imidazol-4-one, 2-amino-1,5-dihydro-	99	$C_3H_5N_3O$	809	0.57
17	Cyclobutanol, TMS derivative	144	$C_7H_{16}OSi$	618	0.57
18	2,4-Di-tert-butylphenol	206	$C_{14}H_{22}O$	856	0.13
19	Eicosane	282	$C_{20}H_{42}$	870	0.27
20	Hydrazinecarboxamide, N,N-diphenyl-	227	$C_{13}H_{13}N_3O$	930	2.00

21	Heneicosane	296	$C_{21}H_{44}$	904	0.26
22	1,2-Benzenedicarboxylic acid, bis(2-methylpropyl) ester	278	$C_{16}H_{22}O_4$	870	0.15
23	1,1,1,5,7,7,7-Heptamethyl-3,3-bis(trimethylsiloxy)tetrasiloxane	444	$C_{13}H_{40}O_5Si_6$	725	0.30
24	Dibutyl phthalate	278	$C_{16}H_{22}O_4$	937	0.53
25	Nonanamide	157	$C_9H_{19}NO$	905	0.35
26	n-Hexadecanoic acid	256	$C_{16}H_{32}O_2$	914	2.81
27	Eicosane	282	$C_{20}H_{42}$	916	0.30
28	Silane, tetramethyl-	88	$C_4H_{12}Si$	693	0.53
29	9-Octadecenamide, (Z)-	281	$C_{18}H_{35}NO$	851	1.03
30	Dodecanamide	199	$C_{12}H_{25}NO$	926	15.30
31	Octadecanoic acid	284	$C_{18}H_{36}O_2$	909	4.09
32	Hexadecanoic acid, butyl ester	312	$C_{20}H_{40}O_2$	892	0.48
33	Hexasiloxane, tetradecamethyl-	458	$C_{14}H_{42}O_5Si_6$	706	0.65
34	Heptadecane, 2-methyl-	254	$C_{18}H_{38}$	922	0.32
35	Dodecanamide	199	$C_{12}H_{25}NO$	906	0.30
36	Benzenecarbothioic acid, 2,6-dichloro-, S-methyl ester	220	$C_8H_6Cl_2OS$	830	0.01
37	Heptacosane	380	$C_{27}H_{56}$	915	0.26
38	9-Octadecenamide, (Z)-	281	$C_{18}H_{35}NO$	772	0.95
39	9-Octadecenamide, (Z)-	281	$C_{18}H_{35}NO$	927	34.89
40	[1,1'-Biphenyl]-4,4'-diamine, N,N'-diphenyl-	336	$C_{24}H_{20}N_2$	566	3.82
41	Hexasiloxane, tetradecamethyl-	458	$C_{14}H_{42}O_5Si_6$	685	1.87
42	6H-Dibenzo[b,d]pyran-1-ol, 6,6,9-trimethyl-3-propyl-	282	$C_{19}H_{22}O_2$	702	0.01

43	Dodecanamide	199	$C_{12}H_{25}NO$	909	9.72
44	Hexadecanoic acid, 1,1-dimethylethyl ester	312	$C_{20}H_{40}O_2$	713	0.46
45	Cyclohexanecarboxylic acid, octyl ester	240	$C_{15}H_{28}O_2$	614	0.46
46	Tetracosane	338	$C_{24}H_{50}$	924	0.41
47	Dicyclohexyl phthalate	330	$C_{20}H_{26}O_4$	846	0.08
48	Hexasiloxane, tetradecamethyl-	458	$C_{14}H_{42}O_5Si_6$	710	0.48
49	Heptadecane, 2-methyl-	254	$C_{18}H_{38}$	902	0.34
50	Diisooctyl phthalate	390	$C_{24}H_{38}O_4$	911	0.44
51	Cannabinol	310	$C_{21}H_{26}O_2$	876	0.14
52	Dotriacontane	450	$C_{32}H_{66}$	921	0.31
53	Hexasiloxane, tetradecamethyl-	458	$C_{14}H_{42}O_5Si_6$	720	0.42
54	Heptacosane	380	$C_{27}H_{56}$	894	0.34
55	Hexasiloxane, tetradecamethyl-	458	$C_{14}H_{42}O_5Si_6$	699	0.33
56	Heptacosane	380	$C_{27}H_{56}$	880	0.30
57	Dotriacontane	450	$C_{32}H_{66}$	897	0.31
58	Hexasiloxane, 1,1,3,3,5,5,7,7,9,9,11,11-dodecamethyl-	430	$C_{12}H_{38}O_5Si_6$	676	0.46
59	2,5-Dihydroxybenzoic acid, 3TMS derivative	370	$C_{16}H_{30}O_4Si_3$	610	0.46
60	Unknown 1	236	$C_8H_{24}O_2Si_3$	386	0.46
61	2-methyloctacosane	408	$C_{29}H_{60}$	864	0.24
62	[1,1'-Biphenyl]-4,4'-diamine, N,N'-diphenyl-	336	$C_{24}H_{20}N_2$	742	0.34
63	Unknown 2	222	$C_6H_{18}O_3Si_3$	428	0.05

64	Hexasiloxane, 1,1,3,3,5,5,7,7,9,9,11,11-dodecamethyl-	430	$C_{12}H_{38}O_5Si_6$	731	0.09
65	1-Iodo-2-methylundecane	296	$C_{12}H_{25}I$	842	0.53
66	Unknown 3	222	$C_6H_{18}O_3Si_3$	476	0.03
67	Unknown 4	222	$C_6H_{18}O_3Si_3$	441	0.05
68	Acetic acid, bis[(trimethylsilyl)oxyl]-, trimethylsilyl ester	308	$C_{11}H_{28}O_4Si_3$	552	0.48
69	Sulfurous acid, decyl 2-propyl ester	264	$C_{13}H_{28}O_3S$	527	0.48
70	1,1,1,5,7,7,7-Heptamethyl-3,3-bis(trimethylsiloxy)tetrasiloxane	444	$C_{13}H_{40}O_5Si_6$	596	0.22
71	Tris(tert-butyldimethylsilyloxy)arsane	468	$C_{18}H_{45}AsO_3Si_3$	561	0.00
72	4,4'-bi-4H-pyran, 2,2',6,6'-tetrakis(1,1-dimethylethyl)-4,4'-dimethyl-	414	$C_{28}H_{46}O_2$	519	0
73	Nonadecane, 1-chloro-	302	$C_{19}H_{39}C_l$	653	0.73
74	Unknown 5	458	$C_{14}H_{42}O_5Si_6$	475	0.17
75	4,4'-bi-4H-pyran, 2,2',6,6'-tetrakis(1,1-dimethylethyl)-4,4'-dimethyl-	414	$C_{28}H_{46}O_2$	541	0.12
76	Unknown 6	412	$C_{24}H_{36}O_2Si_2$	488	0.02
77	Unknown 7	222	$C_6H_{18}O_3Si_3$	444	0.05
78	Unknown 8	430	$C_{12}H_{38}O_5Si_6$	470	0.05
Total					**100**

A: Mass spectral similarity to NIST08 library, B: Relative peak area

333 **Table 3.2. Chemical composition of P5 isolated from the butanol partition of *Juncus lomatophyllus*.**

Peak #	Name	Molecular weight	Formula	Similarity [A]	Area % [B]
1	Hexane, 2,3,4-trimethyl-	128	C_9H_{20}	900	0.27
2	Benzene, 1,3-dimethyl-	106	C_8H_{10}	897	0.06
3	o-Xylene	106	C_8H_{10}	950	0.22
4	o-Xylene	106	C_8H_{10}	931	0.12
5	Ethane, 1,1,2,2-tetrachloro-	166	$C_2H_2Cl_4$	851	0.27
6	Ethane, pentachloro-	200	C_2HCl_5	733	0.24
7	Decane	142	$C_{10}H_{22}$	926	0.36
8	Ethane, hexachloro-	234	C_2Cl_6	884	0.26
9	Decane, 2,3,5,8-tetramethyl-	198	$C_{14}H_{30}$	872	0.41
10	Undecane	156	$C_{11}H_{24}$	944	0.38
11	Silane, cyclohexyldimethoxymethyl-	188	$C_9H_{20}O_2Si$	897	0.10
12	Hexadecane	226	$C_{16}H_{34}$	876	0.32
13	2,4-Di-tert-butylphenol	206	$C_{14}H_{22}O$	896	0.37
14	Eicosane	282	$C_{20}H_{42}$	875	0.38
15	Hexadecane	226	$C_{16}H_{34}$	928	0.83
16	Eicosane	282	$C_{20}H_{42}$	921	0.93
17	Heptadecane, 2,6,10,14-tetramethyl-	296	$C_{21}H_{44}$	895	0.48
18	Eicosane	282	$C_{20}H_{42}$	898	0.33
19	Cetene	224	$C_{16}H_{32}$	915	0.29
20	Eicosane	282	$C_{20}H_{42}$	920	2.67
21	Hexadecane, 2,6,10,14-tetramethyl-	282	$C_{20}H_{42}$	904	0.60

22	1,2-Benzenedicarboxylic acid, bis(2-methylpropyl) ester	278	$C_{16}H_{22}O_4$	878	0.03
23	7,9-Di-tert-butyl-1-oxaspiro(4,5)deca-6,9-diene-2,8-dione	276	$C_{17}H_{24}O_3$	905	0.23
24	Heneicosane	296	$C_{21}H_{44}$	924	1.35
25	Benzenepropanoic acid, 3,5-bis(1,1-dimethylethyl)-4-hydroxy-, methyl ester	292	$C_{18}H_{28}O_3$	799	0.53
26	Hexadecanoic acid, methyl ester	270	$C_{17}H_{34}O_2$	864	0.53
27	1,2-Benzenedicarboxylic acid, butyl 2-ethylhexyl ester	334	$C_{20}H_{30}O_4$	927	0.39
28	Pentanal, oxime	101	$C_5H_{11}NO$	729	0.07
29	Sulfurous acid, butyl octyl ester	250	$C_{12}H_{26}O_3S$	810	7.80
30	1-Octanamine	129	$C_8H_{19}N$	759	8.01
31	Dodecanoic acid, ethyl ester	228	$C_{14}H_{28}O_2$	704	0.19
32	Heptadecane, 2-methyl-	254	$C_{18}H_{38}$	933	1.73
33	Phenylpyruvic acid oxime, 2TMS derivative	323	$C_{15}H_{25}NO_3Si_2$	672	0.14
34	1-Hexadecanol	242	$C_{16}H_{34}O$	928	0.68
35	2-Ethylhexyl methyl isophthalate	292	$C_{17}H_{24}O_4$	805	0.02
36	Heptadecane, 2-methyl-	254	$C_{18}H_{38}$	937	0.70
37	9,12-Octadecadienoic acid (Z,Z)-	280	$C_{18}H_{32}O_2$	867	0.55
38	Hexadecanoic acid, 15-methyl-, methyl ester	284	$C_{18}H_{36}O_2$	765	0.22
39	Oleic Acid	282	$C_{18}H_{34}O_2$	926	1.62

40	Hexanamide	115	$C_6H_{13}NO$	640	1.62
41	1-Ethylsulfanylmethyl-2,8,9-trioxa-5-aza-1-sila-bicyclo[3.3.3]undecane	249	$C_9H_{19}NO_3SSi$	733	0.15
42	Dodecanamide	199	$C_{12}H_{25}NO$	932	5.99
43	Octadecanoic acid	284	$C_{18}H_{36}O_2$	877	1.34
44	Hexasiloxane, tetradecamethyl-	458	$C_{14}H_{42}O_5Si_6$	708	0.27
45	1-Acetoxynonadecane	326	$C_{21}H_{42}O_2$	861	0.29
46	Heptadecane, 2-methyl-	254	$C_{18}H_{38}$	922	0.94
47	Nonanamide	157	$C_9H_{19}NO$	673	0.34
48	Dodecyl acrylate	240	$C_{15}H_{28}O_2$	899	0.82
49	Benzyl butyl phthalate	312	$C_{19}H_{20}O_4$	878	0.09
50	Heptacosane	380	$C_{27}H_{56}$	920	0.63
51	9,12-Octadecadienoic acid, methyl ester, (E,E)-	294	$C_{19}H_{34}O_2$	762	0.31
52	9-Octadecenamide, (Z)-	281	$C_{18}H_{35}NO$	928	13.43
53	Hexasiloxane, 1,1,3,3,5,5,7,7,9,9,11,11-dodecamethyl-	430	$C_{12}H_{38}O_5Si_6$	711	0.74
54	Tetradecanamide	227	$C_{14}H_{29}NO$	910	3.82
55	Hexanedioic acid, bis(2-ethylhexyl) ester	370	$C_{22}H_{42}O_4$	752	0.17
56	Heptacosane	380	$C_{27}H_{56}$	916	0.76
57	Diisooctyl phthalate	390	$C_{24}H_{38}O_4$	807	0.06
58	1H-Indene, 1-hexadecyl-2,3-dihydro-	342	$C_{25}H_{42}$	556	0.09

59	Hexasiloxane, 1,1,3,3,5,5,7,7,9,9,11,11-dodecamethyl-	430	$C_{12}H_{38}O_5Si_6$	707	0.65
60	Decanoic acid, 2-ethylhexyl ester	284	$C_{18}H_{36}O_2$	815	0.73
61	Heptacosane	380	$C_{27}H_{56}$	919	0.44
62	Diisooctyl phthalate	390	$C_{24}H_{38}O_4$	913	20.44
63	Dotriacontane	450	$C_{32}H_{66}$	921	0.56
64	Hexasiloxane, tetradecamethyl-	458	$C_{14}H_{42}O_5Si_6$	709	0.46
65	1H-Indene, 1-hexadecyl-2,3-dihydro-	342	$C_{25}H_{42}$	667	0.09
66	Decanoic acid, 2-ethylhexyl ester	284	$C_{18}H_{36}O_2$	806	0.66
67	Dotriacontane	450	$C_{32}H_{66}$	923	0.56
68	1,3-Benzenedicarboxylic acid, bis(2-ethylhexyl) ester	390	$C_{24}H_{38}O_4$	828	0.19
69	Hexasiloxane, tetradecamethyl-	458	$C_{14}H_{42}O_5Si_6$	723	0.48
70	Decanedioic acid, bis(2-ethylhexyl) ester	426	$C_{26}H_{50}O_4$	634	0.09
71	Heptacosane	380	$C_{27}H_{56}$	870	0.43
72	1-Iodo-2-methylundecane	296	$C_{12}H_{25}I$	882	0.37
73	8,10-Undecadiene-3,7-dione, 6,6,10-trimethyl-, (E)-	222	$C_{14}H_{22}O_2$	543	0.56
74	Benzenamine, 4-octyl-N-(4-octylphenyl)-	393	$C_{28}H_{43}N$	548	0.56
75	Hexasiloxane, tetradecamethyl-	458	$C_{14}H_{42}O_5Si_6$	723	0.56
76	Heptacosane	380	$C_{27}H_{56}$	923	0.24
77	Unknown 1	336	$C_{24}H_{20}N_2$	486	0.02

78	(-)-Neoclovene-(II), dihydro-	206	$C_{15}H_{26}$	729	0.10
79	Hexasiloxane, 1,1,3,3,5,5,7,7,9,9,11,11-dodecamethyl-	430	$C_{12}H_{38}O_5Si_6$	679	0.87
80	Unknown 2	454	$C_{23}H_{35}BrO_4$	485	0.05
81	1-Iodo-2-methylundecane	296	$C_{12}H_{25}I$	862	0.63
82	Unknown 3	142	$C_7H_{14}OSi$	472	0.63
83	4,8,12,16-Octadecatetraen-1-ol, 4,9,13,17-tetramethyl-	318	$C_{22}H_{38}O$	699	0.20
84	Hexasiloxane, tetradecamethyl-	458	$C_{14}H_{42}O_5Si_6$	700	0.58
85	(7a-Isopropenyl-4,5-dimethyloctahydroinden-4-yl)methanol	222	$C_{15}H_{26}O$	689	0.20
86	Methanol, [4-(1,1-dimethylethyl)phenoxy]-, acetate	222	$C_{13}H_{18}O_3$	582	0.03
87	1-Octadecanesulphonyl chloride	352	$C_{18}H_{37}ClO_2S$	751	0.68
88	1,1,1,5,7,7,7-Heptamethyl-3,3-bis(trimethylsiloxy)tetrasiloxane	444	$C_{13}H_{40}O_5Si_6$	690	0.54
89	Unknown 4	468	$C_{18}H_{45}AsO_3Si_3$	449	0.01
90	Hexasiloxane, tetradecamethyl-	458	$C_{14}H_{42}O_5Si6$	710	0.4261
91	4-tert-Amylphenol, TMS derivative	236	$C_{14}H_{24}OSi$	613	0.01
92	3,5-Decadien-7-yne, 6-t-butyl-2,2,9,9-tetramethyl-	246	$C_{18}H_30$	594	0.42
Total					**100**

334 A: Mass spectral similarity to NIST08 library, B: Relative peak area

335
336

3.3.3 Synthesized gold nanoparticle characterization

During the biosynthesis of JLAuNPs, the solution converted immediately from a green to wine color once exposed to the gold salt. This visual color change was confirmed with UV-Vis, as JLAuNPs displayed a spectral peak at 549 nm (Figure 3.3 A). To determine functional groups, present in JL-EtOH and JLAuNPs, FTIR was conducted at a range of 550 to 4000 cm^{-1} (Figure 3.3 B, Table 3.3). The total phenolic content of JLAuNPs was evaluated and was found to be 2.55 mg/mL, while the average diameter and zeta-potential were 166.9 ± 79.64 nm and -23.9 mV, respectively. Furthermore, the morphology of JLAuNPs was determined using HRTEM, which consisted mostly of irregular and round shapes with a few triangular nanoparticles (Figure 3.3 C). A selected area diffraction pattern (SAED) was used to characterize whether JLAuNPs were similar to gold metal. The face-centered lattice of JLAuNP displayed a Bragg reflection of (111), (200), (220) and (311) (Figure 3.3 D). *In vitro* stability indicated that JLAuNPs displayed minimal shifts in the surface plasmon resonance peak (λ_{max}) when exposed to various mediums (Figure 3.4).

Table 3.3. Potential functional groups were identified using Fourier transform infrared spectrometry (FTIR) in the ethanolic extract (JL-EtOH) and synthesized gold nanoparticles (JLAuNPs) of *Juncus lomatophyllus*.

Functional groups	JL-EtOH transmittance (cm^{-1})	JLAuNPs transmittance (cm^{-1})
O-H	3305	3321
C-H	2922	-
C-O	1257	-
Aromatic ring (C-C)	-	1637

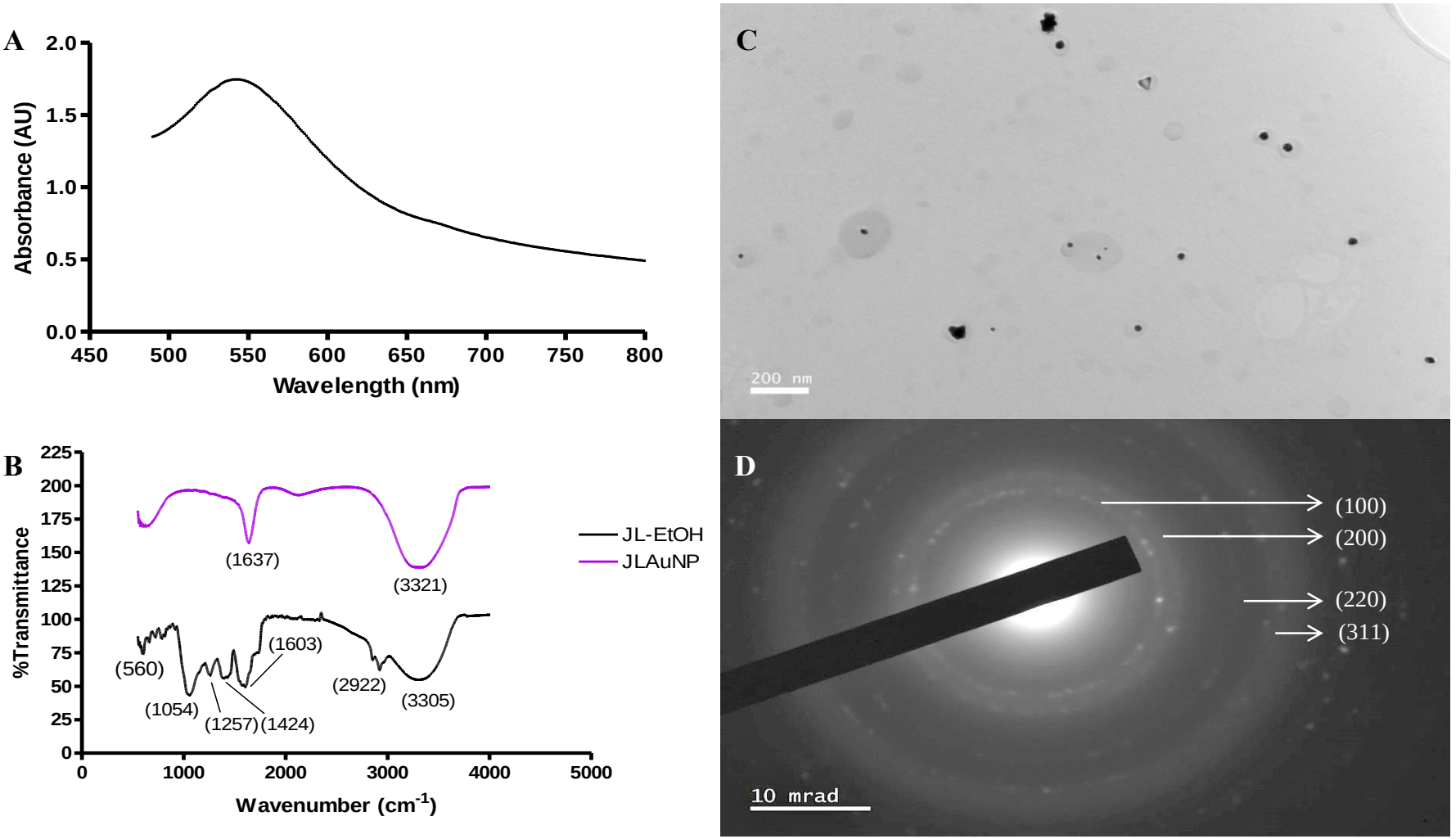

356

357 **Figure 3.3. Gold nanoparticle characterization including ultraviolet-visible (UV-Vis) spectroscopy (A), Fourier-transform infrared spectrometry (FTIR) of the**
358 **ethanolic extract (JL-EtOH) and synthesized gold nanoparticles (JLAuNPs) (B), high-resolution transmission electron microscopy (HRTEM) at 200 nm (C) and**
359 **selected area diffraction pattern (SAED) at 10 mrad (D).**

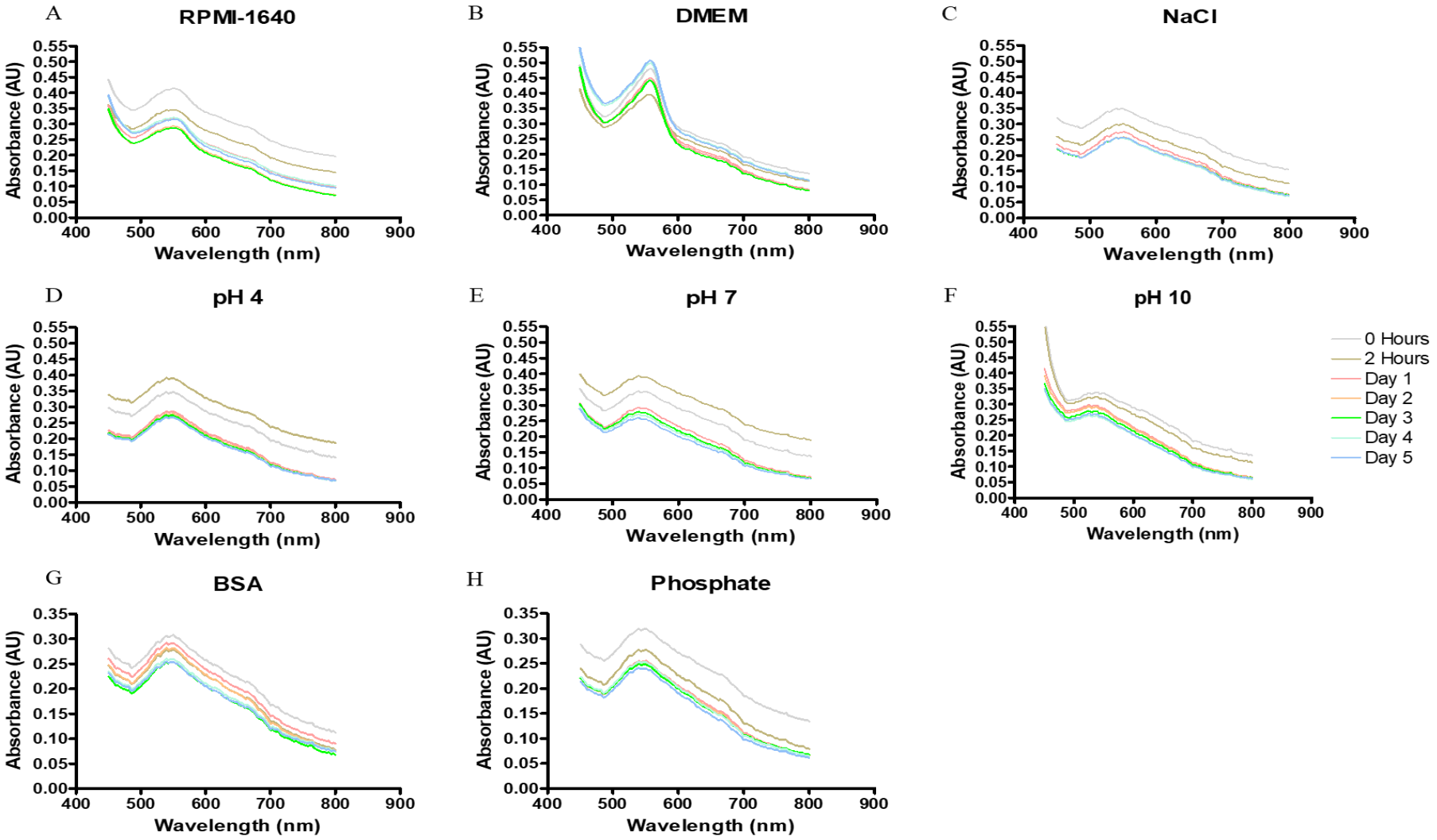

Figure 3.4. ***In vitro*** **stability of** ***Juncus lomatophyllus*** **synthesized gold nanoparticles (JLAuNPs) in different mediums. These solutions include Roswell Park Memorial Institution (RPMI-1640) medium (A), Dulbecco's modified Eagle's Medium (DMEM) (B), 5% sodium chloride (NaCl) (C), pH level of 4 (D), 7 (E) and 10 (F), 0.5% bovine serum albumin (BSA) (G) and phosphate buffer (pH 6.5) (H).**

3.3.4 Tyrosinase inhibition

An anti-tyrosinase activity assay was conducted on JLAuNP, JL-EtOH and JLF. JLAuNP (IC_{50} of 268.8 ± 5.64 µg/mL) displayed higher anti-tyrosinase activity in comparison to JL-EtOH and JLF (IC_{50} > 400 µg/mL).

3.3.5 Antiproliferative activity

The antiproliferative activity of JL-EtOH, JLB and JLAuNPs was evaluated against human keratinocytes (HaCaT) and peripheral blood mononuclear cells (PBMCs). None of the selected samples displayed antiproliferative activity against HaCaT cells and PBMCs (IC_{50} > 400 µg/mL). The positive controls, actinomycin D and 20% DMSO displayed an IC_{50} of 0.01 ± 0.002 µg/mL and 10.41 ± 3.66%, respectively.

3.3.6 TNF-α quantification

Cell viability was conducted to ensure the modulation of lipopolysaccharide (LPS) stimulated TNF-α was not due to cell death. Compared to the respected controls, as displayed in Figures 3.5 and 6, JL-EtOH, JLAuNPs ($p < 0.001$) and JLB ($p < 0.01$) at 400 µg/mL displayed a significant decrease in cell viability. Thus, concentrations of 200, 100 and 50 µg/mL were selected for further evaluation. Furthermore, JL-EtOH, JLB and JLAuNPs were evaluated for their effect against TNF-α production using LPS stimulated PBMCs (Figure 3.7). Compared to the untreated control (42.40 ± 4.17), JLAuNPs (23.59 ± 1.95 pg/mL) significantly inhibited ($p < 0.05$) the production of TNF-α at 200 µg/mL, while 0.25% DMSO (vehicle control) (38.41 ± 0.98), JLAuNPs at 100 (34.28 ± 0.98) and 50 µg/mL (37.00 ± 7.27 pg/mL) displayed no significant effect (Figure 3.7). In comparison to the vehicle control, JL-EtOH (25.48 ± 7.56, 29.45 ± 2.93 and 26.34 ± 1.46 pg/mL) and JLB (30.79 ± 5.80, 26.13 ± 7.02 and 46.83 ± 6.54 pg/mL) at a concentration of 200, 100 and 50 µg/mL displayed no significant effect.

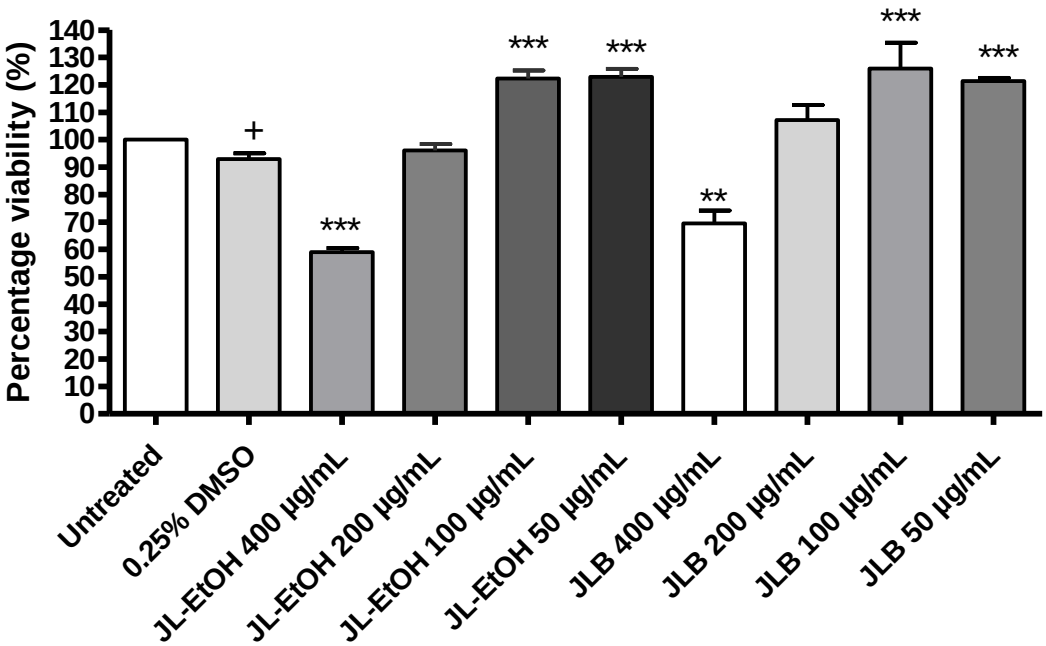

Figure 3.5. Cell viability after treatment with *Juncus lomatophyllus* ethanolic extract (JL-EtOH) and butanol partition (JLB) at a concentration range of 400-50 µg/mL on lipopolysaccharide (LPS) stimulated

peripheral blood mononuclear cells (PBMCs). Data represent mean ± SEM (n=3). Significant difference was determined using a one-way ANOVA followed by Dunnett's multiple comparison test, where $p < 0.05$ (*), $p < 0.01$ (**) and $p < 0.001$ (***) indicate significance when compared to the 0.25% DMSO vehicle control (+).

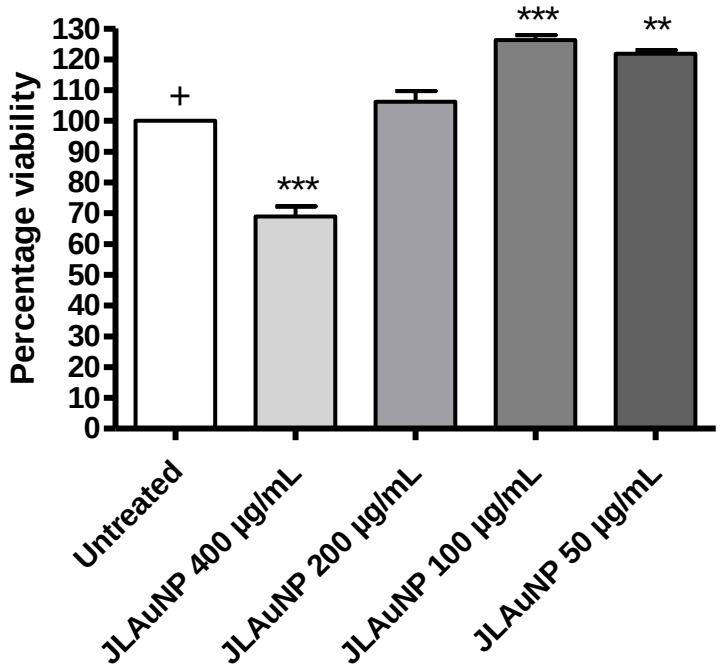

Figure 3.6. Cell viability after treatment with *Juncus lomatophyllus* synthesized gold nanoparticles (JLAuNPs) at a concentration range of 400-50 µg/mL on lipopolysaccharide (LPS) stimulated peripheral blood mononuclear cells (PBMCs). Data represent mean ± SEM (n=3). Significant difference was determined using a one-way ANOVA followed by Dunnett's multiple comparison test, where $p < 0.01$ (**) and $p < 0.001$ (***) indicate significance when compared to the untreated control (+).

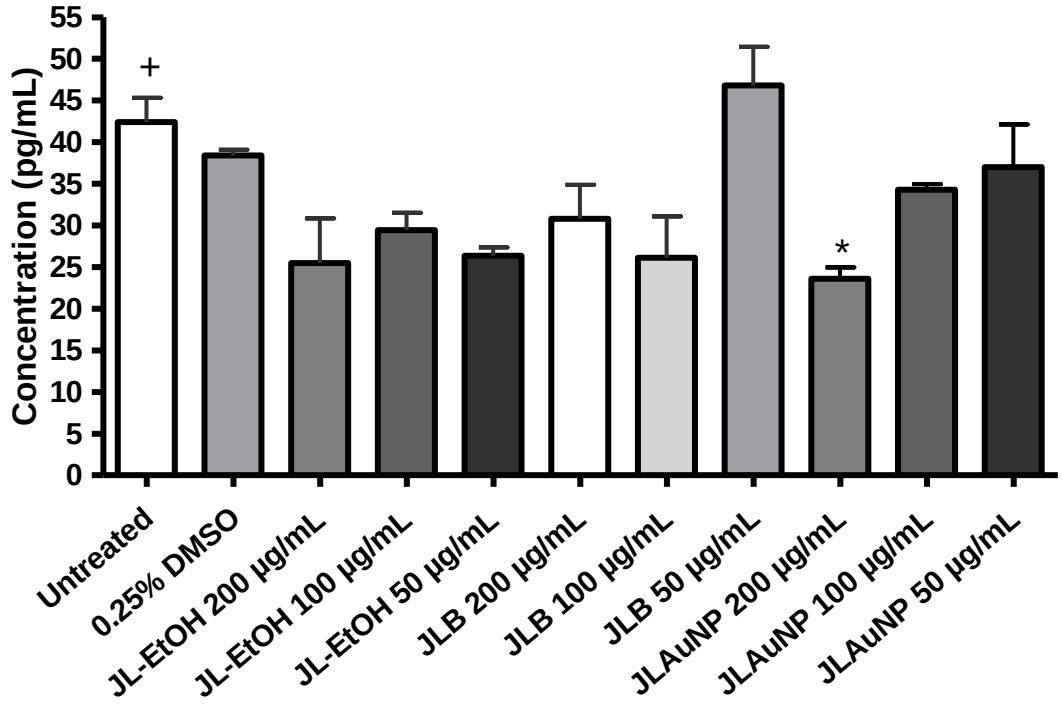

Figure 3.7. Effect of *Juncus lomatophyllus* ethanolic extract (JL-EtOH), butanol partition (JLB) and synthesized gold nanoparticles (JLAuNPs), at a concentration of 200, 100 and 50 µg/mL, against the production of tumor necrosis factor-alpha (TNF-α). Data are represented as mean TNF-α production ± SEM (n=2). A significant difference was determined using one-way ANOVA followed by a Dunnett's multiple comparison test, where $p < 0.05$ (*), indicates a significant difference when compared to the untreated control (+).

3.4 Discussion

Characterization of JLAuNPs was conducted due to the potential impact the size, morphology, stability and the functional groups may have on the biological activity (De Canha et al., 2021). The Bragg reflections observed for JLAuNP during HRTEM were similar to those that were previously reported for gold (Au) (Philip, 2009). Vibration stretches located at the O-H and C-C functional groups indicated the presence of phenolic compounds, supporting the high total phenolic content that was obtained (Sathishkumar et al., 2016).

The stability of the nanoparticles was evaluated in different mediums, which mimicked physiological environments. Furthermore, the duration of the assay was determined by the timeframe required to evaluate the antiproliferative effects of the nanoparticle on HaCaT cells and PBMCs. Minimal shifts in the surface plasmon resonance peak for most of the buffers and media were observed during the *in vitro* stability assay, which could be due to the electrostatic repulsion of JLAuNP (-23.9 mV), which has shown little to no tendency for aggregation. This corresponded with a study conducted by Thipe et al. (2019), as a similar zeta potential was obtained for the synthesized nanoparticles of resveratrol (Thipe et al., 2019).

As of current, no biological activity or compound isolation has been conducted on *J. lomatophyllus*. In a study conducted by Wang et al. (2016), Chinese herbs were selected and inoculated with *B. bifidum* which demonstrated a higher percentage inhibition towards tyrosinase than their crude counterparts (Wang et al., 2016). Thus, the high IC_{50} value obtained for JLF (> 400 µg/mL) could be due to the inability of the bioactive compounds to undergo fermentation resulting in no activity.

JLB and JLAuNPs displayed the highest anti-tyrosinase activity. Previous studies conducted by Pérez et al. (2017) and Chiou et al. (2015) observed similar results (Chiou et al., 2015; Pérez et al., 2017). Pérez et al. (2017) observed that the anti-tyrosinase activity of gold nanoparticles synthesized using ginseng berries (IC_{50}: 7.7 ± 0.6 µg/mL) was enhanced with an IC_{50} of 6.6 ± 0.3 µg/mL (Pérez et al., 2017). The anti-tyrosinase potential of JLAuNPs could be due to the increased bioavailability of flavonoids. This is because previous studies have indicated that plant loaded nanoparticles increase the bioavailability of poorly water-soluble phytochemicals including flavonoids (Husni and Ramadhania, 2021). Furthermore, these compounds could be responsible for the presence of O-H and C-C functional groups that were identified. Moreover, this supports the inhibitory effect JLAuNP displayed against TNF-α production in comparison to JL-EtOH (IC_{50} > 400 µg/mL) as flavonoids have previously displayed anti-inflammatory properties (Guven et al., 2019).

Chiou et al. (2015) indicated that the butanol partition of both the fruit and seed shells of *Camellia tenuifloria* (Hayata) Cohen-Stuart displayed the highest inhibition against tyrosinase with IC_{50} values of 70.0 ± 5.5 and 32.7 ± 0.4 µg/mL, respectively. This could be due to the hydroxyl groups of flavonoids and the presence of terpenes and steroids which have previously shown tyrosinase inhibitory activity and have been isolated from *Juncus* genus (Chiou et al., 2015; El-Shamy et al., 2015). An increase in IC_{50} value for P1 (155.70 ± 4.95), P4 (105.55 ± 7.28) and P5 (125.60 ± 3.68 µg/mL) were observed compared to JLB (40.4 ± 2.31 µg/mL), suggesting that JLB anti-tyrosinase properties may rely on synergistic effects. These effects have been examined in previous studies whereby the combination of more than one compound lowers the IC_{50} value (Rasoanaivo et al., 2011). Furthermore, it was observed that P4 contained n-hexadecanoic acid (2.81%), which has previously displayed anti-tyrosinase properties. According to Panda et al. (2018), n-hexadecanoic acid (peak area of 10.15%) was one of the saturated fatty acids responsible for the anti-tyrosinase activity of *Bauhinia vahlii* Wight & Arn. with an IC_{50} of 98.70 ± 0.70 µg/mL (Panda et al., 2018).

No information, as of current, could be found on the antiproliferative effect of JLB, JL-EtOH and JLAuNP. One study on the effects of gold ions on HaCaT cells displayed no significant effect at a concentration of 100 µM after 24 hours of exposure, which aligns with the IC_{50} value obtained for JLAuNP (Dasari et al., 2015). Moreover, a study conducted by Lorenzo-Anota et al. (2021) concluded that chitosan-coated AuNP displayed no significant effect on cell viability when exposed to concanavalin A stimulated PBMCs at a concentration of 100 µM for 24 hours, which suggests that gold nanoparticles display no antiproliferative activity against PBMCs (Lorenzo-Anota et al., 2021).

3.5 Conclusion

In this study, three main aims were considered due to the limited amount of information that could be found on *Juncus lomatophyllus*. These included identifying the effect JL-EtOH had on the production of tyrosinase and TNF-α and whether the biological activity of JL-EtOH was enhanced when fermented or when used to form gold nanoparticles. Furthermore, this study aims to identify potentially active compounds present using bioassay-guided

fractionation. Seven semi-pure fractions were pooled from JLB, of which P4 and P5 displayed the highest anti-tyrosinase activity. GC-MS concluded that 78 and 92 constituents were present in P4 and P5. n-Hexadenoic acid, which was present in P4 has previously displayed anti-tyrosinase activity.

JLAuNPs displayed enhanced anti-tyrosinase activity in comparison to JL-EtOH and JLF (IC_{50} > 400 µg/mL). JLAuNP, JLB and JL-EtOH were selected for further evaluation and displayed no antiproliferative effects against HaCaT cells and PBMCs (IC_{50} > 400 µg/mL). JLAuNPs significantly inhibited TNF-α production while JL-EtOH and JLB displayed no significant effect at the highest testing concentration (200 µg/mL). In conclusion, JLAuNPs anti-tyrosinase activity and ability to reduce TNF-α production could be due to the increased bioavailability of flavonoids enhancing its biological activity in comparison to JL-EtOH. Furthermore, JLAuNPs potential inhibitory effect against TNF-α correlates with its reducing effects on the expression of tyrosinase in comparison to JL-EtOH. Further isolation and purification should be conducted on JLB to identify potential anti-tyrosinase compounds that could be present. Furthermore, investigations into JLAuNPs potential effect on translators such as nuclear factor kappa beta (NF-κB) that are associated with the production of TNF-α should be considered.

Conflict of Interest

The authors declare that the research was conducted in the absence of any commercial or financial relationships that could be construed as a potential conflict of interest.

Funding

This work was supported by the National Research Foundation [grant number 105169 and 98334] and the Water Research Commission [contract number C2019/2020-00132].

Acknowledgments

The authors would like to acknowledge Mrs. Bianca D. Payne and Mrs. Tenille Esmear (Department of Plant and Soil Sciences, University of Pretoria) for their guidance. Furthermore, the authors would like to acknowledge Dr. Yvette Naudé (Department of Chemistry, University of Pretoria) for conducting the GC-MS analysis, Dr. Suprakas S. Ray (DST/CSIR National Centre for Nanostructured Materials, Council for Scientific and Industrial Research), Prof Kattesh V. Katti, Dr. Velaphi C. Thipe (Department of Radiology, Institute of Green Nanotechnology, University of Missouri Columbia), Dr. Vusani Mandiwana, Michel L. Kalombo (Chemical Cluster, Centre for Nanostructures and Advanced Materials, Council for Scientific and Industrial Research) and Dr. Arno Janse van Vuuren (Centre for High Resolution Transmission Electron Microscopy, Nelson Mandela University) for conducting the FTIR, DLS, zeta potential and HRTEM analysis.

References

Brandt, E.B., and Sivaprasad, U. (2011). Th2 Cytokines and Atopic Dermatitis. *Journal of clinical & cellular immunology* 2(3)**,** 1-25. doi: 10.4172/2155-9899.1000110

Bús, C., Tóth, B., Stefkó, D., Hohmann, J., and Vasas, A. (2018). Family Juncaceae: promising source of biologically active natural phenanthrenes. *Phytochemistry Reviews* 17(4)**,** 833-851.

Chamlin, S.L., Kao, J., Frieden, I.J., Sheu, M.Y., Fowler, A.J., Fluhr, J.W., et al. (2002). Ceramide-dominant barrier repair lipids alleviate childhood atopic dermatitis: changes in barrier function provide a sensitive indicator of disease activity. *Journal of the American Academy of Dermatology* 47(2)**,** 198-208. doi: 10.1067/mjd.2002.124617

Chiou, S.-Y., Ha, C.-L., Wu, P.-S., Yeh, C.-L., Su, Y.-S., Li, M.-P., et al. (2015). Antioxidant, anti-tyrosinase and anti-inflammatory activities of oil production residues from Camellia tenuifloria. *International journal of molecular sciences* 16(12)**,** 29522-29541.

Dasari, T.S., Zhang, Y., and Yu, H. (2015). Antibacterial activity and cytotoxicity of gold (I) and (III) ions and gold nanoparticles. *Biochemistry & pharmacology: open access* 4(6).

Davis, E.C., and Callender, V.D. (2010). Postinflammatory hyperpigmentation: a review of the epidemiology, clinical features, and treatment options in skin of color. *The Journal of Clinical and Aesthetic Dermatology* 3(7)**,** 20-31.

De Canha, M.N., Thipe, V.C., Katti, K.V., Mandiwana, V., Kalombo, L., Ray, S.S., et al. (2021). The activity of gold nanoparticles synthesized using Helichrysum odoratissimum against Cutibacterium acnes biofilms. *Frontiers in cell and developmental biology***,** 2288.

El-Shamy, A.I., Abdel-Razek, A.F., and Nassar, M.I. (2015). Phytochemical review of *Juncus* L. genus (Fam. Juncaceae). *Arabian Journal of Chemistry* 8(5)**,** 614-623.

Gelmetti, C., and Wollenberg, A. (2014). Atopic dermatitis–all you can do from the outside. *British Journal of Dermatology* 170(1)**,** 19-24. doi: 10.1111/bjd.12957

Guven, B., Can, M., Piskin, O., Aydin, B.G., Karakaya, K., Elmas, O., et al. (2019). Flavonoids protect colon against radiation induced colitis. *Regulatory Toxicology and Pharmacology* 104**,** 128-132.

Hengge, U.R., Ruzicka, T., Schwartz, R.A., and Cork, M.J. (2006). Adverse effects of topical glucocorticosteroids. *Journal of the American Academy of Dermatology* 54(1)**,** 1-15.

Husni, P., and Ramadhania, Z.M. (2021). Plant Extract Loaded Nanoparticles. *Indonesian Journal of Pharmaceutics* 3(1)**,** 38-49.

Lall, N., Blom van Staden, A., Rademan, S., Lambrechts, I., De Canha, M.N., Mahore, J., et al. (2019). Antityrosinase and anti-acne potential of plants traditionally used in the Jongilanga community in Mpumalanga. *South African Journal of Botany* 126**,** 241-249. doi: https://doi.org/10.1016/j.sajb.2019.07.015

Lorenzo-Anota, H.Y., Zarate-Triviño, D.G., Uribe-Echeverría, J.A., Ávila-Ávila, A., Rangel-López, J.R., Martínez-Torres, A.C., et al. (2021). Chitosan-Coated Gold Nanoparticles Induce Low Cytotoxicity and Low ROS Production in Primary Leucocytes, Independent of Their Proliferative Status. *Pharmaceutics* 13(7)**,** 942.

Mansouri, Y., and Guttman-Yassky, E. (2015). Immune pathways in atopic dermatitis, and definition of biomarkers through broad and targeted therapeutics. *Journal of clinical medicine* 4(5)**,** 858-873. doi: 10.3390/jcm4050858

Mhlongo, L., and Van Wyk, B.-E. (2019). Zulu medicinal ethnobotany: new records from the Amandawe area of KwaZulu-Natal, South Africa. *South African Journal of Botany* 122**,** 266-290.

Narayanaswamy, R., and Ismail, I.S. (2015). Cosmetic potential of Southeast Asian herbs: an overview. *Phytochemistry Reviews* 14(3)**,** 419-428. doi: https://doi.org/10.1007/s11101-015-9396-2

Oosthuizen, C., Arbach, M., Meyer, D., Hamilton, C., and Lall, N. (2017). Diallyl polysulfides from *Allium sativum* as immunomodulators, hepatoprotectors, and antimycobacterial agents. *Journal of Medicinal Food* 20(7)**,** 685-690. doi: https://doi.org/10.1089/jmf.2016.0137

Panda, P., Dash, P., and Ghosh, G. (2018). Chemometric profile, antioxidant and tyrosinase inhibitory activity of Camel's foot creeper leaves (Bauhinia vahlii). *Natural product research* 32(5)**,** 596-599.

Park, M.-J., and Bae, Y.-S. (2016). Fermented Acanthopanax koreanum root extract reduces UVB-and H 2 O 2-induced senescence in human skin fibroblast cells. *Journal of microbiology and biotechnology* 26(7)**,** 1224-1233.

Parvez, S., Kang, M., Chung, H.S., and Bae, H. (2007). Naturally occurring tyrosinase inhibitors: mechanism and applications in skin health, cosmetics and agriculture industries. *Phytotherapy Research* 21(9)**,** 805-816. doi: https://doi.org/10.1002/ptr.2184

Pérez, Z.E.J., Ramya Mathiyalagan, J.M., Kim, Y.-J., Kang, H.M., Abbai, R., Seo, K.H., et al. (2017). Ginseng-berry-mediated gold and silver nanoparticle synthesis and evaluation of their in vitro antioxidant, antimicrobial, and cytotoxicity effects on human dermal fibroblast and murine melanoma skin cell lines. *International journal of nanomedicine* 12**,** 709.

Philip, D. (2009). Biosynthesis of Au, Ag and Au–Ag nanoparticles using edible mushroom extract. *Spectrochimica Acta Part A: Molecular and Biomolecular Spectroscopy* 73(2)**,** 374-381.

Rasoanaivo, P., Wright, C.W., Willcox, M.L., and Gilbert, B. (2011). Whole plant extracts versus single compounds for the treatment of malaria: synergy and positive interactions. *Malaria journal* 10(1)**,** 1-12.

Rezzani, R. (2004). Cyclosporine A and adverse effects on organs: histochemical studies. *Progress in histochemistry and cytochemistry* 39(2)**,** 85-128.

Sathishkumar, G., Jha, P.K., Vignesh, V., Rajkuberan, C., Jeyaraj, M., Selvakumar, M., et al. (2016). Cannonball fruit (Couroupita guianensis, Aubl.) extract mediated synthesis of gold nanoparticles and evaluation of its antioxidant activity. *Journal of Molecular Liquids* 215**,** 229-236.

Song, M.-Y., Park, S.-K., Kim, C.-S., Yoo, T.H., Kim, B., Kim, M.-S., et al. (2008). Characterization of a novel anti-human TNF-α murine monoclonal antibody with high binding affinity and neutralizing activity. *Experimental & molecular medicine* 40(1)**,** 35-42. doi: 10.3858/emm.2008.40.1.35

Thipe, V.C., Amiri, K.P., Bloebaum, P., Karikachery, A.R., Khoobchandani, M., Katti, K.K., et al. (2019). Development of resveratrol-conjugated gold nanoparticles: Interrelationship of increased resveratrol corona on anti-tumor efficacy against breast, pancreatic and prostate cancers. *International journal of nanomedicine* 14**,** 4413.

Wang, G.-H., Chen, C.-Y., Lin, C.-P., Huang, C.-L., Lin, C.-h., Cheng, C.-Y., et al. (2016). Tyrosinase inhibitory and antioxidant activities of three Bifidobacterium bifidum-fermented herb extracts. *Industrial Crops and Products* 89**,** 376-382.

Wentzel, J., and Wentzel, A. (2020). *Juncus lomatophyllus* [Online]. https://wildflowernursery.co.za/indigenous-plant-database/juncus-lomatophyllus/ [ACCESSED 2020 29 April].

Zari, S.T., and Zari, T.A. (2015). A review of four common medicinal plants used to treat eczema. *Journal of Medicinal Plants Research* 9(24)**,** 702-711.

Chapter 4. Anti-elastase potential of *Elegia tectorum* (L. f.) Moline & H. P. Linder

Chapter 4. Anti-elastase potential of *Elegia tectorum* (L. f.) Moline & H. P. Linder [3]

Abstract

Eczema is a common skin condition that is more prevalent in children and can persist throughout one's life. The outside-in hypothesis states that eczema is caused by a disruption of the skin barrier. One of the main symptoms associated with the condition is an intolerable itching sensation caused by the overproduction of histamine, which further leads to the over-expression of elastase which contributes to the formation of wrinkles. The study aimed to determine if the ethanolic extract of *Elegia tectorum* (ET-EtOH) inhibited the production of elastase and histamine. Furthermore, this study investigated whether the biological activity of ET-EtOH was enhanced when fermented using *Bifidobacterium bifidium* (ETF) or when used in the synthesis of gold nanoparticles (ETAuNP). ET-EtOH displayed anti-elastase activity with a fifty percent inhibitory concentration (IC_{50}) of 28.27 ± 2.02 µg/mL, while ETF and ETAuNP displayed no inhibition (IC_{50} > 500 µg/mL). Due to the anti-elastase activity of ET-EtOH, it was further evaluated for its effect on histamine production using phorbol 12-myristate 13-acetate (PMA) stimulated granulocytes. No antiproliferative activity was observed against human keratinocytes (HaCaT) and granulocytes (IC_{50} > 400 µg/mL). Furthermore, ET-EtOH (0.10 ± 0.009 ng/mL) significantly inhibited ($p < 0.01$) histamine production at 6 µg/mL compared to the vehicle control (0.26 ± 0.02 ng/mL). Further investigation into whether ET-EtOH targets histamine-associated receptors on mast cells as a potential mode of action should be considered.

Keywords: Anti-elastase activity, eczema, *Elegia tectorum*, gold nanoparticles

4.1 Introduction

Atopic dermatitis, commonly known as eczema, occurs at any stage in one's life [1]. Two main hypotheses regarding the causation of the condition has been developed, which include the inside-out and outside-in hypotheses [2]. The outside-in hypothesis states that the condition could be due to a disruption occurring in the skin barrier. This disruption can either be caused by a genetic defect, which controls the formation of the skin barrier or due to environmental changes, which lead to sensitization [2].

In eczema patients, there is an increase in histamine production, which leads to an intolerable itching sensation [3]. Histamine, when synthesised, is stored in secretory granules within mature mast cells and basophils along with other mediators such as proteoglycan heparin and chondroitin sulphate E [4-6]. Increased levels of histamine can affect the expression of genes associated with maintaining the epidermal barrier, which includes filaggrin, keratins and proteases. In response to this, filaggrin levels are reduced and the mRNA expression of some keratins is downregulated, however, the expression of proteases (cathepsins and elastase) is increased [7-10]. These proteases affect the inflammatory system and the epidermal barrier by increasing the pH levels of the skin [11]. Elastase is mainly used to remove foreign proteins, however, when overexpressed these proteases degrade elastin, which leads to the formation of wrinkles [12].

Elegia tectorum (L. f.) Moline & H. P. Linder, previously known as *Chondropetalum tectorum* (L.f) Raf., belongs to the Restionaceae family. This plant is mainly used as an

[3] This chapter will be submitted as an original article to the Journal of Aging Research (Hindawi) with an impact factor of 2.400. The format of this chapter was written based on the author guidelines set by the journal.

attractive garden plant and is traditionally used for thatching roofs, weaving baskets and brooms [13, 14]. This native perennial evergreen is located in marshes and wet areas throughout the Western Cape [14, 15]. Limited information has been published on this genus, specifically the medicinal and traditional usage, however, one study reported that *Elegia equisetacea* (Mast.) Mast. is used by the Western Cape Rasta community to bring good luck to the hunters and to protect the huts and crops from storms [16]. Secondary metabolites within the family include flavones (C-glycosides and luteolin), flavonols (myricetin, quercetin, larycitrin, syringetin) and proanthocyanidins [17]. Previously, anti-elastase properties of *E. tectorum* were reported with a 50% inhibitory concentration (IC_{50}) of 13.5 ± 1.5 µg/mL [18]. Thus, this study aimed to confirm the anti-elastase activity of *E. tectorum* and to determine whether the ethanolic extract (ET-EtOH) inhibited histamine production. Furthermore, this study aimed to determine whether fermenting or synthesizing gold nanoparticles using the extract would enhance the biological activity.

4.2 Materials and Methods

4.2.1 Materials, chemicals and reagents

Human keratinocytes (HaCaT) were donated by Dr. Lester Davids from the University of Cape Town. The Dulbecco's modified Eagle's Medium (DMEM), Roswell Park Memorial Institute (RPMI-1640) medium, phosphate-buffered saline (PBS), fetal bovine serum (FBS), PrestoBlue Cell Viability reagent, ammonium-chloride-potassium (ACK) lysing buffer, amphotericin B, streptomycin, penicillin and Eutech pH buffer solutions (pH 4, 7 and 10) were obtained from ThermoFisher Scientific (Johannesburg, South Africa). Cell culture plates and flasks were purchased from LasecSA (Pty) Ltd. (Midrand, South Africa). The histamine (ab213975) ELISA kit was sourced from BIOCOM Africa (Pty) Ltd. (Lyttleton Manor, South Africa). Phorbol 12-myristate 13-acetate (PMA), histopaque, ethylenediaminetetraacetic acid (EDTA) and other chemicals and reagents such as dimethyl sulfoxide (DMSO), gum arabic, actinomycin D (purity >95%), gold (III) chloride trihydrate ($HAuCl_4.3H_2O$), bovine serum albumin (BSA), sodium chloride (NaCl), *N*-succinyl-Ala-Ala-Ala-ρ-nitroanilide substrate, gentamicin solution, elastase enzyme powder and ursolic acid were obtained from Sigma-Aldrich (Johannesburg, South Africa).

4.2.2 Plant collection and extraction

The stems of *E. tectorum* were collected in March (2016) from Manie van der Schijff Botanical Gardens at the University of Pretoria (PRU: 122257), rinsed with distilled water (dH_2O), placed in a -80˚C freezer for three days. Afterward, the samples were freeze-dried for a week. Once dry, the samples were ground into a fine powder using an IKA grinder (MF 10.1 Head 2870900) with a 2 mm sieve. Afterward, 307.90 g of powder was mixed with 1.54 mL of absolute ethanol (1:5) and placed on a shaker for three days. Thereafter, the solution was filtered using a Whatman no 1 filter paper and concentrated using a rotary evaporator. The percentage yield was calculated for each extract using Equation 1.

$$\%\text{Yield} = \left(\frac{Extract\ weight\ (g)}{Powdered\ or\ fresh\ material\ weight\ (g)}\right) \times 100 \quad (1)$$

The final quantity of the concentrated extract was 11.09 g with a percentage yield of 3.60%. The concentrated plant extract was stored at 4˚C.

4.2.3 Fermentation

ET-EtOH was fermented using *Bifidobacterium bifidum* (ATCC 11863) according to the method of Park and Bae [19], with modifications. *Bifidobacterium bifidum* colonies were cultures from Kwik Sticks on Bifidus Selective Medium (BSM)-Agar supplemented with BSM-Supplement (stock solution of 23.2 g/L) while single colonies were grown on BSM-Broth at 37˚C for 48 hours. Bacterial suspensions were prepared in accordance with an 8 McFarland standard (112×10^8 CFU/mL) at a wavelength of 600 nm. ET-EtOH (10 mg/mL) was supplemented with 1% ethanol solution (w/v), warmed BSM-Broth and inoculated with 4% bacterial suspension (v/v) at a final volume of 50 mL. After fermentation for six weeks at 37˚C with weekly agitations, the extract was sonicated for five minutes at 45˚C, freeze-dried and stored at 4˚C. A vehicle and negative control was included consisting of all the components with one exception. The negative control did not contain any bacteria while the JL-EtOH was substituted with 0.5 mL of EtOH in the vehicle control.

4.2.4 Synthesis of gold nanoparticle

To synthesis gold nanoparticles using *Elegia tectorum*, ET-EtOH was dissolved in dH_2O (2 mg/mL) and heated until 60˚C was reached. Due to the inability of ET-EtOH to homogenize with water, the solution was centrifuged and 50 mL of collected supernatant was combined with 165 mg of gum arabic powder, which was used as a stabilizer. Thereafter, the mixture was heated to 70˚C whereby 0.1 M of gold salt was added. An immediate colour change was observed whereby the solution went from a green to a wine colour.

4.2.5 Characterization of synthesised gold nanoparticles

4.2.5.1 Ultraviolet-visible (UV-Vis) spectrometry

To confirm the formation of gold nanoparticles, a full spectral scan was conducted using ultraviolet-visible spectrometry (UV-Vis) to determine if the surface plasmon resonance (SPR) was similar to gold metal (Au). In a 96-well plate, 100 µL of the synthesized gold nanoparticles (ETAuNPs) solution was added and the absorbance was read between 450-800 nm at 50 nm increments using a Victor Nivo plate reader (PerkinElmer, Midrand, South Africa).

4.2.5.2 *In vitro* stability

In vitro stability of the ETAuNPs was evaluated in various mediums consisting of buffer solutions and cell culture mediums, which included 0.5% bovine serum albumin (BSA), 5% sodium chloride (NaCl), pH buffer solutions of 4, 7 and 10, phosphate buffer (pH 6.5), Dulbecco's Modified Eagles medium (DMEM) and Roswell Park Memorial Institute (RPMI-1640) medium. ETAuNPs were added to the abovementioned solutions at a 1:1 ratio with a final volume of 1.5 mL and were incubated at 37˚C. To confirm whether the nanoparticles were stable, the SPR peaks (λ_{max}) between 450 and 800 nm were measured using a Victor Nivo plate reader at 0, 2, 24 (Day 1), 48 (Day 2), 72 (Day 3), 96 (Day 4) and 120 hours (Day 5).

4.2.5.3 High-resolution transmission electron microscopy (HRTEM)

High-resolution transmission electron microscopy was used to identify the particle size and shape of ETAuNPs. Furthermore, the crystallinity was identified through selected area electron diffraction (SAED). Five microlitres of ETAuNPs solution were loaded onto a carbon-coated copper TEM grid and allowed to dry. Thereafter, the grids were loaded into a JEOL JEM- ARM200F double Cs-corrected transmission electron microscope equipped with

a large solid angle energy dispersive spectrometer (EDS) (Akishima, Tokyo, Japan) and images were captured.

4.2.5.4 Quantification of the total phenolic content present in the synthesized nanoparticles

The total phenolic content was quantified using the Folin Cioalteau as described by De Canha [20]. A standard curve was prepared from ET-EtOH that was serially diluted two-fold, in dH_2O, resulting in a final concentration range of 4000-31.25 µg/mL. In a 2 mL Eppendorf tube, 125 µL of 7.5% (w/v) sodium bicarbonate solution (Na_2CO_3) and 125 µL 10% (v/v) Folin Cioalteau reagent (1 in 10 mL dH_2O) were added to 250 µL of each dilution and to 250 µL of ETAuNPs solution. Thereafter, 100 µL of each solution was transferred into a 96-well plate and incubated at 30˚C for 30 minutes in the dark. Blanks for ET-EtOH and ETAuNPs consisted of 250 µL of sample, 7.5% Na_2CO_3 and dH_2O in the place of 10% Folic Cioalteau. The absorbance was measured at 765 nm using a Victor Nivo plate reader and the phenolic content of ETAuNPs was determined using the equation generated from the standard curve ($y = 0.0001x + 0.0157$, $R^2 = 0.9414$). The quantified phenolic content was used as the highest stock concentration in each of the bioassays that were conducted.

4.2.5.5 Dynamic light scattering (DLS)

To determine the hydrodynamic size of the ETAuNPs, 1 mL of the ETAuNPs was transferred into a zeta cell and read using a Zetasizer Nano ZS instrument (Malvern Instruments Ltd., Malvern, Worcestershire, UK). Three reads were performed, and the average was obtained Dynamic light scattering (DLS).

4.2.5.6 Zeta potential

The electrostatic charge of ETAuNPs was identified by transferring 1 mL of solution into a cuvette, which was read three times using a Zetasizer Nano ZS instrument and the average of three reads was recorded.

4.2.5.7 Fourier transform infrared spectrometry (FTIR)

To identify potential phytochemical groups, present in ETAuNPs, Fourier transform infrared spectrometry was conducted using 9 mg of ET-EtOH as a blank. The percentage transmittance was detected over an infrared range of 550-4000 cm^{-1} using a Perkin Elmer spectrum 100 FTIR spectrometer (Perkin Elmer, Midrand, South Africa).

4.2.6 Anti-elastase assay

The method used to determine the inhibition of elastase was described by Nel [21]. Briefly, stock concentrations of ET-EtOH, the fermented (ETF) extract and ursolic acid (positive control) were prepared at 20 mg/mL (in DMSO). From the ursolic stock solution, 4.8 µL was transferred into 35.2 µL of DMSO to obtain a final concentration range from 60-0.94 µg/mL. The stock solutions of ET, ETF and ETAuNP were serially diluted in DMSO to obtain a concentration ranging from 500-7.81 µg/mL. A vehicle control (1 % DMSO) was prepared in the same manner as the plant samples. A blank control (0%) was included that contained all the reagents including 5 µL of 1 % DMSO, however, no enzyme was added. The absorbance values were determined using a BIO-TEK Power-Wave XS plate reader at a wavelength of $OD_{405\ nm}$ at a temperature of 37˚C for 15 minutes. To calculate the percentage inhibition, Equation 2 was used:

$$\% \ Inhibition = 100 - \left(\frac{Absorbance\ sample\ at\ 15\ min - absorbance\ at\ 0\ min}{Absorbance\ control\ at\ 15\ min - absorbance\ at\ 0\ min}\right) \text{ x } 100 \qquad (2)$$

4.2.7 Cell culture

Human keratinocytes (HaCaT) were used to determine the antiproliferative activity of the plant samples. To maintain the HaCaT cell line DMEM media was used supplemented with 10% fetal bovine serum and 1% antibiotics consisting of penicillin (100 U/mL), streptomycin (100 µg/mL) and amphotericin B (250 µg/mL). The cells were incubated at 5% CO_2 and 37˚C until a confluent monolayer was obtained. The cells were sub-cultured using 0.25% trypsin-EDTA once a monolayer had formed.

4.2.8 Antiproliferative activity against HaCaT cells

The method used to determine antiproliferative activity was described by Lall [22]. In this method, the PrestoBlue cell viability reagent was used to measure the antiproliferative activity. Within a 96-well microtiter culture plate, cells were seeded into each well at a concentration of 5×10^4 cells/mL and the plate were incubated overnight at 37˚C and 5% CO_2. A stock solution of the ET-EtOH was prepared at a concentration of 20 mg/mL in DMSO and serially diluted two-fold with 20% DMSO and actinomycin D as the positive control. Once the cells adhered, ET-EtOH and 20% DMSO were added in triplicate. The final concentration of ET-EtOH and actinomycin D ranged between 400-3.125 and 0.05-3.9×10^{-4} µg/mL with 20% DMSO between 20-0.63%. Media (100%), PrestoBlue reagent and a 1% DMSO control were added, however, the PrestoBlue control contained no cells (0%). After 72 hours, PrestoBlue reagent was added and incubated for a further two hours Thereafter, the fluorescence was measured at an excitation/emission wavelength of 560/590 nm using a Victor Nivo plate reader. To calculate the cell viability of each sample, Equation 3 was used.

$$\% \ Viability = \frac{Fluorescence\ \ sample - Fluorescence\ 0\%\ control}{(Fluorescence\ \ 100\%\ control - Fluorescence\ \ 0\%\ control)} \text{ x } 100 \qquad (3)$$

4.2.9 Granulocyte extraction

Granulocytes were extracted and analysed based on their histamine production once treated with the prepared extract. The selection criteria of the volunteer were based on whether they had eczema and were above the age of 21 with no history of major diseases. Ethics approval was obtained by the ethics committee of the Faculty of Natural and Agricultural Science (EC120411-046, University of Pretoria, South Africa). To isolate the granulocytes a method described by Oosthuizen [23] was used with alterations. Briefly, 15 mL of freshly collected blood was diluted with incomplete RPMI-1640 media at a 1:1 ratio, at room temperature. Thereafter, 15 mL of diluted blood was layered on 7.5 mL of histopaque and centrifuged at 1500×*g* for 30 minutes. After centrifugation, the erythrocyte and granulocyte layer were collected and transferred into a falcon tube. The erythrocytes were lysed with 10% lysis buffer at a ratio of 1:5 (v/v). After 15 minutes, the cells were centrifuged for seven minutes at 540 x *g* at room temperature. The collected pellet was washed with buffer A containing 45 mL PBS, 0.18 g trisodium citrate and 5 mL pasteurized plasma (8:1:1) and resuspended in complete RPMI-1640 media containing 10% heat-inactivated fetal bovine serum and 1% gentamicin (10 mg/mL).

4.2.10 Histamine quantification

Histamine from granulocyte cell supernatant was quantified using a Histamine ELISA kit, in accordance with the manufacturer's protocol. Granulocytes were stimulated with phorbol 12-

myristate 13-acetate (PMA) at a final concentration of 1 µg/mL. The cells were seeded in a 48-well plate at a concentration of 1.5×10^5 cells/mL. After a 24-hour incubation at 37˚C and 5% CO_2, ET-EtOH was added, in duplicate, at a final concentration of 6, 3 and 2 µg/mL and incubated for 30 minutes. An untreated and vehicle (0.25% DMSO) control was prepared in the same manner. Thereafter, 200 µL of cell supernatant was transferred to a 96-well plate and stored at -80˚C until used. Cell viability was measured using ImageJ at 20x magnification due to the small size of the stimulated granulocytes. The average size of the granulocytes after 30 minutes of incubation was determined using the following protocol, the image type was set to 8-bit and a bandpass filter was applied. The gray morphology of the image was set at a radius of 2 pixels with a circular structure element. Thereafter, the background with a rolling ball of more than 12 pixels was subtracted. The threshold was adjusted to the automatic setting and a watershed binary option was selected to ensure that cells were recognised as separate entities. The image particle size at 120-infinity $pixels^2$ with a circularity of 0.0-1 was measured and the average size was recorded. Thereafter, the same equation as Equation 2 was used to calculate percentage viability.

4.2.11 Statistical analysis

Results are reported as mean ± standard error (or standard deviation) as displayed in the results section. Three repeats were performed for each assay, with two repeats conducted for histamine quantification. To obtain the IC_{50} values, a nonlinear regression analysis of the sigmoidal dose-response curves (4-parameter logistic) using GraphPad Prism 4 was conducted. Statistical analysis was done using one-way analysis of variance (ANOVA) followed by Dunnett's multiple comparison tests (GraphPad, version 4), where $p < 0.05$ (*), $p < 0.01$ (**) and $p < 0.001$ (***) were considered statistically significant.

4.3 Results

4.3.1 Characterization of gold nanoparticles

During the preparation of the ETAuNP, an immediate colour change was observed whereby the green tinge of the solution converted to a wine colour once exposed to the gold salt, which indicated the presence of gold nanoparticles. This was confirmed with UV-Vis, as ETAuNP displayed a spectral peak at 535 nm (Figure 4.1 A). The total phenolic content of ETAuNP was 3.04 mg/mL. Furthermore, the functional groups present in ET-EtOH and ETAuNP that were identified were tabulated (Figure 4.1 B, Table 4.1). The average diameter and zeta-potential of the synthesized nanoparticles were measured and found to be 115 ± 77.74 nm and -9.42 mV, respectively. Furthermore, the morphology of ETAuNP was determined using HRTEM, which consisted mostly of round shapes (Figure 4.1 C). A selected area diffraction pattern (SAED) was used to characterize whether ETAuNP was similar to gold metal. The face centred lattice planes of ETAuNP displayed a diffraction index of (111), (200), (220) and (311) (Figure 4.1 D). Lastly, ETAuNP displayed minimal shifts in the surface plasmon resonance peak (λ_{max}) when exposed to the various mediums except for BSA whereby low λ_{max} peaks were observed, which were evident after one day (Figure 4.2 G).

Table 4.1. Potential functional groups were identified using Fourier transform infrared spectrometry (FTIR) in the ethanolic extract (ET-EtOH) and synthesized gold nanoparticles (ETAuNPs) of *Elegia tectorum*.

Functional groups	ET-EtOH transmittance (cm^{-1})	ETAuNPs transmittance (cm^{-1})
O-H	3321	3353
C-H	2924	-
C-O	1058	-
Aromatic ring (C-C)	-	1637
C=O	1734	-

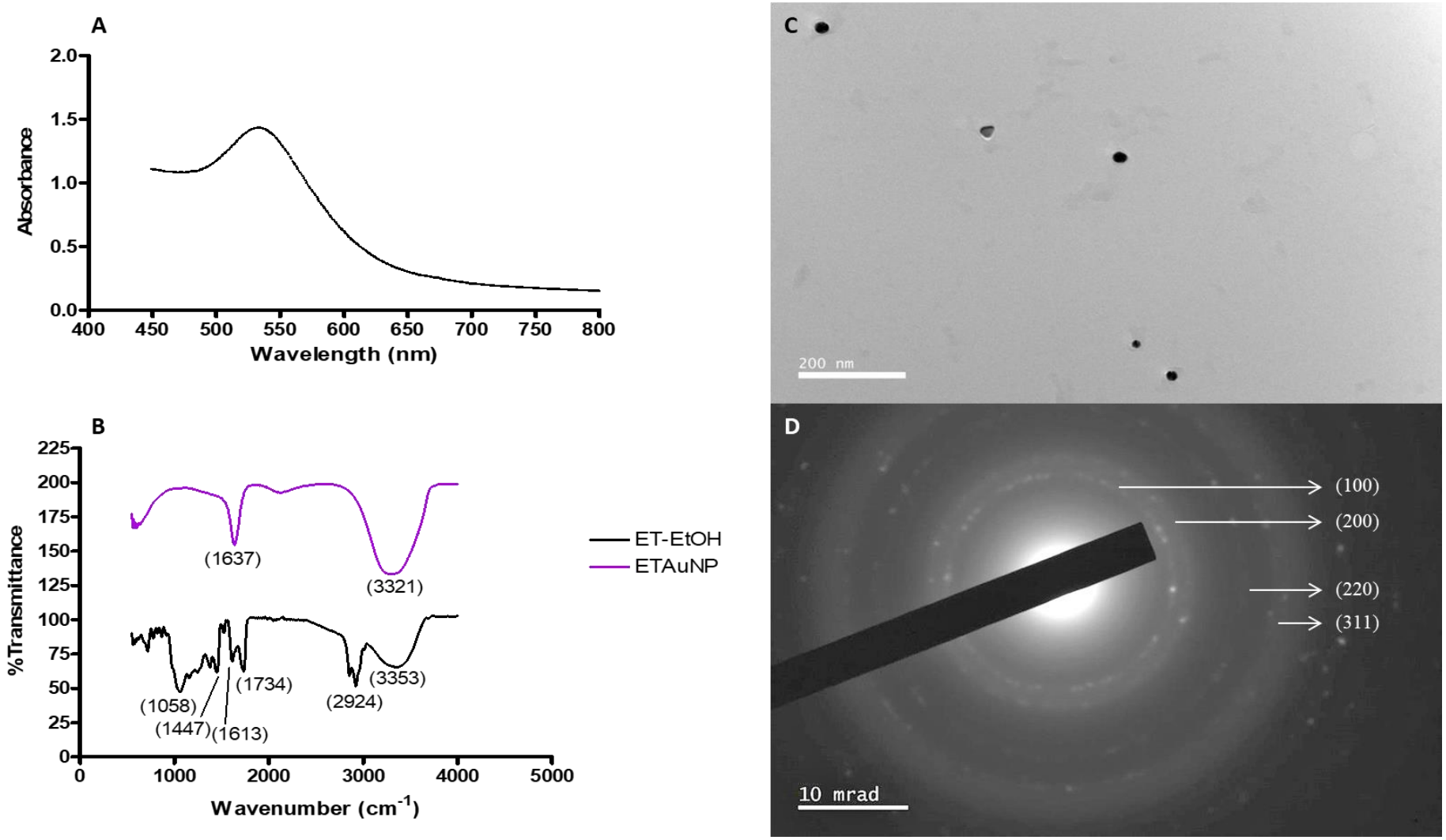

Figure 4.1. Gold nanoparticle characterization including ultraviolet-visible (UV-Vis) spectroscopy (A), Fourier-transform infrared spectrometry (FTIR) of the ethanolic extract (ET-EtOH) and synthesized gold nanoparticles (ETAuNP) (B), high-resolution transmission electron microscopy (HRTEM) at 200 nm (C) and selected area diffraction pattern (SAED) at 10 mrad (D).

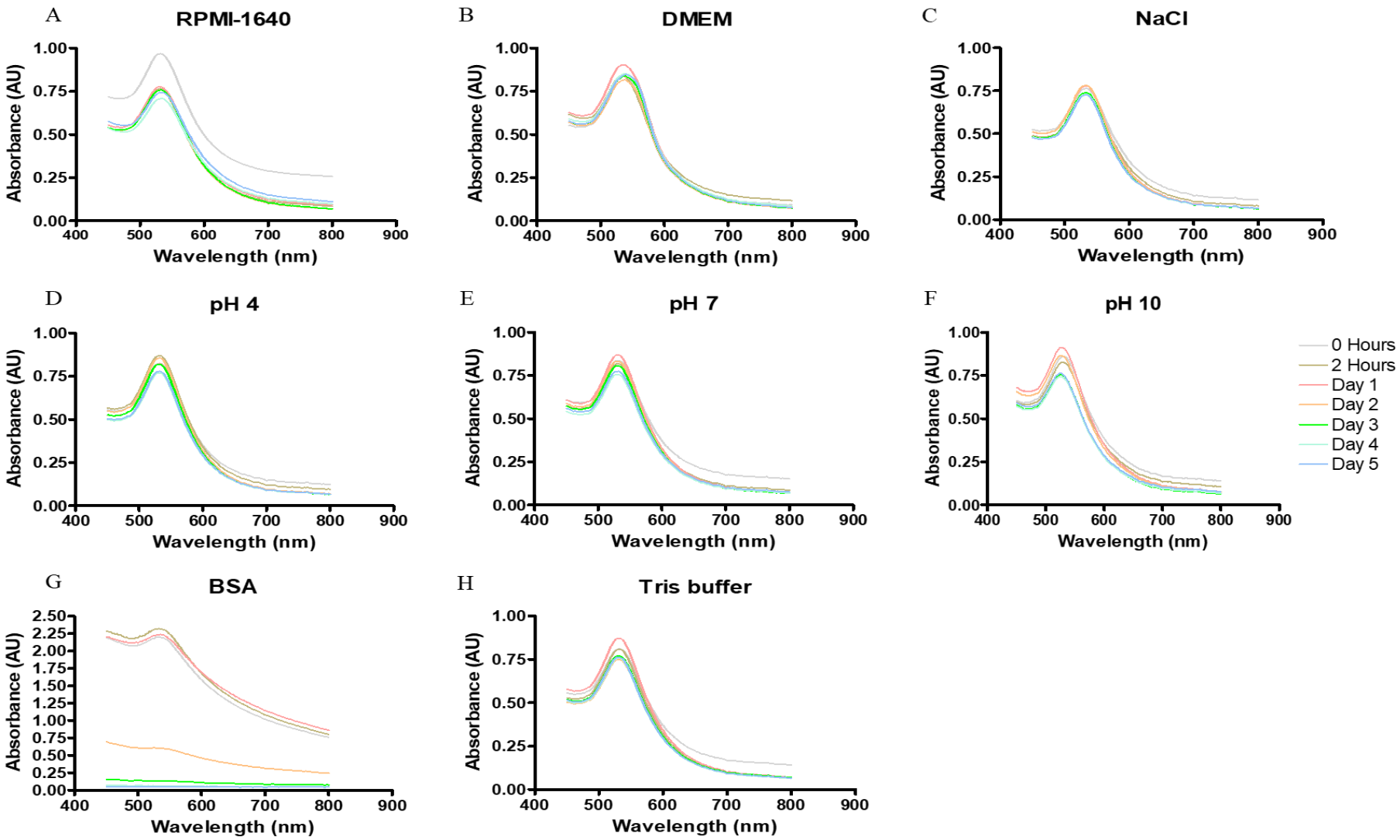

Figure 4.2. ***In vitro*** **stability of** ***Elegia tectorum*** **synthesized gold nanoparticles (ETAuNPs) in different mediums. These solutions include Roswell Park Memorial Institution (RPMI-1640) medium (A) and Dulbecco's modified Eagle's Medium (DMEM) (B), 5% sodium chloride (NaCl) (C), pH level of 4 (D), 7 (E) and 10 (F), 0.5% bovine serum albumin (BSA) (G) and tris buffer (pH 8.1) (H).**

4.3.2 Elastase inhibition

The elastase inhibitory activity was evaluated for ET-EtOH, ETF and ETAuNP. ET-EtOH displayed an IC_{50} of 28.27 ± 2.02 µg/mL, while the positive control (ursolic acid) showed an IC_{50} of 22.30 ± 2.79 µg/mL, respectively. Furthermore, ETAuNP and ETF displayed no activity (IC_{50} > 500 µg/mL).

4.3.3 Antiproliferative activity

ET-EtOH was selected for further evaluation due to its high anti-elastase activity and displayed no antiproliferative activity against human keratinocytes (HaCaT) and granulocyte cells (IC_{50} > 400 µg/mL). The positive controls, while the positive control, actinomycin D and 20% DMSO, displayed an IC_{50} of 0.01 ± 0.002 µg/mL and 6.06 ± 0.77%, respectively.

4.3.4 Quantification of histamine

To ensure the selected concentration did not modulate cell death, a cell viability assay was conducted. When compared to the 0.25% vehicle control, ET-EtOH at a concentration of 50 and 13 µg/mL ($p < 0.001$) significantly reduced the viability of the cells (Figure 4.3). Thus, lower concentrations of 6, 3 and 2 µg/mL were selected for histamine quantification.

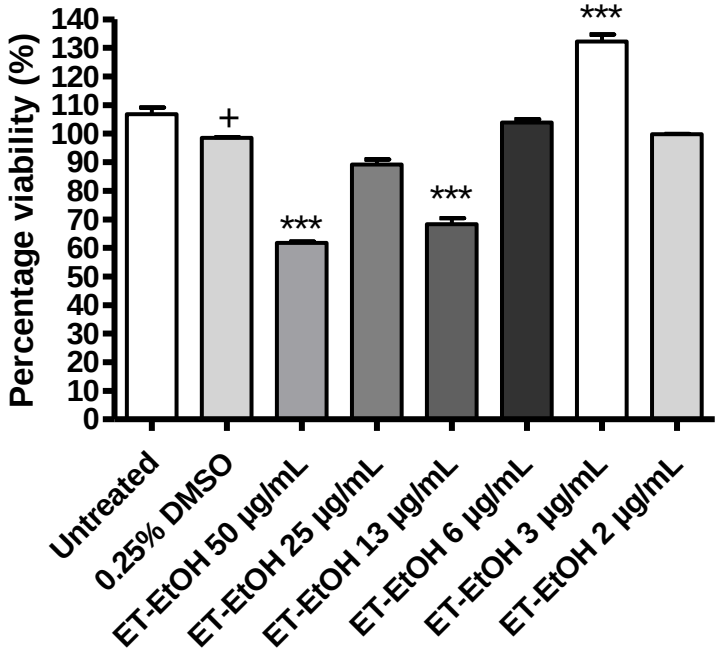

Figure 4.3. Cell viability after treatment with *Elegia tectorum* ethanolic extract (ET-EtOH) at a concentration range of 50-2 µg/mL on phorbol 12-myristate 13-acetate (PMA) stimulated granulocytes. Data represent mean ± SEM (n=3). A significant difference was determined using a one-way ANOVA followed by Dunnett's multiple comparison test, where $p < 0.001$ (***) indicate significance when compared to the 0.25% vehicle control (+).

Furthermore, the potential effect of ET-EtOH against histamine production was evaluated. The vehicle control (0.26 ± 0.02 ng/mL), when compared to the untreated control (0.30 ± 0.02 ng/mL) displayed no significant effect. ET-EtOH significantly ($p < 0.05$) inhibited histamine production at a concentration of 6 (0.10 ± 0.01) and 3 µg/mL (0.11 ± 0.01 ng/mL), while no significant effect was observed at a concentration 2 µg/mL (0.14 ± 0.04 ng/mL) when compared to the vehicle control (Figure 4.4).

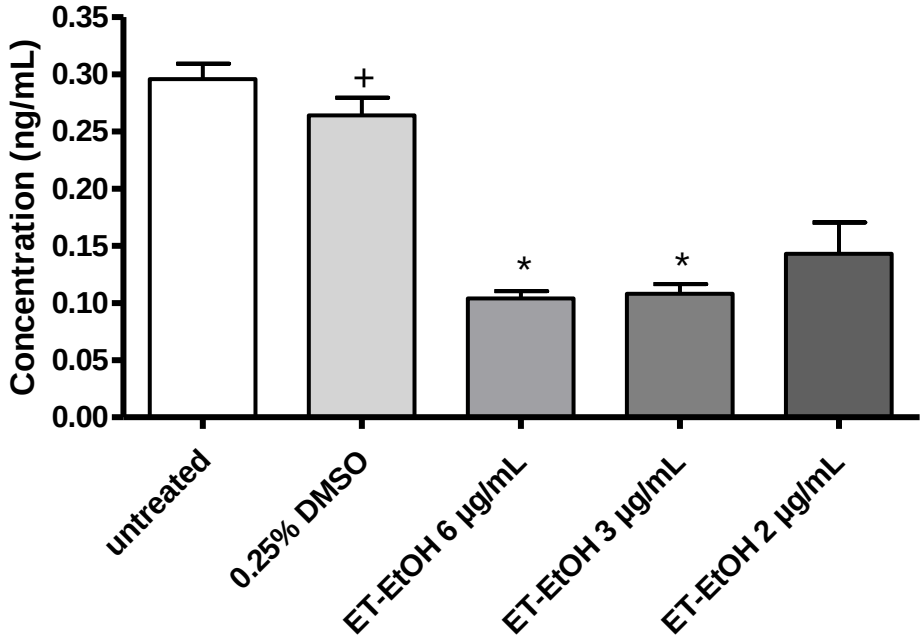

Figure 4.4. Effects of *Elegia tectorum* ethanolic extract (ET-EtOH) on histamine production at a concentration of between 6, 3 and 2 µg/mL on phorbol 12-myristate 13-acetate (PMA) stimulated granulocytes. Data represent mean ± SEM (n=2). Significant difference was determined using a one-way ANOVA followed by Dunnett's multiple comparison test, where $p < 0.05$ (*) indicate significance when compared to 0.25% DMSO vehicle control (+).

4.4 Discussion

To identify the impact size, morphology or stability of ETAuNP may have on its biological activity characterization was conducted [20]. Vibration stretches were located at each of the functional groups mentioned in Table 4.1, which indicate the presence of phenolic compounds [24]. This supports the total phenolic content that was measured for ETAuNPs. Furthermore, the SAED diffraction index observed for ETAuNPs aligns with the Bragg reflections for gold as reported by Philip [25].

The buffers used during the *in vitro* stability were selected to mimic physiological environments while the duration was based on the timeframe required to determine the antiproliferative activity. Minimal shifts in the surface plasmon resonance (SPR) peaks for most of the mediums were observed, however, low SPR peaks were seen when ETAuNP was exposed to BSA. These low SPR peaks could be due to the electrostatic repulsion of the nanoparticle as a study conducted by Salopek et al. (1992), indicated that a zeta potential above or below ± 30 mV is considered stable while nanoparticles that do not fall within this range may precipitate and agglomerate [26]. In accordance with this study, ETAuNP (-9.42 mV) displayed strong agglomeration and precipitation, which may have resulted in the low SPR peaks when exposed to BSA.

Anti-elastase activity was conducted on ET-EtOH, ETAuNP and ETF of which ETAuNP and EFT displayed no activity. Ali et al. (2017) indicated that an increase in the concentration of zinc peroxide nanoparticles (ZnO_2-NP) significantly decreased elastase activity [27]. This suggests further evaluation into the potential effect other types of nanoparticles synthesised using ET may have on elastase production should be considered. Furthermore, a study done by Park and Bae (2016) demonstrated that *B. bifidum* fermented *Acanthopanax koreanum* root extract displayed greater anti-photoaging activity, which is characterized by the presence

of wrinkles, in comparison to the ethanolic extract. This was due to the repression of specific signalling pathways, which included hydrogen peroxide (H_2O_2)-induced activities of matrix metalloproteinase (MMP)-1 and -3 [19, 28]. Thus, ETF may have anti-photoaging activity, which indirectly reduces wrinkle formation, however, further investigation is required. One of the aims of this study was to validate the anti-elastase activity of ET-EtOH reported by Lymperis [18]. The IC_{50} values obtained in this study were roughly double than those reported. Furthermore, the antiproliferative activity of ET-EtOH against HaCaT cells was the same as Lymperis [18].

No current information on the antiproliferative activity against PBMCs and the potential effect of *E. tectorum*, the genus or isolated compounds have on histamine production could be found. However, kaempferol, which has previously been isolated from *Elegia macrocarpa* (Kunth) Moline and H.P Linder, was reported to increase the percentage viability of PBMCs at a concentration of 50 µg/mL [18, 29]. Furthermore, quercetin which has been isolated from *E. macrocarpa*, is known for its antihistamine properties [18, 30]. Compound isolation of ET-EtOH should be considered to identify whether kaempferol and quercetin are present.

Conclusion

This study focused on the potential effect ET-EtOH had on elastase and histamine production and whether the biosynthesis of ETAuNP and ETF enhanced the biological activity. ETAuNP and EFT displayed no anti-elastase activity (IC_{50} > 500 µg/mL), while ET-EtOH showed an IC_{50} of 28.27 ± 2.02 µg/mL. ET-EtOH was further evaluated for its effects on histamine production using granulocytes. Further investigation of ET-EtOH indicated that no antiproliferative activity against HaCaT and granulocytes (IC_{50} > 400 µg/mL) was observed. At a concentration of 6 and 3 µg/mL, ET-EtOH significantly inhibited the production of histamine in comparison to the vehicle control. In conclusion, ET-EtOH anti-elastase activity correlates with its ability to reduce histamine production. Further investigation into whether ET-EtOH targets histamine-associated receptors on mast cells as a potential mode of action should be considered.

Conflicts of Interest

The author(s) declare(s) that there is no conflict of interest regarding the publication of this paper.

Funding Statement

This work was supported by the National Research Foundation [grant number 105169 and 98334] and the Water Research Commission [contract number C2019/2020-00132].

Acknowledgments

The authors would like to acknowledge Mrs. Bianca D. Payne and Mrs. Tenille Esmear (Department of Plant and Soil Sciences, University of Pretoria) for their guidance. Furthermore, the authors would like to acknowledge Dr. Suprakas S. Ray (DST/CSIR National Centre for Nanostructured Materials, Council for Scientific and Industrial Research), Prof Kattesh V. Katti, Dr. Velaphi C. Thipe (Department of Radiology, Institute of Green Nanotechnology, University of Missouri Columbia), Dr. Vusani Mandiwana, Michel L. Kalombo (Chemical Cluster, Centre for Nanostructures and Advanced Materials, Council for Scientific and Industrial Research) and Dr. Arno Janse van Vuuren (Centre for

High Resolution Transmission Electron Microscopy, Nelson Mandela University) for conducting the FTIR, DLS, zeta potential and HRTEM analysis.

References

[1] C. A. Akdis, M. Akdis, T. Bieber, C. Bindslev-Jensen, M. Boguniewiz, P. Eigenmann, et al., "Diagnosis and treatment of atopic dermatitis in children and adults: European Academy of Allergology and Clinical Immunology/American Academy of Allergy, Asthma and Immunology/PRACTALL Consensus Report," *The Journal of Allergy and Clinical Immunology*, vol. 118, no. 1, pp. 152-169, 2006.

[2] E. B. Brandt, U. Sivaprasad, "Th2 Cytokines and Atopic Dermatitis.," *Journal of clinical & cellular immunology*, vol. 2, no. 3, pp. 1-25, 2011.

[3] J. Buddenkotte, M. Maurer, M. Steinhoff. Histamine and antihistamines in atopic dermatitis. Histamine in Inflammation. Boston: Springer; 2010. p. 73-80.

[4] M. Castells, "Mast cell mediators in allergic inflammation and mastocytosis," *Immunology and Allergy Clinics*, vol. 26, no. 3, pp. 465-485, 2006.

[5] Y. Abe, S. Ogino, M. Irifune, I. Imamura, H. Fukui, H. Wada, et al., "Histamine content, synthesis and degradation in human nasal mucosa," *Clinical & Experimental Allergy*, vol. 23, no. 2, pp. 132-136, 1993.

[6] A. D. Hogan, L. B. Schwartz, "Markers of mast cell degranulation," *Methods*, vol. 13, no. 1, pp. 43-52, 1997.

[7] M. Gschwandtner, M. Mildner, V. Mlitz, F. Gruber, L. Eckhart, T. Werfel, et al., "Histamine suppresses epidermal keratinocyte differentiation and impairs skin barrier function in a human skin model," *Allergy*, vol. 68, no. 1, pp. 37-47, 2013.

[8] D. Gutowska-Owsiak, L. Greenwald, C. Watson, T. Selvakumar, X. Wang, G. Ogg, "The histamine-synthesizing enzyme histidine decarboxylase is upregulated by keratinocytes in atopic skin," *British Journal of Dermatology*, vol. 171, no. 4, pp. 771-778, 2014.

[9] R. Voegeli, A. Rawlings, M. Breternitz, S. Doppler, T. Schreier, J. Fluhr, "Increased stratum corneum serine protease activity in acute eczematous atopic skin," *British Journal of Dermatology*, vol. 161, no. 1, pp. 70-77, 2009.

[10] R. Agrawal, J. A. Woodfolk, "Skin barrier defects in atopic dermatitis," *Current allergy and asthma reports*, vol. 14, no. 5, pp. 1-11, 2014.

[11] C. Gelmetti, A. Wollenberg, "Atopic dermatitis–all you can do from the outside.," *British Journal of Dermatology*, vol. 170, no. 1, pp. 19-24, 2014.

[12] T. S. Thring, P. Hili, D. P. Naughton, "Anti-collagenase, anti-elastase and anti-oxidant activities of extracts from 21 plants," *BMC complementary and alternative medicine*, vol. 9, no. 1, pp. 27, 2009.

[13] SA-Venues. *Elegia tectorum* 2020 [Available from: https://www.sa-venues.com/plant-life/elegia.php.

[14] S. Turner, H. Jamieson. *Elegia tectorum* 2016 [Available from: http://pza.sanbi.org/elegia-tectorum.

[15] Immediate Media Co. *Elegia tectorum* 2020 [Available from: https://www.gardenersworld.com/plants/elegia-tectorum/.

[16] L. A. Philander, "An ethnobotany of Western Cape Rasta bush medicine," *Journal of ethnopharmacology*, vol. 138, no. 2, pp. 578-594, 2011.

[17] J. B. Harborne, "Arsenal for survival: secondary plant products," *Taxon*, vol. 49, no. 3, pp. 435-449, 2000.

[18] P. Lymperis, E.-M. Tomou, M. N. De Canha, N. Lall, H. Skaltsa, "Traditional Uses, Phytochemistry, and Pharmacology of Elegia Species: A Review," *Scientia Pharmaceutica*, vol. 90, no. 1, pp. 4, 2021.

[19] M.-J. Park, Y.-S. Bae, "Fermented Acanthopanax koreanum root extract reduces UVB- and H 2 O 2-induced senescence in human skin fibroblast cells," *Journal of microbiology and biotechnology*, vol. 26, no. 7, pp. 1224-1233, 2016.
[20] M. N. De Canha, V. C. Thipe, K. V. Katti, V. Mandiwana, L. Kalombo, S. S. Ray, et al., "The activity of gold nanoparticles synthesized using Helichrysum odoratissimum against Cutibacterium acnes biofilms," *Frontiers in cell and developmental biology*, vol., no., pp. 2288, 2021.
[21] M. Nel, A. B. van Staden, D. Twilley, C. B. Oosthuizen, D. Meyer, S. Kumar, et al., "Potential of succulents for eczema-associated symptoms," *South African Journal of Botany*, vol., no., pp., 2022.
[22] N. Lall, A. Blom van Staden, S. Rademan, I. Lambrechts, M. N. De Canha, J. Mahore, et al., "Antityrosinase and anti-acne potential of plants traditionally used in the Jongilanga community in Mpumalanga," *South African Journal of Botany*, vol. 126, no., pp. 241-249, 2019.
[23] L. Koenderman, P. Kok, M. Hamelink, A. Verhoeven, P. Bruijnzeel, "An improved method for the isolation of eosinophilic granulocytes from peripheral blood of normal individuals," *Journal of leukocyte biology*, vol. 44, no. 2, pp. 79-86, 1988.
[24] G. Sathishkumar, P. K. Jha, V. Vignesh, C. Rajkuberan, M. Jeyaraj, M. Selvakumar, et al., "Cannonball fruit (Couroupita guianensis, Aubl.) extract mediated synthesis of gold nanoparticles and evaluation of its antioxidant activity," *Journal of Molecular Liquids*, vol. 215, no., pp. 229-236, 2016.
[25] D. Philip, "Biosynthesis of Au, Ag and Au–Ag nanoparticles using edible mushroom extract," *Spectrochimica Acta Part A: Molecular and Biomolecular Spectroscopy*, vol. 73, no. 2, pp. 374-381, 2009.
[26] B. Salopek, D. Krasic, S. Filipovic, "Measurement and application of zeta-potential," *Rudarsko-geolosko-naftni zbornik*, vol. 4, no. 1, pp. 147, 1992.
[27] S. S. Ali, R. Morsy, N. A. El-Zawawy, M. F. Fareed, M. Y. Bedaiwy, "Synthesized zinc peroxide nanoparticles (ZnO2-NPs): a novel antimicrobial, anti-elastase, anti-keratinase, and anti-inflammatory approach toward polymicrobial burn wounds," *International journal of nanomedicine*, vol. 12, no., pp. 6059, 2017.
[28] Y.-M. Kang, C.-H. Hong, S.-H. Kang, D.-S. Seo, S.-O. Kim, H.-Y. Lee, et al., "Anti-photoaging effect of plant extract fermented with Lactobacillus buchneri on CCD-986sk fibroblasts and HaCaT keratinocytes," *Journal of Functional Biomaterials*, vol. 11, no. 1, pp. 3, 2020.
[29] M. Kluska, M. Juszczak, D. Wysokiński, J. Żuchowski, A. Stochmal, K. Woźniak, "Kaempferol derivatives isolated from Lens culinaris Medik. reduce DNA damage induced by etoposide in peripheral blood mononuclear cells," *Toxicology Research*, vol. 8, no. 6, pp. 896-907, 2019.
[30] K. M. Brodowska, "Natural flavonoids: classification, potential role, and application of flavonoid analogues," *European Journal of Biological Research*, vol. 7, no. 2, pp. 108-123, 2017..

Chapter 5. Potential antihistamine activity of gold nanoparticles biosynthesized from *Bulbine frutescens* (L.) Willd.

Potential antihistamine activity of gold nanoparticles biosynthesized from *Bulbine frutescens* (L.) Willd. [4]

Short title: Antihistamine potential of *Bulbine frutescens*

Abstract

One of the proposed causations of atopic dermatitis is the outside-in hypothesis, which states that eczema is caused by a disruption within the skin barrier. These disruptions include dry, cracked skin which promotes the production of histamine. The study aimed to determine whether *Bulbine frutescens* (BF) alleviated skin damage through wound healing and reduced the production of histamine. Furthermore, this study investigated whether gold nanoparticles formed using BF would enhance biological activity. Eight samples were prepared from BF and their antiproliferative effects against human keratinocyte (HaCaT) cells were evaluated. The commercial spray (BFS) and its respected gold nanoparticles (BFSAuNP) displayed antiproliferative activity against HaCaT cells with fifty percent inhibitory concentrations (IC_{50}) of 4.63 ± 0.05 and 3.50 ± 0.40%, respectively. Furthermore, the ethanolic whole leaf (BFE^{+}) extract significantly reduced cell viability at the highest tested concentration (400 µg/mL). The ethanolic leaf juice (BFE; $p < 0.01$) extract and its respected gold nanoparticles (BFEAuNP; $p < 0.05$) displayed significant wound closure at 100 µg/mL and were further evaluated against histamine production. None of the selected samples displayed antiproliferative activity against phorbol 12-myristate 13-acetate (PMA) stimulated granulocytes (IC_{50} > 200 µg/mL). In comparison to the untreated control (0.30 ± 0.02 ng/mL), BFEAuNP significantly inhibited histamine production at a concentration of 100 ($p < 0.01$) and 50 µg/mL ($p < 0.001$). Furthermore, in comparison to the vehicle control (0.26 ± 0.02 ng/mL), BFE significantly stimulated ($p < 0.001$) the production of histamine at the highest concentration (200 µg/mL).

[4] This chapter will be submitted as an original article to PLoS ONE with an impact factor of 3.240. The format of this chapter was written based on the author guidelines set by the journal.

Further investigation into the potential *in vivo* wound healing capabilities of BFEAuNP and whether the sample targets histamine-associated receptors on mast cells should be considered.

5.1) Introduction

The basis of the outside-in hypothesis, a proposed causation of atopic dermatitis, is the loss-of-function mutation within the filaggrin gene, which further impairs the barrier function [1]. The filaggrin gene is located on chromosome 1q21 and translates into a polyprotein known as profilaggrin, which is the main component of keratohyalin granules [2, 3]. These profilaggrins are comprised of a calcium-binding N-terminal domain and are dephosphorylated and cleaved into 10-12 filaggrin monomers that contribute to the strength and integrity of the epidermis [2, 4]. When these monomers aggregate, the keratin cytoskeleton forms a protein-lipid matrix, which maintains epidermal hydration [5].

In eczema patients who have an impaired barrier function, there is an increase in trans-epidermal water loss and a decrease in water-binding capacity, which manifests as dry cracked skin [1, 2]. Due to the presence of cracked skin, there is an increase in histamine production, which leads to an intolerable itching sensation [6]. Increased levels of histamine can affect the expression of genes associated with maintaining the epidermal barrier including filaggrin, keratins and proteases. In response to this, filaggrin levels are reduced and the mRNA expression of some keratins is downregulated, further drying the skin and leading to more severe cracks [7, 8].

Bulbine frutescens (L.) Willd, part of the Asphodelaceae family, is found within Southern and Eastern Africa and is indigenous to South Africa, mainly located in the Free State, KwaZulu-Natal and within the Cape Province of South Africa [9, 10]. *Bulbine frutescens* is used in traditional medicine to treat numerous ailments and conditions. The leaf sap is prepared into a warm poultice for the treatment of wounds, eczema and arthritis [9, 10]. An infusion prepared

from fresh leaves is used by Rastafarians for coughs and colds [11]. The jelly-like juice within the leave is used for burns, blisters, cracked lips, acne and mouth ulcers [11]. Other traditional uses of *B. frutescens* include treating diarrhea, ringworms, herpes and insect bites using dried leaf bases [12, 13].

Numerous studies have reported the chemical composition of *B. frutescens*. Secondary metabolites that have been isolated include anthraquinones such as chrysophanol, isofuranonaphthoquinones and phenylanthraquinones, which display anticancer properties [9, 10, 14]. Other secondary metabolites include jowones A and B, which display unique antimalarial activity [15]. However, none of these compounds has been evaluated for their effect on eczema-associated symptoms. This study aimed to determine whether *Bulbine frutescens* alleviated skin damage through wound healing and reduced the production of histamine. Furthermore, this study investigated whether gold nanoparticles formed using *B. frutescens* would enhance biological activity.

5.2) Methods and materials

5.2.1) Materials, chemicals and reagents

The human keratinocytes (HaCaT) were donated by Dr. Lester Davids from the University of Cape Town. The Dulbecco's modified Eagle's Medium (DMEM), Roswell Park Memorial Institute (RPMI-1640) medium, ammonium-chloride-potassium (ACK) lysing buffer, amphotericin B, streptomycin, penicillin, Eutech pH buffer solutions (pH 4, 7 and 10), phosphate-buffered saline (PBS), fetal bovine serum (FBS) and PrestoBlue Cell Viability reagent were obtained from ThermoFisher Scientific (Johannesburg, South Africa). Cell culture plates and flasks were purchased from LasecSA (Pty) Ltd. (Midrand, South Africa). The histamine (ab213975) ELISA kit was sourced from BIOCOM Africa (Pty) Ltd. (Lyttleton

Manor, South Africa). Phorbol 12-myristate 13-acetate (PMA), histopaque, ethylenediaminetetraacetic acid (EDTA) and other chemicals and reagents such as dimethyl sulfoxide (DMSO), gum arabic, actinomycin D (purity >95%), gold (III) chloride trihydrate ($HAuCl_4.3H_2O$), bovine serum albumin (BSA), sodium chloride (NaCl) and gentamicin solution were obtained from Sigma-Aldrich (Johannesburg, South Africa).

5.2.2) Plant collection and extraction

Fresh leaves were collected in March (2016) at the University of Pretoria (UP) and a herbarium sample was prepared accordingly with a PRU number of 122179. To prepare an ethanolic whole leaf extract, the leaves were dried and grounded into a fine powered using an IKA MF10 grinder (MF 10.1 Head 2870900) with a 2 mm sieve. The powdered material (46.14 g) was homogenized with 231 mL of absolute ethanol and agitated on a shaker for 48 hours. Thereafter, the solution was filtered using a Buchner funnel, with the pulp undergoing a second extraction. The remaining solution was further concentrated using a rotary evaporator. To prepare the gel extract, 6.06 g of gel was scrapped from the remaining leaves, filtered using a Buchner funnel and freeze-dried into a powder. The percentage yield was calculated for each extract using Equation 1.

$$\%\text{Yield} = \left(\frac{Extract\ weight\ (g)}{Powdered\ or\ fresh\ material\ weight\ (g)}\right) \times 100 \quad (1)$$

The yield of the leaves and gel was 23.25 and 2.31%. Furthermore, two commercial products namely a freeze-dried ethanolic leaf juice and a commercial spray, consisting of pure organic leaf extracts, were obtained from Botanica Natural Products. All of the prepared and obtained extracts were stored at 4˚C.

5.2.3) Synthesis of gold nanoparticles

Gold nanoparticles were synthesized using the ethanolic whole leaf (BFE^+), freeze-dried ethanolic leaf juice (BFE), gel (BFG) extracts and commercial spray (BFS). For BFE, BFE^+ and BFG, the extracts were dissolved in 100 ml of distilled water (dH_2O) (0.2 mg/mL) and were heated to 60˚C. Thereafter, the solutions were centrifuged at 1700 rpms for 10 minutes and the supernatant was collected, due to the insolubility of the samples in dH_2O. Thirty grams of gum arabic powder was added to 20 mL of BFE and BFE^+, 60 mg was added to 40 mL of BFG and the solutions were heated to 60˚C. Thereafter, 500 µl of 0.01 M gold salt ($HAuCl_4.3H_2O$) was added to BFE and BFE^+, while 380 µl of 0.1 M $HAuCl_4.3H_2O$ was added to BFG, per 20 ml of solution. To synthesize nanoparticles from BFS, 8 mL of BFS was added to 12 mg of gum arabic powder. Afterward, the solution was heated (60-65˚C) and 1 mL of 0.01 M $HAuCl_4.3H_2O$ was added. To wash the synthesized nanoparticles of BFS, the sample was centrifuged at 13,500 rpms for 5 minutes. The pellet was resuspended in dH_2O, centrifuged and the supernatant was collected. Each of the synthesized nanoparticles was stored at 4˚C.

5.2.4) Characterization of synthesized gold nanoparticles

5.2.4.1) Ultraviolet-visible (UV-Vis) spectrometry

To confirm the formation of gold nanoparticles (AuNPs), a full spectral scan was conducted using ultraviolet-visible spectrometry (UV-Vis) to determine if the surface plasmon resonance (SPR) was similar to gold metal (Au). In a 96-well plate, 100 µL of the AuNPs were added and the absorbance was read between 450-800 nm at 50 nm increments using a Victor Nivo plate reader (PerkinElmer, Midrand, South Africa).

5.2.4.2) *In vitro* stability

In vitro stability of the AuNPs was evaluated in various mediums consisting of buffer solutions and cell culture mediums, which included 0.5% bovine serum albumin (BSA), 5% sodium chloride (NaCl), pH buffer solutions of 4, 7 and 10, phosphate buffer (pH 6.5), Dulbecco's Modified Eagles medium (DMEM) and Roswell Park Memorial Institute (RPMI-1640) medium. AuNPs were added to the abovementioned solutions at a 1:1 ratio with a final volume of 1.5 mL and were incubated at 37˚C. To confirm whether the nanoparticles were stable, the SPR peaks (λ_{max}) between 450 and 800 nm were measured using a Victor Nivo plate reader at 0, 2, 24 (Day 1), 48 (Day 2), 72 (Day 3), 96 (Day 4) and 120 hours (Day 5).

5.2.4.3) High-resolution transmission electron microscopy (HRTEM)

High-resolution transmission electron microscopy was used to identify the particle size and shape of AuNPs. Furthermore, the crystallinity was identified through selected area electron diffraction (SAED). Five microlitres of AuNPs solutions were loaded onto a carbon-coated copper TEM grid and allowed to dry. Thereafter, the grids were loaded into a JEOL JEM-ARM200F double Cs-corrected transmission electron microscope equipped with a large solid angle energy dispersive spectrometer (EDS) (Akishima, Tokyo, Japan) and images were captured.

5.2.4.4) Quantification of the total phenolic content present in the synthesized nanoparticles

The total phenolic content was quantified using the Folin Cioalteau as described by De Canha [16]. A standard curve was prepared from BFE, BFE^{+}, BFG and BFS that was serially diluted two-fold, in dH_2O, resulting in a final concentration range of 4000-31.25 µg/mL for BFE and BFE^{+}, 2000-15.63 µg/mL for BFG and 50-0.39% for BFS. In a 2 mL Eppendorf tube, 125 µL of 7.5% (w/v) sodium bicarbonate solution (Na_2CO_3) and 125 µL 10% (v/v) Folin Cioalteau

reagent (1 in 10 mL dH_2O) were added to 250 µL of each dilution and to 250 µL of AuNPs solution. Thereafter, 100 µL of each solution was transferred into a 96-well plate and incubated at 30˚C for 30 minutes in the dark. Blanks for the samples and AuNPs consisted of 250 µL of sample, 7.5% Na_2CO_3 and dH_2O in the place of 10% Folic Cioalteau. The absorbance was measured at 765 nm using a Victor Nivo plate reader and the phenolic content of the AuNPs was determined using the equations generated from the standard curves (BFE: $y = 9\times10^{-5}x + 0.0092$, $R^2 = 0.9887$, BFE^+: $y = 0.0001x + 0.0031$, $R^2 = 0.9992$, BFG: $y = 0.0002x – 0.0137$, $R^2 = 0.9975$ and BFS: $y = 0.0074x + 0.0024$, $R^2 = 0.9924$). The quantified phenolic content was used as the highest stock concentration in each of the bioassays that were conducted.

5.2.4.5) Dynamic light scattering (DLS)

To determine the hydrodynamic size of the AuNPs, 1 mL of the solutions were transferred into a zeta cell and read using a Zetasizer Nano ZS instrument (Malvern Instruments Ltd., Malvern, Worcestershire, UK). Three reads were conducted and the averages were obtained.

5.2.4.6) Zeta potential

The electrostatic charge of the AuNPs was evaluated by transferring 1 mL of the solutions into a cuvette, which was read three times using a Zetasizer Nano ZS instrument and the averages of three reads were recorded.

5.2.4.7) Fourier transform infrared spectrometry (FTIR)

To identify potential phytochemical groups, present in the AuNPs, Fourier transforms infrared spectrometry was conducted using BFE, BFE^+, BFG and BFS as blanks. The percentage transmittance was detected over an infrared range of 550-4000 cm^{-1} using a Perkin Elmer spectrum 100 FTIR spectrometer (Perkin Elmer, Midrand, South Africa).

5.2.5) Cell culture

Human keratinocytes (HaCaT) were used to determine the antiproliferative and wound healing activity of the samples. To maintain the HaCaT cells, DMEM media was supplemented with 10% fetal bovine serum and 1% antibiotics consisting of penicillin (100 U/mL), streptomycin (100 µg/mL) and amphotericin B (250 µg/mL). The cells were incubated at 5% CO_2 and 37˚C until a confluent monolayer was obtained. The cells were sub-cultured using 0.25% trypsin-EDTA once a monolayer had formed.

5.2.6) Antiproliferative activity against HaCaT cells

The method used to determine antiproliferative activity against HaCaT was described by Lall [17]. In this method, the PrestoBlue cell viability reagent was used to measure the antiproliferative effect. Within 96-well microtiter culture plates, cells were seeded into each well at a concentration of 5×10^4 cells/mL and the plates were incubated overnight at 37˚C and 5% CO_2. Stock solutions of the BFE, BFE^+ and BFG were prepared at 20 mg/mL (w/v) in DMSO. The stock solutions were diluted two-fold with 20% DMSO and actinomycin D used as the positive control. Once the cells adhered, the stock solutions, BFS, AuNPs, 20% DMSO and actinomycin D were added in triplicate, resulting in a final concentration ranging between 400-3.125 µg/mL for BFE, BFE^+, their respective AuNPs and BFG, actinomycin D between $0.05\text{-}3.9\times10^{-4}$ µg/mL, 20% DMSO between 20-0.63% and BFS at 10-0.31%. Media (100%), PrestoBlue reagent and a 1% DMSO control were added, however, the PrestoBlue control contained no cells (0%). After 72 hours, PrestoBlue reagent was added and incubated for a further two hours Thereafter, the fluorescence was measured at an excitation/emission wavelength of 560/590 nm using a Victor Nivo plate reader. To calculate the cell viability of each sample, Equation 2 was used.

$$\%\ Viability = \frac{Fluorescence\ \ sample - Fluorescence\ 0\%\ control}{(Fluorescence\ 100\%\ control - Fluorescence\ \ 0\%\ control)} \times 100 \quad (2)$$

5.2.7) Wound healing assay

The wound-healing assay was conducted using a similar method as Liang, Park and Guan [18], with slight modifications. Briefly, 500 µL of 1.5×10^5 cells/mL was seeded into a 48-well plate and incubated overnight at 37˚C and 5% CO_2. Once a confluent layer was formed, a cross was scratched into the cells using a 1 mL pipette tip and the debris was removed and replaced with fresh complete media (500 µL). A stock solution (20 mg/mL) of BFE, BFE^+ and BFG dissolved in DMSO was diluted in DMEM media to a final concentration of 1 mg/mL. These stock solutions, BFS and AuNPs were added in duplicates. The final concentration for BFE, BFE^+, their AuNPs and BFG was 100 and 50 µg/mL, while for BFS, BFSAuNP and BFGAuNP were 10 and 5%. A media (untreated) control and a 0.5% DMSO vehicle control were added, resulting in a final volume of 1.5 ml. Thereafter, the plates were incubated for 15 hours. Images at a magnification of 4× were taken before and after the final incubation period and were processed using ImageJ to determine the percentage wound closure. The following protocol was followed, image type was altered to 8-bit and a bandpass filter was applied. Thereafter, the threshold was adjusted (automatic setting) and minimal radium was applied to enhance the scratch outline. Using the wand tool, the borders of the scratch were selected and the analysis measure function was used to obtain the area, which was recorded. To calculate the percentage wound closure Equation 3 was used.

$$\%\text{Wound closure} = \left(\frac{Area\ of\ scratch\ at\ 0\ hours - Area\ of\ scratch\ at\ 15\ hours}{Area\ of\ scratch\ at\ 0\ hours}\right) \times 100\% \quad (3)$$

A cell viability assay was conducted thereafter using a same method as described in section 5.2.6, whereby 30 µL of Prestoblue viability reagent was added to 300 µL of media and incubated for two hours. Equation 2 was used to calculate the percentage viability.

5.2.8) Granulocyte extraction

Granulocytes were extracted and analyzed based on their histamine production once treated with the prepared samples. The selection criteria of the volunteer were based on whether they had eczema and were above the age of 21 with no history of major diseases. Ethics approval was obtained by the ethics committee of the Faculty of Natural and Agricultural Science (EC120411-046, University of Pretoria, South Africa). To isolate the granulocytes a method described by Oosthuizen [19] was used with alterations. Briefly, 15 mL of freshly collected blood was diluted with incomplete RPMI-1640 media at a 1:1 ratio, at room temperature. Thereafter, 15 mL of diluted blood was layered on 7.5 mL of histopaque and centrifuged at 1500×*g* for 30 minutes. After centrifugation, the erythrocyte and granulocyte layer were collected and transferred into a falcon tube. The erythrocytes were lysed with 10% lysis buffer at a ratio of 1:5 (v/v). After 15 minutes, the cells were centrifuged for seven minutes at 540 x *g* at room temperature. The collected pellet was washed with buffer A containing 45 mL PBS, 0.18 g trisodium citrate and 5 mL pasteurized plasma (8:1:1) and resuspended in complete RPMI-1640 media containing 10% heat-inactivated fetal bovine serum and 1% gentamicin (10 mg/mL).

5.2.9) Quantification of histamine

Histamine from granulocytes cell supernatant was quantified using a Histamine ELISA kit, following the manufacturer's protocol. Granulocytes were stimulated with phorbol 12-myristate 13-acetate (PMA) at a final concentration of 1 µg/mL. The cells were seeded in a 48-well plate at a concentration of 1.5×10^5 cells/mL. After a 24-hour incubation at 37˚C and 5% CO_2, BFE and BFEAuNP were added, in duplicate, at final concentrations of 200, 100 and 50 µg/mL and incubated for 30 minutes. A vehicle control consisting of 0.25% DMSO was prepared in the same manner. Thereafter, 200 µL of cell supernatant was transferred to a 96-

well plate and stored at -80˚C until used. Cell viability was measured using ImageJ at 20x magnification due to the size of the stimulated granulocytes. The average size of the granulocytes after 30 minutes of incubation was determined using the following protocol, the image type was set to 8-bit and a bandpass filter was applied. The gray morphology of the image was set at a radius of 2 pixels with a circular structure element. Thereafter, the background with a rolling ball of more than 12 pixels was subtracted. The threshold was adjusted to the automatic setting and a watershed binary option was selected to ensure that cells were recognized as separate entities. The image particle size at 120-infinity pixels^2 with a circularity of 0.0-1 was measured and the average size was recorded. Thereafter, a same equation as Equation 2 was used to calculate percentage viability.

5.2.10) Statistical analysis

Results are reported as mean ± standard error (or standard deviation) as displayed in the results section. Three repeats were performed, with two repeats conducted for histamine quantification. Furthermore, AuNPs, where applicable, were compared to the untreated control as the stock solutions does not contain DMSO. To obtain the IC_{50} values, a nonlinear regression analysis of the sigmoidal dose-response curves (4-parameter logistic) using GraphPad Prism 4 was conducted. Statistical analysis was done using one-way analysis of variance (ANOVA) followed by Dunnett's multiple comparison tests (GraphPad, version 4), where $p < 0.05$ (*), $p < 0.01$ (**) and $p < 0.001$ (***) were considered statistically significant.

5.3) Results

5.3.1) Characterization of gold nanoparticles

Gold nanoparticles were synthesized from BFE, BFE+, BFG and BFS. During the preparation of the gold nanoparticles, the crude solutions immediately converted from a green or brown to

a wine color once exposed to the gold salt. This was confirmed with UV-Vis as the AuNPs displayed a spectral peak between 540 and 550 nm. Furthermore, the total phenolic content of each nanoparticle was determined to be 2171.62 µg/mL (BFEAuNP), 2005.57 µg/mL (BFE^{+}AuNP), 99.41 µg/mL (BFGAuNP) and 49.01% (BFSAuNP). To determine functional groups present, FTIR was conducted (Fig 5.1-4 A, Table 5.1).

Table 5.1. Potential functional groups. Potential functional groups were identified using Fourier transform infrared spectrometry (FTIR) in *Bulbine frutescens* samples and synthesized gold nanoparticles (AuNPs).

Functional group	***Bulbine frutescens* Sample**	**Transmittance of sample**	**Transmittance of AuNPs**
O-H	BFE [a]	3289	3321
	BFE^{+} [b]	3259	
	BFG [c]	3243	
	BFS [d]	3273	3274
Aromatic rings (C-C)	BFE	-	1637
	BFE+	-	
	BFG	-	
	BFS	1041	
C-H	BFE+	2924	-
C-O	BFE	1072	-
	BFE+	1022	-
	BFG	1055	-
	BFS	1041	-
C=O	BFE+	1620	-
	BFS	1643	-

A: *Bulbine frutescens* ethanolic leaf juice extract, B: *Bulbine frutescens* ethanolic whole leaf extract, C: *Bulbine frutescens* gel extract, D: *Bulbine frutescens* commercial spray solution

The average diameter and zeta-potential for each synthesized nanoparticles were found to be 128.7 ± 78.51 and -10.5 (BFEAuNP), 132.0 ± 96.47 and -14.5 (BFE^{+}AuNP), 51.82 ± 33.76 and -9.27 (BFGAuNP) and 289.3 ± 88.68 nm and -4.02 mV (BFSAuNP). A high-resolution transmission electron microscopy (HRTEM) was used to evaluate the morphology of the synthesized nanoparticles. As displayed in Fig. 5.1-4 B, the morphology of the synthesized nanoparticles consisted mostly of round or hexagonal shapes with one or two triangular shapes while BFSAuNP contained irregularly shaped nanoparticles. Furthermore, a selected area diffraction pattern (SAED) was used to characterize whether the AuNPs displayed a similar plane as gold metal. The face-centered lattice planes of the synthesized nanoparticles displayed a diffractive index of (111), (200), (220) and (311) (Fig. 5.1-4 C).

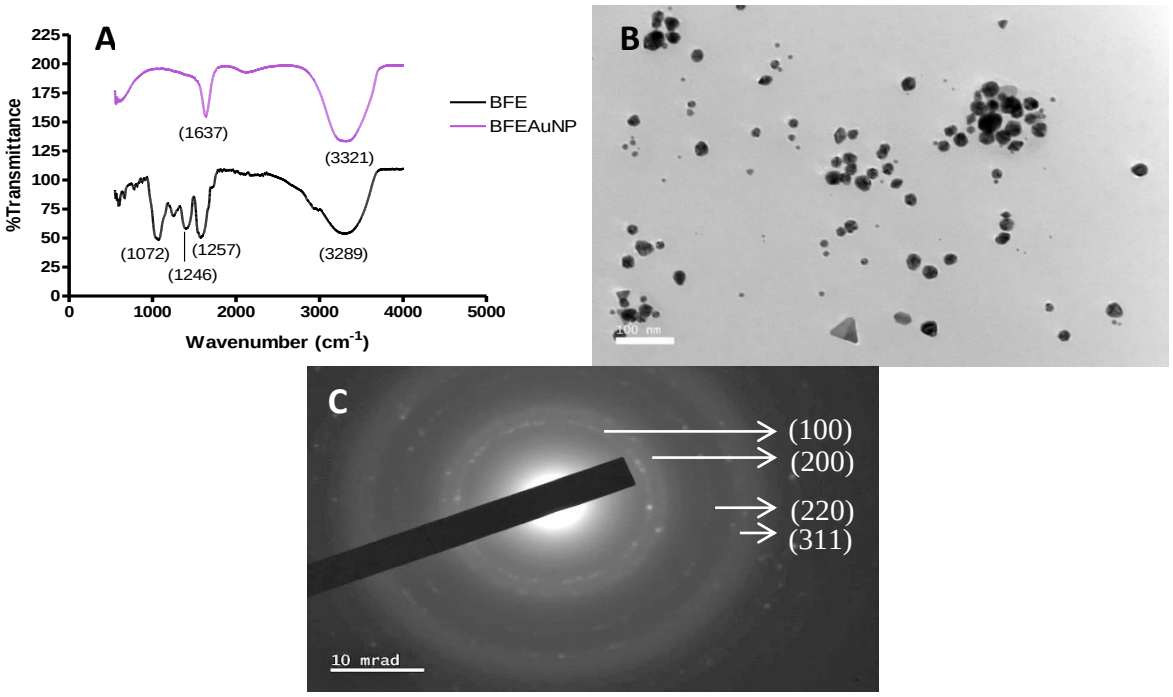

Fig. 5.1. Characterization of *Bulbine frutescens* gold nanoparticles biosynthesized from the freeze-dried ethanolic leaf juice extract (BFEAuNP). Gold nanoparticle characterization including Fourier-transform infrared spectrometry (FTIR) of the ethanolic leaf juice extract (BFE) and synthesized gold nanoparticles (BFEAuNP) (A), high-resolution transmission electron microscopy (HRTEM) at 100 nm (B) and selected area diffraction pattern (SAED) at 10 mrad (D).

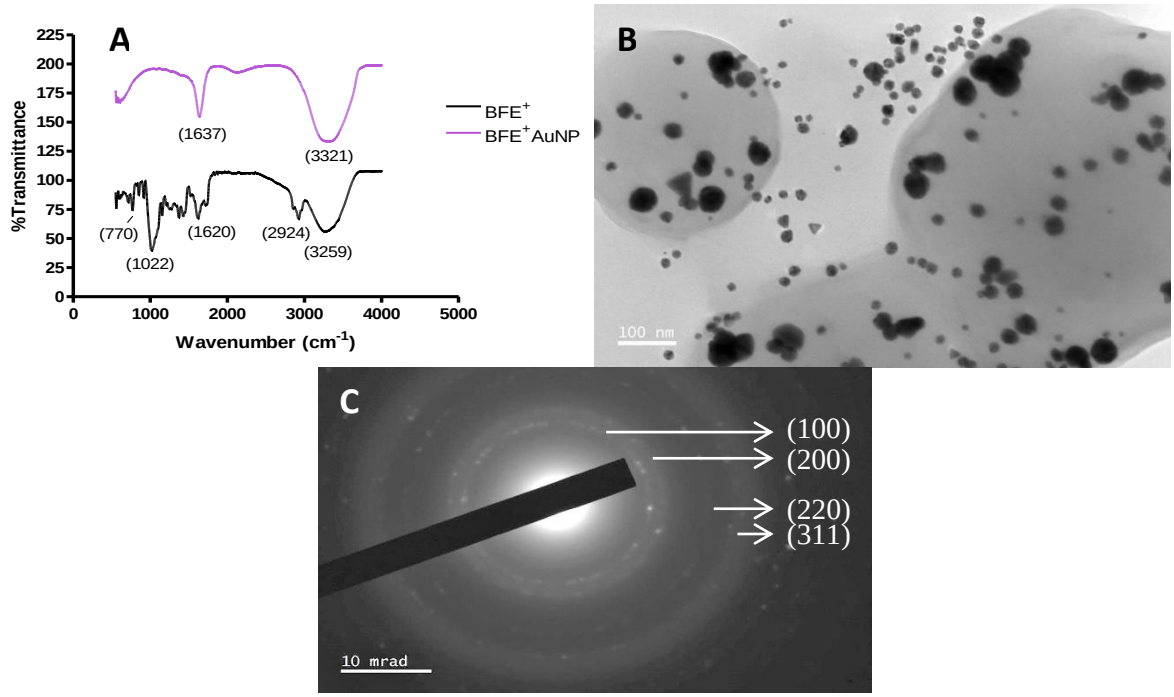

277

278 **Fig. 5.2. Characterization of *Bulbine frutescens* gold nanoparticles biosynthesized from the ethanolic whole**
279 **leaf extract (BFE$^+$AuNP).** Gold nanoparticle characterization including Fourier-transform infrared spectrometry
280 (FTIR) of the ethanolic whole leaf extract (BFE$^+$) and synthesized gold nanoparticles (BFE$^+$AuNP) (A), high-
281 resolution transmission electron microscopy (HRTEM) at 100 nm (B) and selected area diffraction pattern
282 (SAED) at 10 mrad (D).

283

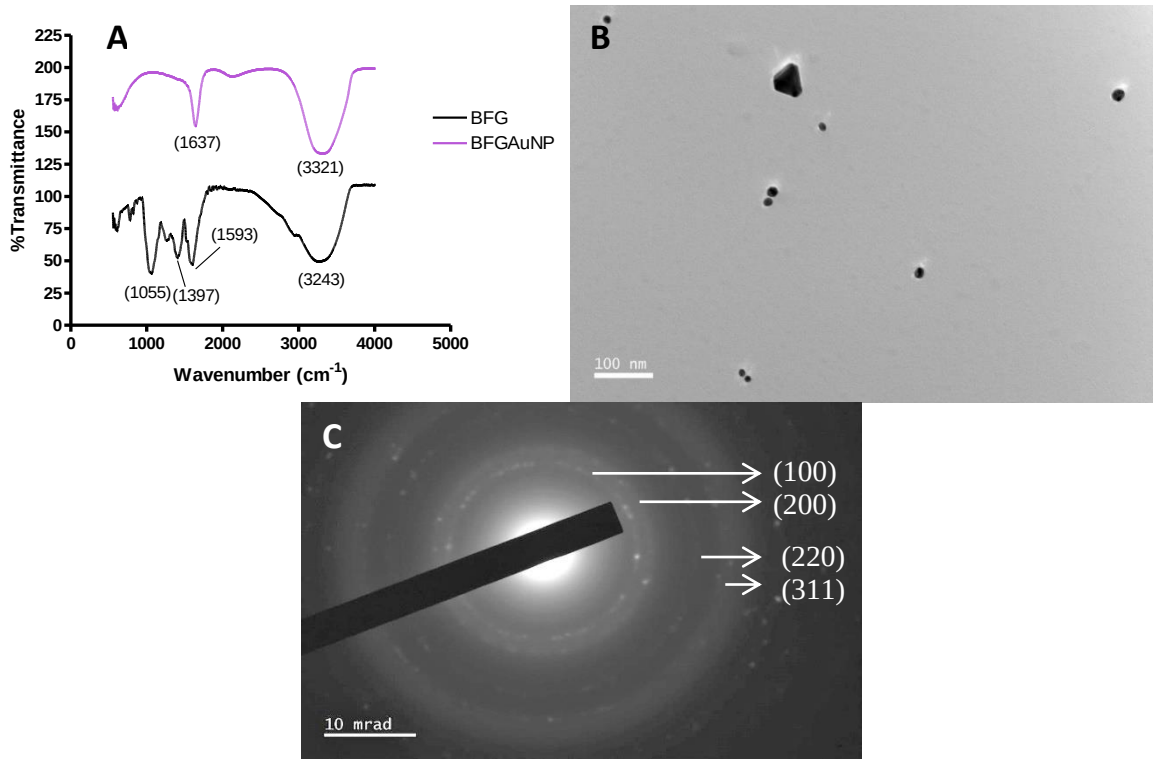

284

285 **Fig. 5.3. Characterization of *Bulbine frutescens* gold nanoparticles biosynthesized from the gel extract**
286 **(BFGAuNP).** Gold nanoparticle characterization including Fourier-transform infrared spectrometry (FTIR) of the
287 freeze-dried gel extract (BFG) and synthesized gold nanoparticles (BFGAuNP) (A), high-resolution transmission
288 electron microscopy (HRTEM) at 100 nm (B) and selected area diffraction pattern (SAED) at 10 mrad (D).

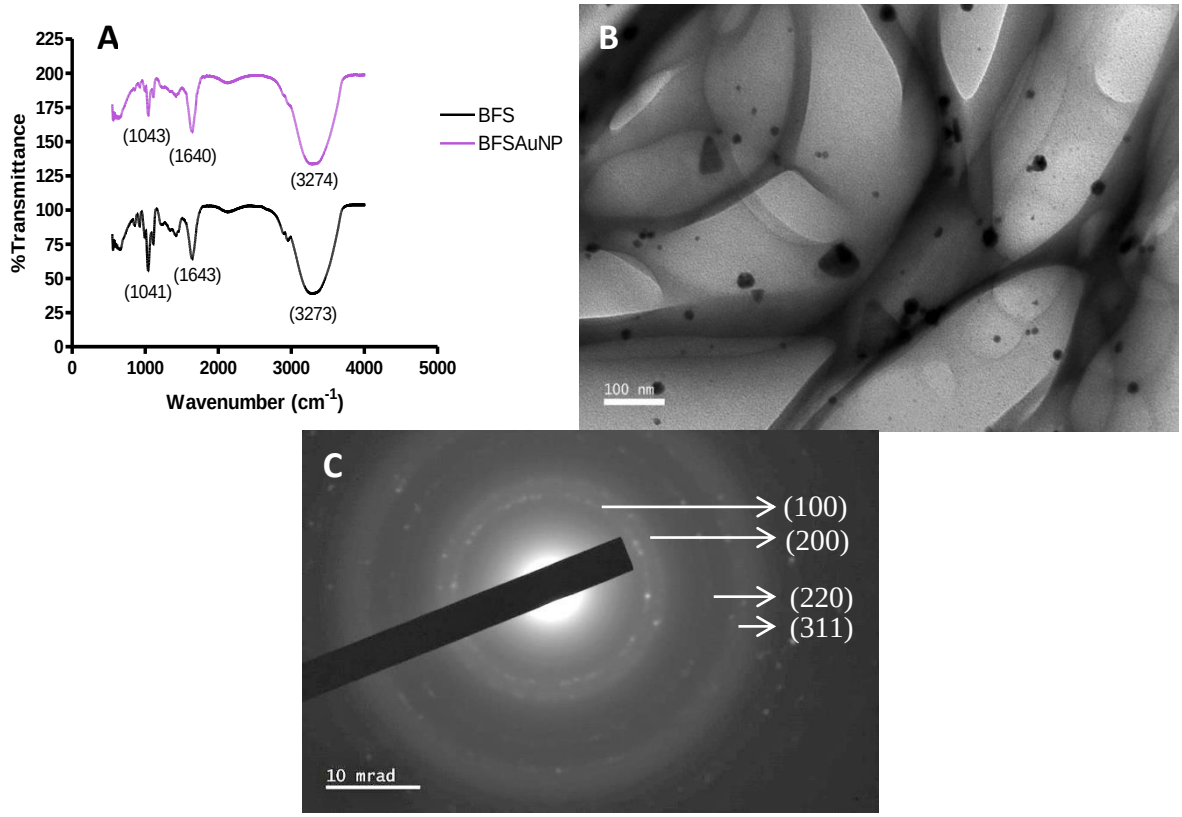

289

290 **Fig. 5.4. Characterization of *Bulbine frutescens* gold nanoparticles biosynthesized from the commercial**
291 **spray (BFSAuNP).** Gold nanoparticle characterization including Fourier-transform infrared spectrometry (FTIR)
292 of the commercial spray obtained from Botanica (BFS) and synthesized gold nanoparticles (BFSAuNP) (A), high-
293 resolution transmission electron microscopy (HRTEM) at 100 nm (B) and selected area diffraction pattern
294 (SAED) at 10 mrad (D).

295

296 Lastly, *in vitro* stability indicated that AuNPs displayed minimal shifts in the surface plasmon
297 resonance peaks (λ_{max}) when exposed to most of the mediums (Fig. 5.5-8). Furthermore,
298 BFEAuNP displayed low peaks when exposed to solutions with a pH level of 7 or containing
299 NaCl (Fig. 5.5 C and E), while BFGAuNP and BFSAuNP showed low peaks when added to
300 BSA (Fig. 5.7 and 8 G).

301

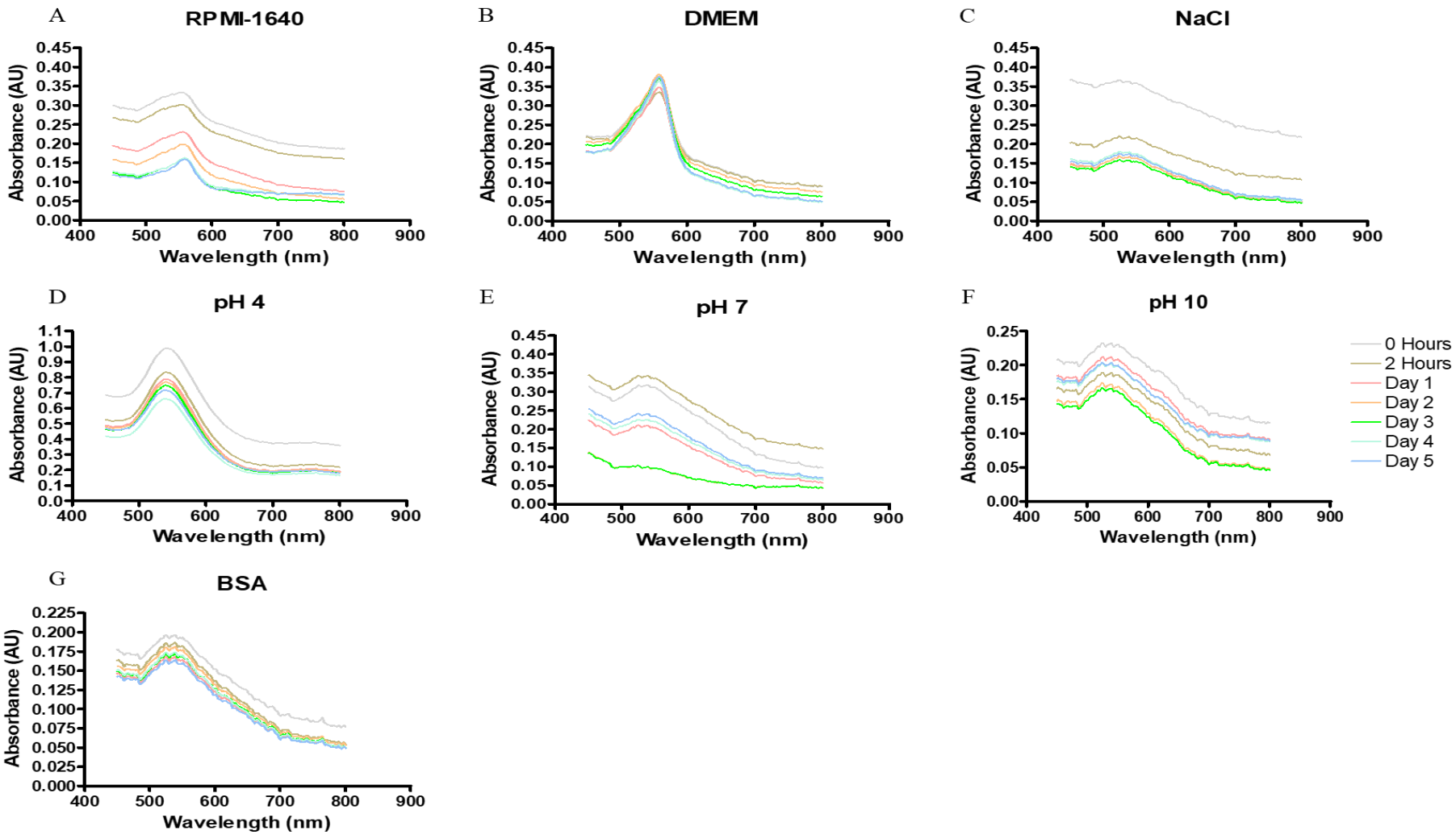

Fig. 5.5. *In vitro* stability of *Bulbine frutescens* ethanolic leaf juice synthesized gold nanoparticles (BFEAuNP). *In vitro* stability of *Bulbine frutescens* ethanolic synthesized leaf juice gold nanoparticles (BFEAuNP) in different mediums. These solutions include Roswell Park Memorial Institution (RPMI-1640) medium (A) and Dulbecco's modified Eagle's Medium (DMEM) (B), 5% sodium chloride (NaCl) (C), pH level of 4 (D), 7 (E) and 10 (F) and 0.5% bovine serum albumin (BSA) (G).

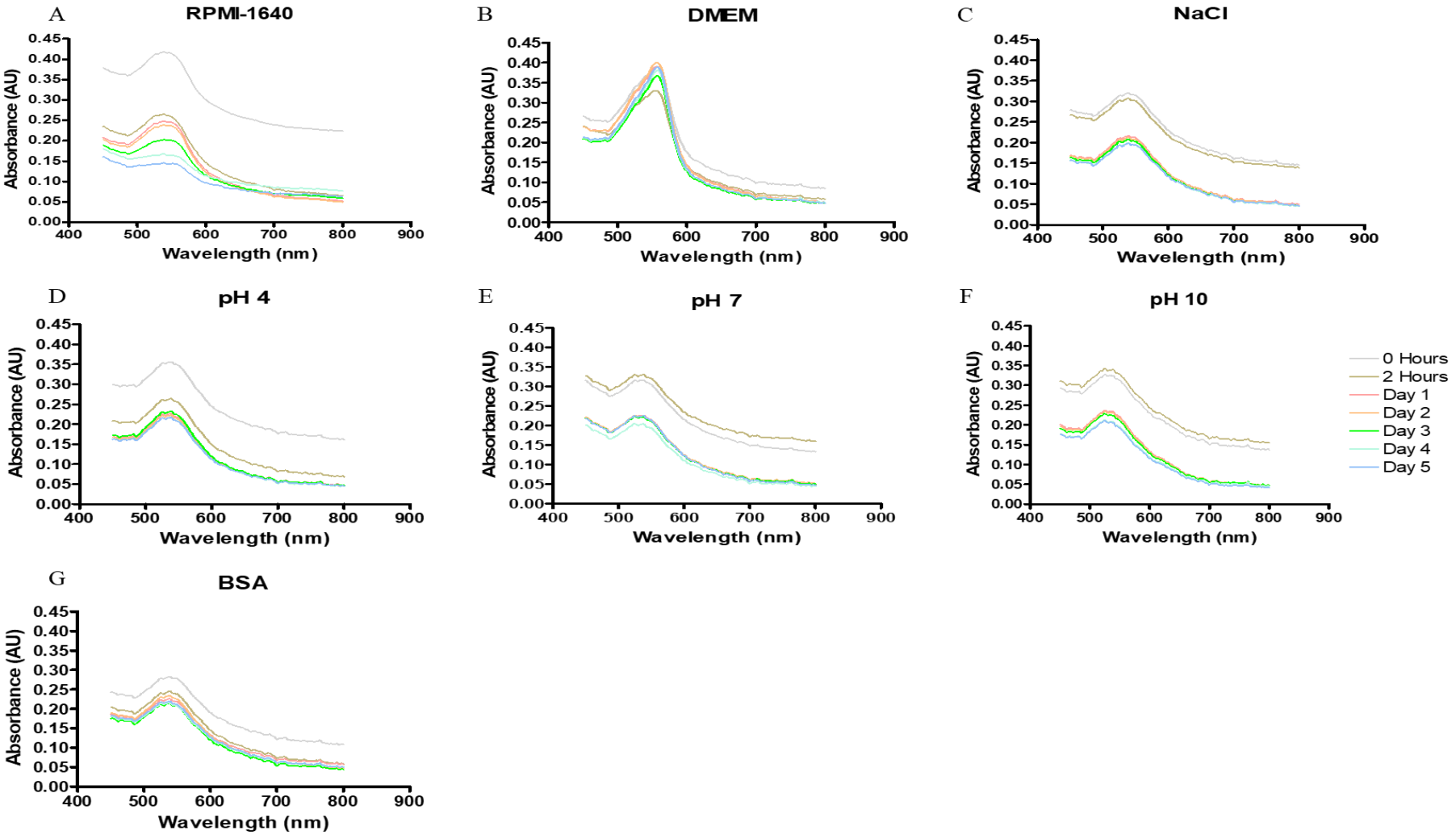

306

307 **Fig. 5.6. *In vitro* stability of *Bulbine frutescens* ethanolic whole leaf synthesized gold nanoparticles (BFE^{+}AuNP).** *In vitro* stability of *Bulbine frutescens* ethanolic whole
308 leaf synthesized gold nanoparticles (BFE^{+}AuNPs) in different mediums. These solutions include incomplete Roswell Park Memorial Institution (RPMI-1640) medium (A) and
309 Dulbecco's modified Eagle's Medium (DMEM) (B), 5% sodium chloride (NaCl) (C), pH level of 4 (D), 7 (E) and 10 (F) and 0.5% bovine serum albumin (BSA) (G).

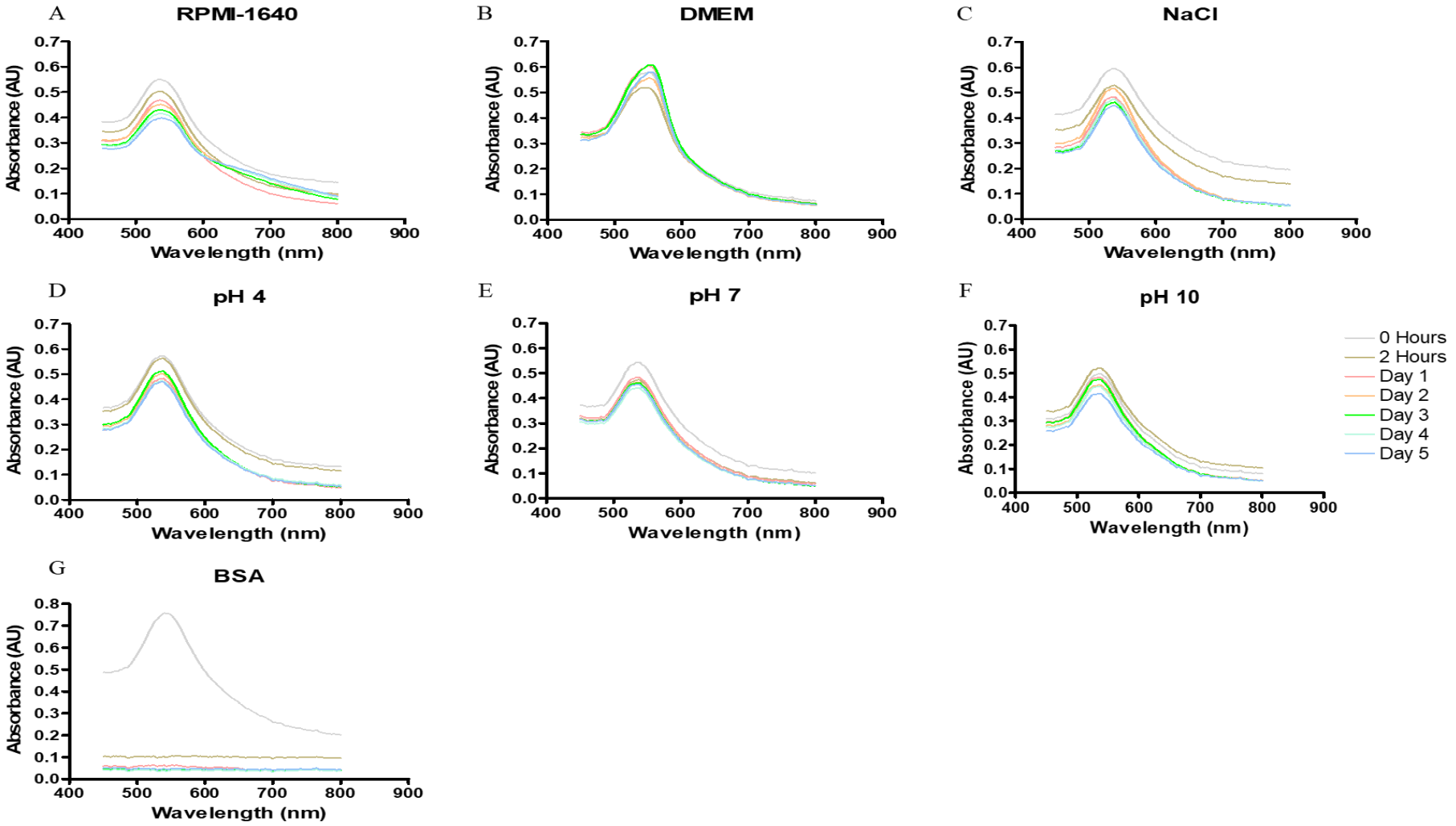

Fig. 5.7. *In vitro* stability of *Bulbine frutescens* freeze-dried gel synthesized gold nanoparticles (BFGAuNP). *In vitro* stability of *Bulbine frutescens* freeze-dried gel synthesized gold nanoparticles (BFGAuNP) in different mediums. These solutions include incomplete Roswell Park Memorial Institution (RPMI-1640) medium (A) and Dulbecco's modified Eagle's Medium (DMEM) (B), 5% sodium chloride (NaCl) (C), pH level of 4 (D), 7 (E) and 10 (F) and 0.5% bovine serum albumin (BSA) (G).

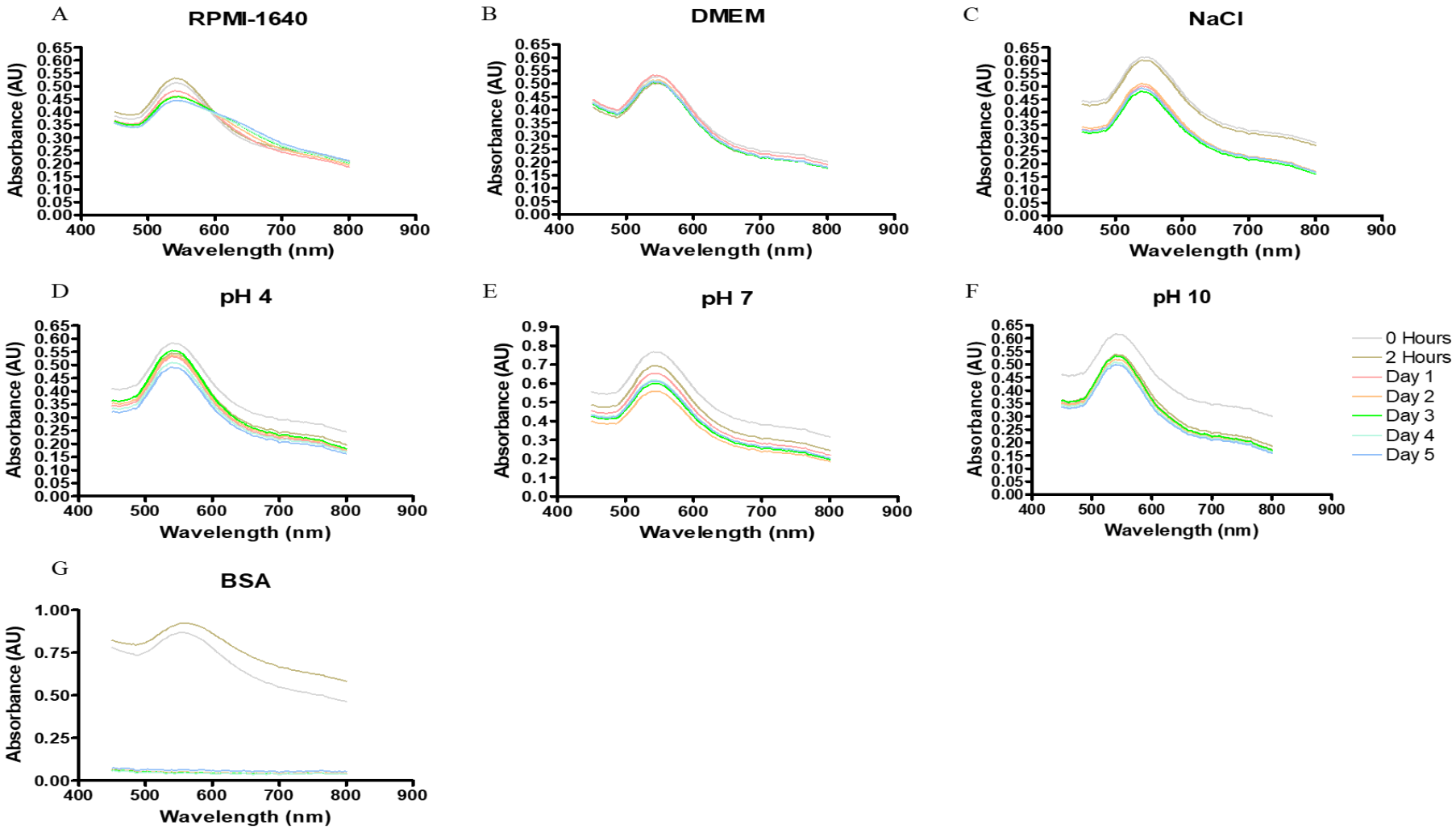

Fig. 5.8. *In vitro* stability of *Bulbine frutescens* commercial spray synthesized gold nanoparticles (BFSAuNP). *In vitro* stability of *Bulbine frutescens* commercial spray synthesized gold nanoparticles (BFSAuNPs) in different mediums. These solutions include incomplete Roswell Park Memorial Institution (RPMI-1640) medium (A) and Dulbecco's modified Eagle's Medium (DMEM) (B), 5% sodium chloride (NaCl) (C), pH level of 4 (D), 7 (E) and 10 (F) and 0.5% bovine serum albumin (BSA) (G).

5.3.2) Antiproliferative activity

BFS and BFSAuNPs displayed antiproliferative activity against HaCaT cells with an IC_{50} of 4.63 ± 0.05 and 3.50 ± 0.40%, respectfully while BFE, BFE^+, BFG, BFEAuNP, BFE^+AuNP (IC_{50} > 400 µg/mL) and BFGAuNP (IC_{50} > 10%) displayed no activity. Samples that displayed significant wound closure as shown in section 5.3.3 were further evaluated for histamine production. None of the selected samples displayed antiproliferative activity against granulocyte cells (IC_{50} > 200 µg/mL). Moreover, the positive controls (actinomycin D and 20% DMSO) displayed antiproliferative properties with an IC_{50} of 0.01 ± 0.002 µg/mL and 6.06 ± 0.77%.

5.3.3) Wound healing assay

A cell viability assay on the stimulated wound inflicted HaCaT cells was conducted. At a concentration of 400 µg/mL, BFE^+ (49.56 ± 9.10%) significantly reduced ($p < 0.001$) cell viability in comparison to the vehicle control (97.46 ± 3.90%), thus a concentration of 100 and 50 µg/mL was selected for further evaluation against wound closure (Fig. 5.9).

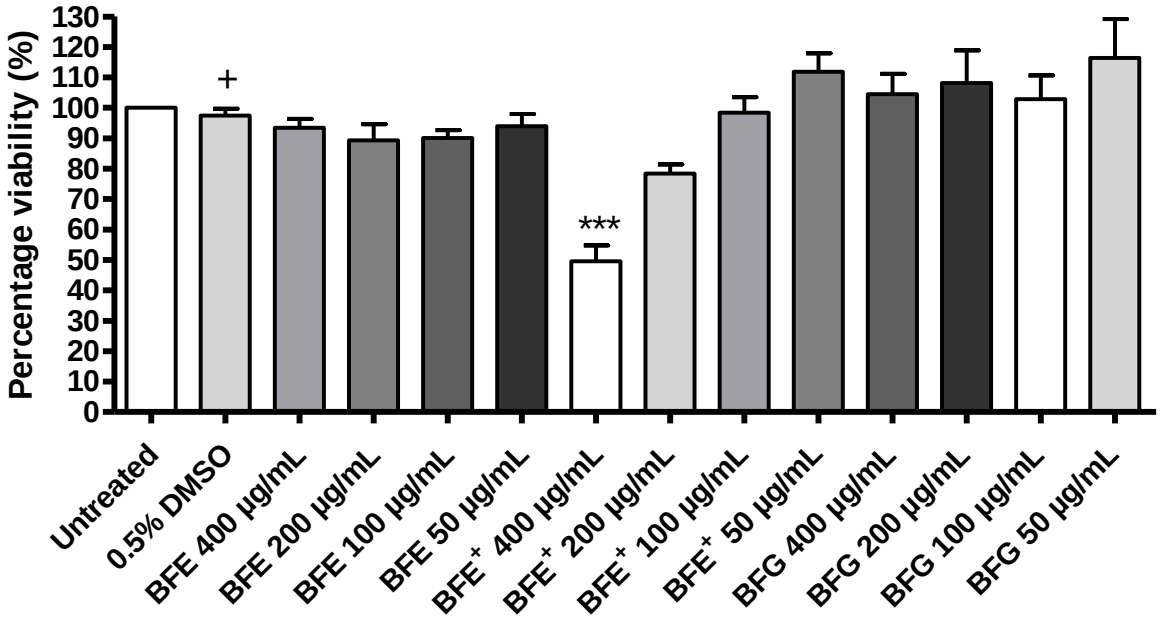

Fig. 5.9. Cell viability after treatment with *Bulbine frutescens* on wound stimulated human keratinocytes (HaCaT) cells. Cell viability after treatment with the ethanolic leaf juice (BFE), ethanolic whole leaf (BFE+) and gel extract (BFG) of *Bulbine frutescens* at a concentration of 400-50 µg/mL on wound stimulated human keratinocytes (HaCaT) cells. Data represent mean ± SEM (n=2). A significant difference was determined using a one-way ANOVA followed by Dunnett's multiple comparison test, where $p < 0.05$ (*), $p < 0.01$ (**) and $p < 0.001$ (***) indicate significance when compared to the vehicle (0.5% DMSO) control (+).

Furthermore, the percentage wound closure was measured and recorded for *B. frutescens* samples (Fig. 5.10 and 5.11). At a concentration of 100 (31.40 ± 0.88 %, $p < 0.01$) and 50 µg/mL (22.22 ± 1.73 %, $p < 0.05$), BFE displayed significant wound closure in comparison to the vehicle control (9.63 ± 0.22 %). BFE^+ and BFG at 100 µg/mL and BFS at 2% displayed no significant effect when compared to the vehicle control. Moreover, BFEAuNP (20.87 ± 0.69 %) at 100 µg/mL significantly enhanced ($p < 0.05$) wound closure when compared to the untreated control (9.30 ± 0.15 %). BFE^+AuNP at 100 µg/mL, BFGAuNP at 10% and BFSAuNP at 2% displayed no significant effect when compared to the untreated control.

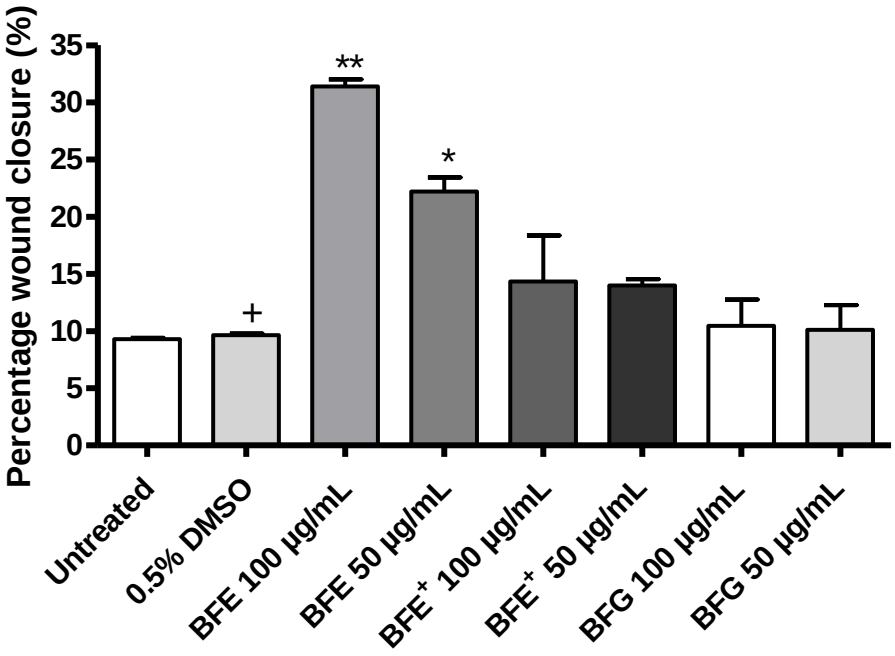

348

349 **Fig. 5.10. Wound healing properties.** Percentage wound closure of *Bulbine frutescens* ethanolic leaf juice (BFE),
350 ethanolic whole leaf (BFE^{+}) and gel extract (BFG) at a concentration range of 100 and 50 µg/mL on wound
351 stimulated human keratinocytes (HaCaT). Data represent mean ± SEM (n=2). A significant difference was
352 determined using a one-way ANOVA followed by Dunnett's multiple comparison test, where $p < 0.05$ (*) and p
353 < 0.01 (**) indicate significance when compared to the vehicle (0.5% DMSO) control (+).

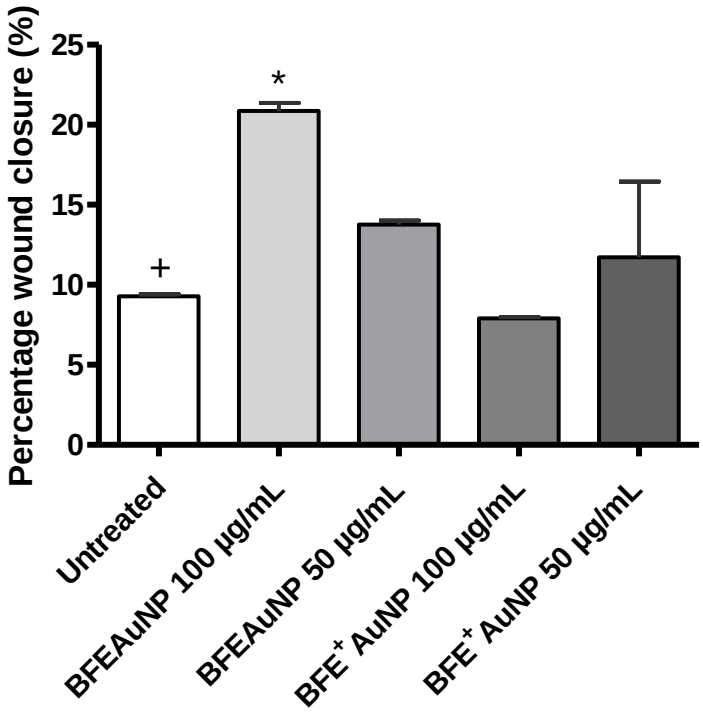

354

355 **Fig. 5.11. Wound healing properties.** Percentage wound closure of *Bulbine frutescens* ethanolic leaf juice
356 synthesized gold nanoparticle (BFEAuNP) and ethanolic whole leaf synthesized gold nanoparticle (BFE^{+}AuNP)
357 solutions at a concentration range of 100 and 50 µg/mL on wound stimulated human keratinocytes (HaCaT). Data

represent mean ± SEM (n=2). A significant difference was determined using a one-way ANOVA followed by Dunnett's multiple comparison test, where $p < 0.05$ (*) and $p < 0.01$ (**) indicate significance when compared to the untreated control (+).

5.3.4) Quantification of histamine

The effects of BFE and BFEAuNP against histamine production were quantified due to the significant wound closure observed. A cell viability assay on PMA stimulated granulocytes was conducted to ensure the modulation of histamine was not due to cell death. The samples displayed no significant difference in cell viability compared to the untreated control (Fig. 5.12).

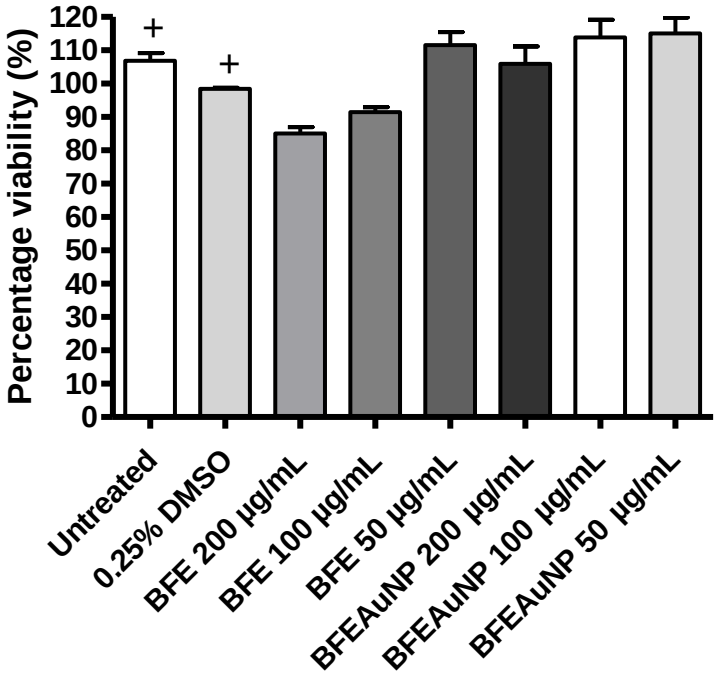

Fig. 5.12. Cell viability after treatment with *Bulbine frutescens* on PMA stimulated granulocytes. Cell viability after treatment with the ethanolic leaf juice (BFE) extract and synthesized gold nanoparticles (BFEAuNP) of *Bulbine frutescens* at a concentration of 200, 100 and 50 µg/mL on phorbol 12-myristate 13-acetate (PMA) stimulated granulocytes. Data represent mean ± SEM (n=2). A significant difference was determined using a one-way ANOVA followed by Dunnett's multiple comparison test when compared to the untreated and vehicle control (+).

Compared to the untreated control (0.30 ± 0.02 ng/mL), BFEAuNP significantly inhibited histamine production at a concentration of 100 (0.12 ± 0.04, $p < 0.01$) and 50 µg/mL (0.02 ± 0.008 ng/mL, $p < 0.001$) (Fig. 5.13), while BFE (0.42 ± 0.02 ng/mL) significantly stimulated ($p < 0.01$) histamine production at 200 µg/mL when compared to the vehicle control (0.26 ± 0.02 ng/mL) (Fig. 5.14).

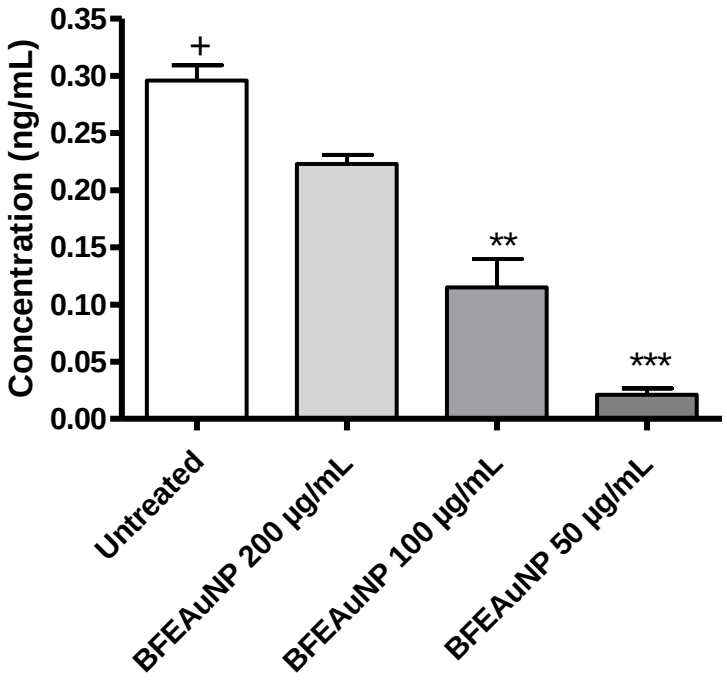

Fig. 5.13. Effects of *Bulbine frutescens* synthesized gold nanoparticles against histamine production. *Bulbine frutescens* ethanolic leaf juice synthesized gold nanoparticles (BFEAuNPs) effect on histamine production at a concentration of 200, 100 and 50 µg/mL on phorbol 12-myristate 13-acetate (PMA) stimulated granulocytes. Data represent mean ± SEM (n=2). Significant difference was determined using a one-way ANOVA followed by Dunnett's multiple comparison test, where $p < 0.01$ (**) and $p < 0.001$ (***) indicate significance when compared to the untreated control (+).

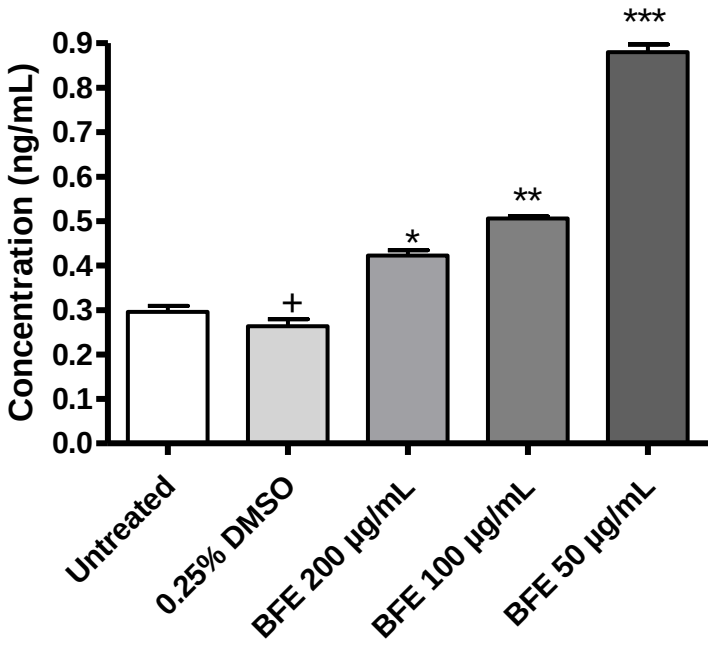

388

389 **Fig. 5.14. Effects of *Bulbine frutescens* ethanolic leaf juice extract (BFE).** *Bulbine frutescens* ethanolic leaf
390 juice extracts (BFE) antihistamine production at a concentration of 200, 100 and 50 µg/mL on phorbol 12-
391 myristate 13-acetate (PMA) stimulated granulocytes. Data represent mean ± SEM (n=2). Significant difference
392 was determined using a one-way ANOVA followed by Dunnett's multiple comparison test, where $p < 0.05$ (*),
393 $p < 0.01$ (**) and $p < 0.001$ (***) indicate significance when compared to the vehicle control (+).

394

395 5.4) Discussion

396 Characterization of the synthesized gold nanoparticles using various methods was conducted
397 to identify the potential effect the size, morphology and stability of the AuNPs would have on
398 the biological activity focused on in this study [16]. Using FTIR analysis, numerous functional
399 groups were found in the prepared samples of *B. frutescens*, which display vibration stretches.
400 These stretches indicate the presence of phenolic compounds within the AuNPs. This supports
401 the high phenolic content observed for BFE, BFE+ and BFS. Moreover, minimal functional
402 groups were found in BFG, supporting the low phenolic content that was observed for
403 BFGAuNP [20].

The stability of the AuNP's was evaluated in different mediums that mimicked physiological environments. Mediums, where a low SPR peak was observed, could be due to the electrostatic repulsion of the nanoparticle as nanoparticles with a zeta potential above or below ± 30 mV are considered stable. In accordance the study conducted by Salopek [21], BFEAuNP (-10.5) and BFE^{+}AuNP (-14.5 mV) displayed slight agglomeration while BFGAuNP (-9.27) and BFSAuNP (-4.02 mV) showed strong agglomeration and precipitation. This suggests that BFEAuNP, BFSAuNP and BFGAuNP may have agglomerated when exposed to the different mediums resulting in a low SPR peak.

A study conducted by Nguyen et al (2016) indicated that the leaf juice of *Carica papaya* L. significantly reduced cell viability ($p < 0.001$) of HaCaT cells at a concentration of 20 mg/mL [22]. Since the commercial spray is comprised of organic leaf juice at an unknown concentration, it was suggested that the high antiproliferative effect of BFS could be due to the high concentration of extract present in the spray. Thus, the composition of BFS needs to be confirmed in order to support this. Similar antiproliferative properties against HaCaT cells for the BFE^{+} and BFG were found in a study conducted by Nel et al. (2022) [23].

A study conducted by Tambama et al. (2014), indicated that a compound previously isolated from *B. frutescens* known as isofuranonaphthoquinone displayed no effect on cell viability at the highest concentration (37.5 µg/mL) compared to the negative control when exposed to Jurkat T cells for 24 hours [14]. This study supports the cell viability obtained for BFE and BFEAuNP as Jurkat T cells are similar to granulocytes since both of these cell lines are white blood cells.

Though *B. frutescens* is traditionally used to treat wounds, no studies could be found on the sample's *in vitro* healing effect on HaCaT cells [24]. Anthraquinone knipholone, a compound previously isolated from the leaf juice of *B. frutescens,* has previously displayed high

antioxidant activity with an IC_{50} of 22 ± 1.5 µM [25, 26]. Since reactive oxygen species are known to reduce wound healing capabilities, this study concluded that anthraquinone knipholone may possess wound healing properties. This could potentially provide an explanation for the wound healing properties observed for BFE and BFEAuNP, however, further investigation is required.

Furthermore, studies have shown that chrysophanol displayed anti-inflammatory activity at a concentration of 20 µM and is thought to reduce histamine production. A derivative of this compound, known as chrysophanol glucuronide, was previously isolated from *B. frutescens* [27, 28]. This derivative could potentially have the same effect as chrysophanol, as BFEAuNP displayed antihistamine activity, however, further studies are needed.

5.5) Conclusion

For the purpose of this study, the potential wound healing and antihistamine properties of *Bulbine frutescens* were evaluated and whether the biosynthesis of AuNPs would enhance the biological activity. Of the eight samples that were evaluated, BFS and BFSAuNP displayed antiproliferative activity against HaCaT cells (IC_{50} of 4.63 ± 0.05 and 3.50 ± 0.40%), while the remaining samples including BFE, BFE+, BFG and their respected AuNPs displayed no effect (IC_{50} > 400 µg/mL and 10%). Furthermore, BFE (31.40 ± 0.88%, $p < 0.01$) and BFEAuNP (20.87 ± 0.69%, $p < 0.05$) displayed significant wound closure at the highest testing concentration (100 µg/mL) and were further evaluated against histamine production.

None of the selected samples displayed antiproliferative properties against granulocytes (IC_{50} > 200 µg/mL). In comparison to the untreated control, BFEAuNP at a concentration of 100 and 50 µg/mL significantly inhibited the production of histamine. Moreover, BFE, when compared to the vehicle control, significantly stimulated histamine production at a concentration of 200 µg/mL. This contrast in activity between BFE and BFEAuNP could be due to the

encapsulation of compounds causing a potential increase in symbiotic interactions, however, further studies are required. In conclusion, the potential wound healing properties of BEFAuNP correlates with the antihistamine effect displayed at a concentration of 100 µg/mL. Thus, further investigations into the potential *in vivo* wound healing properties of BFEAuNP and whether the sample targets histamine-associated receptors on mast cells as a potential mode of action should be considered.

Funding statement

This work was supported by the National Research Foundation [grant number 105169 and 98334].

Acknowledgement

The authors would like to acknowledge Mrs. Bianca D. Payne and Mrs. Tenille Esmear (Department of Plant and Soil Sciences, University of Pretoria) for their guidance. Furthermore, the authors would like to acknowledge Dr. Suprakas S. Ray (DST/CSIR National Centre for Nanostructured Materials, Council for Scientific and Industrial Research), Prof Kattesh V. Katti, Dr. Velaphi C. Thipe (Department of Radiology, Institute of Green Nanotechnology, University of Missouri Columbia), Dr. Vusani Mandiwana, Michel L. Kalombo (Chemical Cluster, Centre for Nanostructures and Advanced Materials, Council for Scientific and Industrial Research) and Dr. Arno Janse van Vuuren (Centre for High Resolution Transmission Electron Microscopy, Nelson Mandela University) for conducting the FTIR, DLS, zeta potential and HRTEM analysis. Lastly the authors would like to thank the Department of Science and Innovation (DSI) for funding contributions.

References

1. Sullivan M, Silverberg NB. Current and emerging concepts in atopic dermatitis pathogenesis. Clinics in dermatology. 2017;35(4):349-53. doi: 10.1016/j.clindermatol.2017.03.006.
2. Lee H, Lee S. Epidermal permeability barrier defects and barrier repair therapy in atopic dermatitis. Allergy, asthma & immunology research. 2014;6(4):276-87. doi: 10.4168/aair.2014.6.4.276.
3. Palmer CNA, Irvine AD, Terron-Kwiatkowski A, Zhao Y, Liao H, Lee SP, et al. Common loss-of-function variants of the epidermal barrier protein filaggrin are a major predisposing factor for atopic dermatitis. Nature Genetics. 2006;38:441-6. doi: https://doi.org/10.1038/ng1767.
4. Brown SJ, McLean WHI. One remarkable molecule: filaggrin. Journal of Investigative Dermatology. 2012;132(3):751-62. doi: 10.1038/jid.2011.393.
5. Voisin T, Chiu IM. Molecular link between itch and atopic dermatitis. Proceedings of the National Academy of Sciences. 2018;115(51):12851-3. doi: 10.1073/pnas.1818879115.
6. Buddenkotte J, Maurer M, Steinhoff M. Histamine and antihistamines in atopic dermatitis. Histamine in Inflammation. Boston: Springer; 2010. p. 73-80.
7. Gschwandtner M, Mildner M, Mlitz V, Gruber F, Eckhart L, Werfel T, et al. Histamine suppresses epidermal keratinocyte differentiation and impairs skin barrier function in a human skin model. Allergy. 2013;68(1):37-47. doi: 10.1111/all.12051.
8. Gutowska-Owsiak D, Greenwald L, Watson C, Selvakumar T, Wang X, Ogg G. The histamine-synthesizing enzyme histidine decarboxylase is upregulated by keratinocytes in atopic skin. British Journal of Dermatology. 2014;171(4):771-8. doi: 10.1111/bjd.13199.
9. Abdissa N, Heydenreich M, Midiwo JO, Ndakala A, Majer Z, Neumann B, et al. A xanthone and a phenylanthraquinone from the roots of *Bulbine frutescens*, and the revision of six seco-anthraquinones into xanthones. Phytochemistry Letters. 2014;9:67-73. doi: https://doi.org/10.1016/j.phytol.2014.04.004.
10. Hoffman D-D. Snake Flower – *Bulbine frutescens* 2020 [cited 2020 28 April]. Available from: https://herbclass.com/bulbine-frutescens/.
11. Harris S. *Bulbine frutescens* 2003 [cited 2020 28 April]. Available from: http://pza.sanbi.org/bulbine-frutescens.
12. Pather N, Kramer B. *Bulbine natalensis* and *Bulbine frutescens* promote cutaneous wound healing. Journal of ethnopharmacology. 2012;144(3):523-32.
13. Coopoosamy R. Traditional information and antibacterial activity of four Bulbine species (Wolf). African journal of Biotechnology. 2011;10(2):220-4.
14. Tambama P, Abegaz B, Mukanganyama S. Antiproliferative activity of the isofuranonaphthoquinone isolated from *Bulbine frutescens* against jurkat T cells. BioMed Research International. 2014;2014:1-14. doi: https://doi.org/10.1155/2014/752941.
15. Bringmann G, Mutanyatta-Comar J, Maksimenka K, Wanjohi JM, Heydenreich M, Brun R, et al. Joziknipholones A and B: the first dimeric phenylanthraquinones, from the roots of *Bulbine frutescens*. Chemistry–A European Journal. 2008;14(5):1420-9.
16. De Canha MN, Thipe VC, Katti KV, Mandiwana V, Kalombo L, Ray SS, et al. The activity of gold nanoparticles synthesized using Helichrysum odoratissimum against Cutibacterium acnes biofilms. Frontiers in cell and developmental biology. 2021:2288.
17. Lall N, Blom van Staden A, Rademan S, Lambrechts I, De Canha MN, Mahore J, et al. Antityrosinase and anti-acne potential of plants traditionally used in the Jongilanga community in Mpumalanga. South African Journal of Botany. 2019;126:241-9. doi: https://doi.org/10.1016/j.sajb.2019.07.015.

18. Liang C-C, Park AY, Guan J-L. In vitro scratch assay: a convenient and inexpensive method for analysis of cell migration in vitro. Nature protocols. 2007;2(2):329-33.
19. Oosthuizen C, Arbach M, Meyer D, Hamilton C, Lall N. Diallyl polysulfides from *Allium sativum* as immunomodulators, hepatoprotectors, and antimycobacterial agents. Journal of Medicinal Food. 2017;20(7):685-90. doi: https://doi.org/10.1089/jmf.2016.0137.
20. Sathishkumar G, Jha PK, Vignesh V, Rajkuberan C, Jeyaraj M, Selvakumar M, et al. Cannonball fruit (Couroupita guianensis, Aubl.) extract mediated synthesis of gold nanoparticles and evaluation of its antioxidant activity. Journal of Molecular Liquids. 2016;215:229-36.
21. Salopek B, Krasic D, Filipovic S. Measurement and application of zeta-potential. Rudarsko-geolosko-naftni zbornik. 1992;4(1):147.
22. Nguyen TT, Parat M-O, Shaw PN, Hewavitharana AK, Hodson MP. Traditional aboriginal preparation alters the chemical profile of Carica papaya leaves and impacts on cytotoxicity towards human squamous cell carcinoma. PLoS One. 2016;11(2):e0147956.
23. Nel M, van Staden AB, Twilley D, Oosthuizen CB, Meyer D, Kumar S, et al. Potential of succulents for eczema-associated symptoms. South African Journal of Botany. 2022.
24. Hutchings A. Zulu medicinal plants: An inventory: University of Natal press; 1996.
25. Habtemariam S. Antioxidant activity of Knipholone anthrone. Food chemistry. 2007;102(4):1042-7.
26. Prisa D. Effective Microorganisms Improve Growth and Minerals Content in the Medicinal Plant Bulbine frutescens. Indian Journal of Natural Sciences. 2022;12(70):37763-70.
27. Xie L, Tang H, Song J, Long J, Zhang L, Li X. Chrysophanol: a review of its pharmacology, toxicity and pharmacokinetics. Journal of Pharmacy and Pharmacology. 2019;71(10):1475-87.
28. Kushwaha PP, Maurya SK, Singh A, Prajapati KS, Singh AK, Shuaib M, et al. Bulbine frutescens phytochemicals as novel ABC-transporter inhibitor: a molecular docking and molecular dynamics simulation study. Journal of Cancer Metastasis and Treatment. 2021;7:2.

Chapter 6. Conclusion and future studies

6.1. Conclusion and future studies

Three South African plants namely *Juncus lomatophyllus* (JL), *Elegia tectorum* (ET) and *Bulbine frutescens* (BF) were evaluated for their potential effect against eczema-associated symptoms including tyrosinase expression, elastase production and wound healing properties as well as the effect these plants may have on the production of either tumor necrosis factor-alpha (TNF-α) or histamine. Furthermore, this study observed whether synthesizing gold nanoparticles (AuNP) from JL, ET and BF or fermenting JL and ET using *Bifidobacterium bifidum* would enhance the biological activity. Lastly, due to the limited amount of information on the compound composition of JL, a bioassay guided fractionation was conducted.

Seven semi-pure fractions were pooled from the butanol partition (JLB), of which P4 and P5 displayed the highest anti-tyrosinase activity. Gas chromatography-mass spectrometry (GC-MS) concluded that 78 and 92 peaks were present in P4 and P5 of which n-hexadenoic acid, which was present in P4, has previously displayed anti-tyrosinase activity. The gold synthesized nanoparticle of JL (JLAuNPs) displayed enhanced anti-tyrosinase activity in comparison to the ethanolic (JL-EtOH) and fermented (JLF) extract of JL (IC_{50} > 400 µg/mL). Thus, JLAuNP, JLB and JL-EtOH were further evaluated for their effects against TNF-α using lipopolysaccharide (LPS) stimulated peripheral blood mononuclear cells (PBMCs). None of the samples displayed antiproliferative effects against human keratinocyte (HaCaT) cells and PBMCs (IC_{50} > 400 µg/mL). JLAuNPs (23.59 ± 1.95 pg/mL), when compared to the untreated control (42.40 ± 4.17 pg/mL), significantly inhibited TNF-α production while JL-EtOH and JLB displayed no effect at 200 µg/mL.

The effects of the ethanolic extract of ET (ET-EtOH) against elastase production (IC_{50} of 28.27 ± 2.02 µg/mL) was not enhanced by the formation of gold nanoparticles or through fermentation (IC_{50} > 500 µg/mL). Thus, ET-EtOH was selected for further evaluation against histamine production using phorbol 12-myristate 13-acetate (PMA) stimulated granulocytes. ET-EtOH significantly inhibited histamine production at a concentration of 6 (0.10 ± 0.01) and 3 µg/mL (0.11 ± 0.01 ng/mL) in comparison to the vehicle control (0.26 ± 0.02 ng/mL).

Four extracts were prepared from the leaves and gel of BF and were evaluated for their potential wound healing properties on HaCaT cells. The commercial spray (BFS) and the synthesized gold nanoparticles (BFSAuNP) displayed antiproliferative activity with an IC_{50} of 4.63 ± 0.05 and 3.50 ± 0.40%, while the ethanolic leaf juice (BFE), ethanolic whole leaf, gel extract and their respected gold nanoparticles (AuNPs) showed no activity (IC_{50} > 400 µg/mL and 10%).

The synthesized gold nanoparticles (BFEAuNP, 20.87 ± 0.69%) showed significant wound closure ($p < 0.05$) when compared to the media control (9.30 ± 0.15%) at the highest testing concentration (100 µg/mL). Due to the significant wound closure displayed by BFE and BFEAuNP, these samples were selected for further evaluation for their effects against histamine production using PMA stimulated granulocytes at a concentration of 200, 100 and 50 µg/mL. None of the selected samples displayed antiproliferative effects against granulocyte cells (IC_{50} > 200 µg/mL). In comparison to the untreated control (0.30 ± 0.02 ng/mL), BFEAuNP at a concentration of 100 (0.12 ± 0.04, $p < 0.05$) and 50 µg/mL (0.02 ± 0.008 ng/mL, $p < 0.01$) significantly inhibited the production of histamine.

Future studies include isolation and purification of JLB to identify potential anti-tyrosinase compounds that could be present. Furthermore, investigations into JLAuNPs potential effect on translators such as nuclear factor kappa beta (NF-κB) that are associated with the production of TNF-α should be considered. Moreover, the potential mechanism of action by which ET-EtOH may inhibit symptoms associated with eczema should be considered. Lastly, investigations into the potential *in vivo* wound healing properties of BFEAuNP and whether the BFEAuNP and ET-EtOH targets histamine-associated receptors on mast cells as a potential mode of action should be considered.